Aus dem Institut für Zelluläre und Molekulare Immunologie
(Prof. Dr. rer. nat. J. Wienands)
der Medizinischen Fakultät der Universität Göttingen

Role of the glucocorticoid receptor in the development of ulcerative colitis and colorectal carcinoma in a murine model

Inaugural-Dissertation

zur Erlangung des Doktorgrades
der Medizinischen Fakultät der
Georg-August-Universität zu Göttingen

vorgelegt von

Eric Phillip Twomey
aus
Windhoek, Namibia

Göttingen, 2021

Dekan	Prof. Dr. med. W. Brück

Betreuungsausschuss

Betreuer/in:	Prof. Dr. rer. nat. H. M. Reichardt
Ko-Betreuer/in	Prof. S. A. Johnsen, Ph.D.

Prüfungskommission

Referent/in:	_____
Ko-Referent/in	_____
Drittreferent/in	_____

Datum der mündlichen Prüfung: _____

Eidesstattliche Versicherung

Ich versichere hiermit an Eides statt,

1. dass ich die vorgelegte Arbeit mit dem Titel

   Role of the glucocorticoid receptor in the development of ulcerative colitis and colorectal carcinoma in a murine model

   selbstständig und ohne Anwendung anderer als der angegebenen Hilfsmittel angefertigt habe; nicht selbst erhobene Befunde und/oder Ergebnisse habe ich nach ihrer Herkunft eindeutig gekennzeichnet;

2. dass die eingereichte Druckfassung und die elektronische Fassung identisch sind. Mit der Übermittlung meiner Dissertation an externe Dienste zum Zwecke der Überprüfung mittels Plagiatssoftware bin ich einverstanden.

3. dass die Ergebnisse dieser Arbeit an keiner anderen Fakultät Gegenstand eines Promotionsverfahrens gewesen sind.

4. dass die Arbeit in folgender Form bereits veröffentlicht (oder zur Publikation eingereicht) wurde:

   Muzzi C, Watanabe N, **Twomey E**, Meers GK, Reichardt HM, Bohnenberger H, Reichardt SD. The Glucocorticoid Receptor in Intestinal Epithelial Cells Alleviates Colitis and Associated Colorectal Cancer in Mice. Cell Mol Gastroenterol Hepatol. 2021;11(5):1505-1518.

   Twomey E, Reichardt SD (2017): Role of the glucocorticoid receptor in intestinal epithelial cells for the development of colitis-associated colorectal cancer. Accepted poster within the Conference of Comprehensive Cancer Research in Göttingen, 12/2017

   Erläuterung: Teile der Dissertation können vorab publiziert worden sein; dabei muss der Name des Doktoranden als Autor oder Mitautor verzeichnet sein; Angaben über das Thema der Veröffentlichung, die Zeitschrift (mit Bandzahl, Jahreszahl, Seitenzahl) und Autorennamen

5. dass ein früherer Promotionsversuch weder in Medizin noch in Zahnmedizin stattgefunden hat

6. dass ich keine Hilfe von Promotionsberatern in Anspruch genommen habe und Dritten keine geldwerten Leistungen für Arbeiten gezahlt habe, die mit der Dissertation im Zusammenhang stehen.

Table of Contents

List of Figures

List of Tables

Abbreviations

5-ASA ..... 5-aminosalicylic acid
6-MP 6-Mercaptopurine
AB ..... antibodies
ACF ..... aberrant crypt foci
ACTH ..... Adrenocorticotropin
AMP ..... antimicrobial peptide
APC ..... adenomatous polyposis coli
AZA ..... Azathioprine
B-cells ..... bursa of Fabricius lymphocytes
CA-CRC ..... colitis-associated colorectal carcinoma
CD ..... Crohn's disease, cluster of differentiation
cDNA ..... complementary deoxyribonucleic acid
CRH ..... corticotropin-releasing-hormone
CSA ..... Cyclosporin A
CTL ..... cytotoxic T lymphocyte
CXCL ..... C-X-C motif ligand
DAB ..... diaminobenzidine
DBD ..... DNA-binding domain
DC ..... dendritic cell
ddH_2O ..... double-distilled water
DEPC ..... diethylpyrocarbonate
DEX ..... dexamethasone
DNA ..... deoxyribonucleic acid
dNTP ..... deoxy nucleoside triphosphate
FAB ..... antigen binding fragment
FACS ..... fluorescence-activated cell sorting
FAP ..... familial adenomatous polyposis
Fc ..... crystallizable fragment
G ..... gauge
GCs ..... glucocorticoids
GR ..... glucocorticoid receptor
GRE ..... glucocorticoid-responsive-elements
HE ..... Hematoxylin Eosin
HNPCC ..... hereditary nonpolyposis colorectal cancer
HPA ..... hypothalamic-pituitary-adrenal axis
HPRT ..... hypoxanthine phosphoribosyl transferase
HSP ..... heatshock-protein
i. v. ..... intravenously
IECs ..... intestinal epithelial cells
IHC ..... Immunohistochemistry
IL ..... Interleukin
IVC ..... individually ventilated cages
kDa ..... kilodalton
KO ..... knock-out
KRAS ..... Kirsten Rat Sarcoma
LAVES ..... Lower Saxony State Office for Consumer Protection and Food Safety
LBD ..... ligand binding domain
MALT ..... mucosa-associated lymphatic tissue

MAPK ..... mitogen-activated protein kinase
MCP ..... monocyte chemotactic protein
MFACs .....medium fatty acid chains
MHC .....major histocompatibility complex
MLH .....MutL homolog
mTOR ..... mechanistic target of Rapamycin
NFAT ..... nuclear factors of activated T-cells
NFκB .....nuclear factor of kappa-light chain-enhancer of activated B-cells
nGRE ..... negative glucocorticoid responsive element
NTD ..... N-terminal domain
PAMP ..... pathogen-associated molecular pattern
PAS .....Periodic acid-Schiff
PCR .....polymerase chain reaction
PfuS .....pyrococcus furiosus
PPAR-γ ..... proliferator activated receptor gamma
PRR ..... pattern-recognition receptor
PSC ..... primary sclerosing cholangitis
qRT-PCR ..... quantitative reverse transscription-polymerase chain reaction
rcf ..... relative centrifugal force
RE ..... response element
RNA ..... ribonucleic acid
RONS .....reactive oxygen and nitrogen species
RT ..... room temperature
SEM .....standard error of the mean
SFACs .....short fatty acid chains
SPF .....specific-pathogen-free
TBS/T .....Tris-buffered-saline-Tween
T cells .....Thymus cell lymphocytes
TF .....transcription factors
T_H1 .....type 1 helper T-cells
T_H2 .....type 2 helper T-cells
TLR-2 ..... toll-like receptor
TNFR .....TNF-α receptor
TNF-α ..... tumor necrosis factor alpha
TNM .....tumor-nodes-metastasis
TP53 .....tumor protein p53
T_{reg} ..... cells regulatory T cells
UC ..... ulcerative colitis
UICC ..... Union for International Cancer Control
w/v .....weight per volume
ZTE .....Zentrale Tierexperimentelle Einheit

Abstract

For many decades, glucocorticoids (GCs) have been an essential pillar of the therapy of many inflammatory diseases. The beneficial effects of this class of hormones occur quickly and reliably after administration, although they are accompanied by the risk of various side effects. GCs have also been used successfully in the therapy of ulcerative colitis for many years. Nevertheless, the exact mode of action of their effect on the inflammatory processes in the bowel is still largely unknown. Since GCs trigger most of their effects through binding to the GC receptor (GR), we aimed to elucidate the role of the GR in the gut, especially in intestinal epithelial cells. To reach this objective, we triggered colitis in a mouse model expressing a modified GR whose function was restricted to DNA-binding independent activities, or in mice in which the GR in intestinal epithelial cells was switched off. We hypothesized that under these conditions the disease course was altered. A special focus was laid on the activity of macrophages being a switch point of inflammatory processes. We used clinical parameters to assess the disease course and characterized the molecular processes by investigating cytokine production and gene expression. Immunohistochemical analyses were performed to identify and quantify infiltrating cells. Most importantly, we could show that switching off GR expression in enterocytes worsened the disease course. Both clinically and biochemically, aggravated episodes were observed. Increased gene expression of CCL2 in intestinal epithelial cells could at least be partially accountable for this observation. In the end, we assumed that deletion of the GR also affected colitis-associated colorectal carcinoma in mice. Using the mouse model with a deletion of the GR in intestinal epithelial cells, we could show that more and larger tumors developed under these conditions. In summary, our work demonstrates that the GR expressed in cell of the intestinal tract plays an essential role as an immunoregulatory entity. Hereby, it represents a major factor in the development of both ulcerative colitis and colitis-associated colorectal carcinoma, and thus could serve as a potential target of further therapeutic regimens.

1. Introduction

1.1. Anatomy and Structure of the Colon

The human colon depicts the end of the gastrointestinal tract (GIT), beginning at the side-to-end connection to the ileum and ending with the transition from rectum to anus (Fig. 1). The cecum is separated from the ileum by the ileocecal valve which prevents feces backflow and forms the first part of the ascending colon. In the upper right flexure, the colon transverses to the left, where it bends again, forming the upper left flexure, descends and after creating the sigmoidal colon finally, ends in the rectum. In contrast to the ileum, which maintains a highly sterile environment, the colon is characterized by its huge microbiome variety and its vast amount of microbiota (Gill et al. 2006).

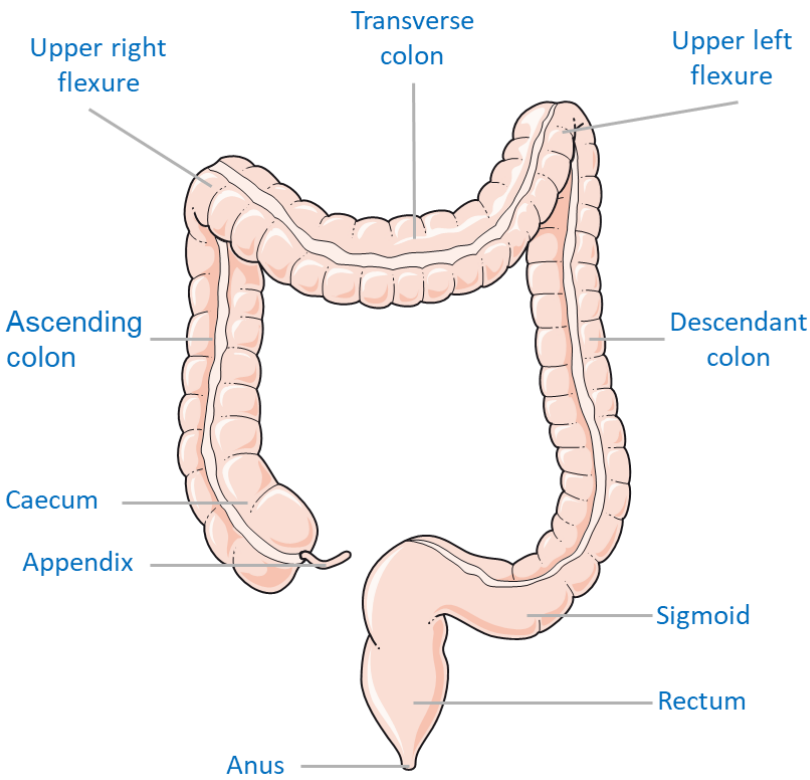

Fig. 1 Anatomy of the human colon. Depicted is a typical human colon with its nomenclature. Adapted with kind permission from Medical Art by Servier (Servier 2018).

In histological terms, the colon shows high similarity to the preceding small intestine (Fig. 2). The histological layers consist of the *lamina epithelialis mucosae*, or *epithelium*, *lamina propria mucosae*, *lamina muscularis mucosae*, *tela submucosa*, *tunica muscularis*, *tunica adventitia*. However, the colon shows two key differences to the small intestine. Firstly, its *mucosa* displays no villi, but only crypts. In the fundus of the crypts, basal

epithelial cells are permanently dividing and thus regenerating the epithelial layer of the mucosa. Secondly, the colonic epithelium shows a higher amount of goblet cells than the preceding small intestine, producing mucus and thus lubricating the surface of the mucosa. The cryptic structure of the mucosa is upheld by fibrocytes, myocytes and resident cells of the immune system like macrophages. Colonic crypts are supplied by mesenteric arteries and arterioles and drained by venules, and lymphatic vessels, which provide a constant flow of lymph towards lymph nodes (Fig. 2) (Kaiserling et al. 2003).

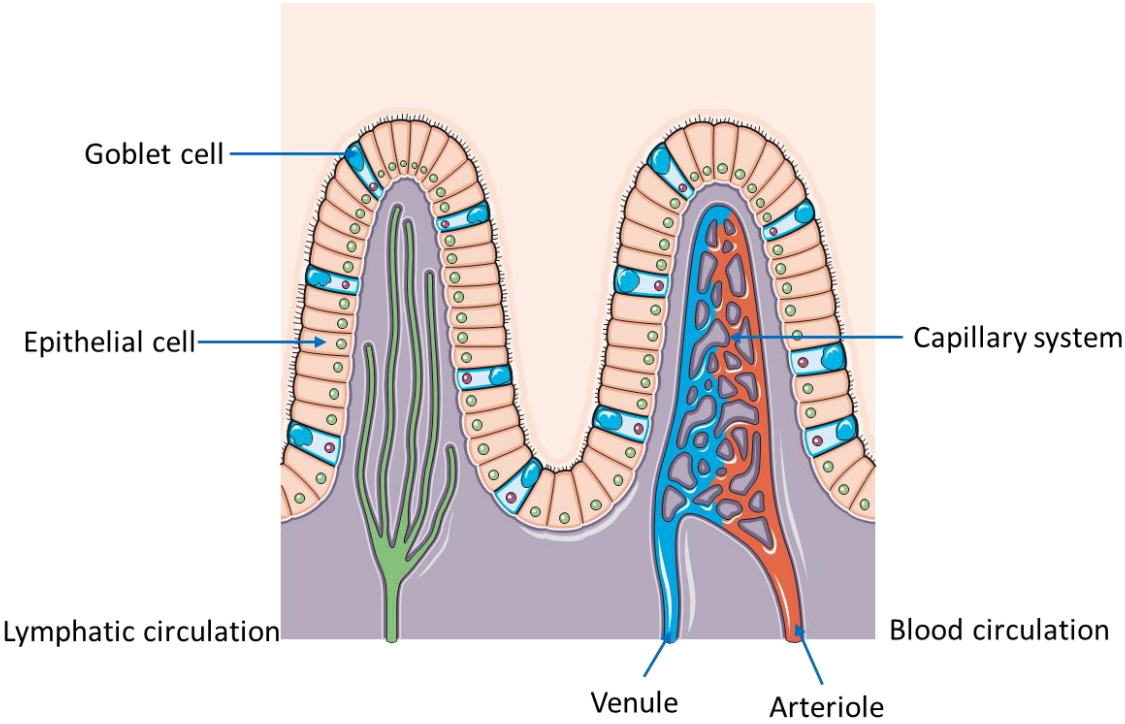

Fig. 2 Structure of the colon's crypts. In contrast to the preceding part of the gut, the colon epithelium does not possess any villi but only crypts. The cells of the pseudo-rectified columnar epithelium are constantly scaled off by luminal ordure and renew themselves by replicating basal cells at the crypt's basis. Goblet cells produce mucus that allows a lubrication of the epithelial surface. The epithelium is strongly vascularized and well supplied by lymphatic drainage (Michael Ross 2016). Adapted with kind permission from Medical Art by Servier (Servier 2018).

1.2. Physiology and Functions of the Colon

The colon and the rectum represent the last section of the GIT. The colon has multiple functions and is irreplaceable for an intact physiology of the human body. With a total surface area of about 2 m^2, it represents a large interaction surface for substances and organisms of the external environment with the body (Helander and Fändriks 2014). Through sodium-hydrogen exchange channels for instance, up to 6 liters of fluids from the food pulp can be extracted per day and the stool can thus be thickened (Sandle 1998; Muanprasat and Chatsudthipong 2013). By doing so, it contributes significantly to the

regulation of the water and electrolyte balance of the body (Phillips and Giller 1973). At the same time, the colon, together with the rectum, is considered a reservoir of stool and allows controlled defecation (Ford et al. 1995). In recent years, the colon has also increasingly come into the spotlight of scientific attention and public interest as being the organ with the highest immune-microbiome interaction within the human body (Enders 2014). The composition of the microbiota even seems to have an effect on the origin and course of colorectal cancer (Garrett 2019). In contrast to the mostly sterile preceding small intestine, the colon harbors large amounts of microbiota, collectively referred to as the microbiome. It is estimated that there are roughly 30 trillion bacteria within the human colon, almost as many as cells within the human body itself (Sender et al. 2016). Approximately 500 - 1000 different strains of bacteria, fungi, protozoa and occasionally helminths colonize the colon (Ramakrishna 2007). Most of these microorganisms are in equilibrium with each other as well as with the host. In this context, the physical, chemical, and immunological barrier function of the epithelial cells within the mucosa is essential (Sartor 2008; Pastorelli et al. 2013). A complex interplay of the epithelial cells, macrophages and other immune cells residing in the mucosa, such as T cells, results in the inability of harmful bacteria to enter the human body in healthy individuals and lead to systemic inflammation or infection (Kaistha and Levine 2014). The colon holds a large arsenal of immune cells that contribute to homeostasis in the colon with the mucosa associated lymphogenic tissue (MALT), consisting of Peyer's patches and tissue-resident immune cells (Shao et al. 2005; Ahluwalia et al. 2017). If this finely tuned balance within the colon becomes deranged, e. g. due to an infiltration with enteric germs, chronic malnutrition or chronic stress, local inflammation or even infection is often the result, which in turn can lead to systemic inflammation. It is evident that a healthy colon with its numerous functions and particularly its role as a barrier is essential for an intact gut homeostasis and an abiding well-being of any individual.

1.3. Ulcerative Colitis

1.3.1. Epidemiology of UC

Ulcerative colitis (UC) or *Colitis Ulcerosa* belongs to the group of inflammatory bowel diseases. Despite intensive research in the past decades, its etiology and pathological mechanisms remain partially idiopathic. In comparison to Crohn’s disease (CD) or *Morbus Crohn*, UC is defined by the sole affection of the colon. In most cases, UC predominantly affects the rectal part of the colon and its extension is limited to the mucosa and submucosa

(Kumar et al. 2016). In contrast to CD, the course of UC is milder and can be cured by total colectomy in many cases (German S3-Guideline Ulcerative Colitis 2020).

Both, UC and CD mainly occur in modern societies such as in populations of North America and Northern Europe. Since the past century, numbers of newly affected patients and existing cases are constantly increasing. An incidence of 1.2 to 20.3 cases per 100.000 individuals per year, and a prevalence of 7.6 to 246.0 cases per 100,000 were reported in literature (Loftus 2004). The lifestyle in industrialized countries including high fat and high sugar diets and the frequent use of medication especially antibiotics seems to be accountable for this phenomenon. Interestingly, a high socio-economic status seems to be linked to higher disease rates (Danese et al. 2004).

Until today, 47 gene loci with an effect on UC have been discovered. 28 of these loci are shared with CD (Turnbaugh et al. 2007). Despite the knowledge of these loci, a genetic screening is not indicative yet due to a small impact of each one of the genes.

Focusing on the influence of the microbiota to the course of UC, it has been shown that a loss of tolerance from the host towards the microbiota correlates with the severeness of the course of disease. These observations were made in animal models have not been confirmed in human trials as of yet (Kaistha and Levine 2014). However, patients with UC do have a distinct composition of the microbiotic flora and tend to have a higher density of microbiota compared to healthy individuals. Surprisingly, antibiotic therapies does not seem to have any effect on the course of UC (Sartor 2008). The existence of microbiota appears to be a compulsory precondition to the development of UC, at least in a murine model (Podolsky 2002). Within the response of the mucosal immune system no explicit evidence regarding innate immune defects can be detected. Increased expression of TLR-2 (toll-like receptor 2) and TLR-4 (toll-like receptor 4) for example has been identified but are considered to be secondary effects of the disease (Cario and Podolsky 2000; Hermoso et al. 2004).

1.3.2. Immunological Homeostasis and Barrier of the Colon

The immunological homeostasis of the colon appears to be a delicate balance of sufficient protection against potentially harmful organisms on the one hand and adequate tolerance against commensal bacteria that are beneficial to the host on the other hand (Fig. 3). The central communication and barrier function between the luminal microbiome and the resident immune cells is performed by the intestinal epithelial cells (IECs) (Kagnoff 2014).

Under physiological conditions, the mucosa and the microbiotic flora interact in a harmonic homeostasis. Some organisms get in contact with the epithelial layer or even surpass it, where they eventually encounter resident macrophages. These macrophages recognize the specific surface pattern of the organism and will eliminate those from the colon's own microbiome without any inflammatory response occurring (Podolsky 2002). Also, epithelial cells tolerate tangent or intruding bacteria to a certain extent, without an inflammation being triggered.

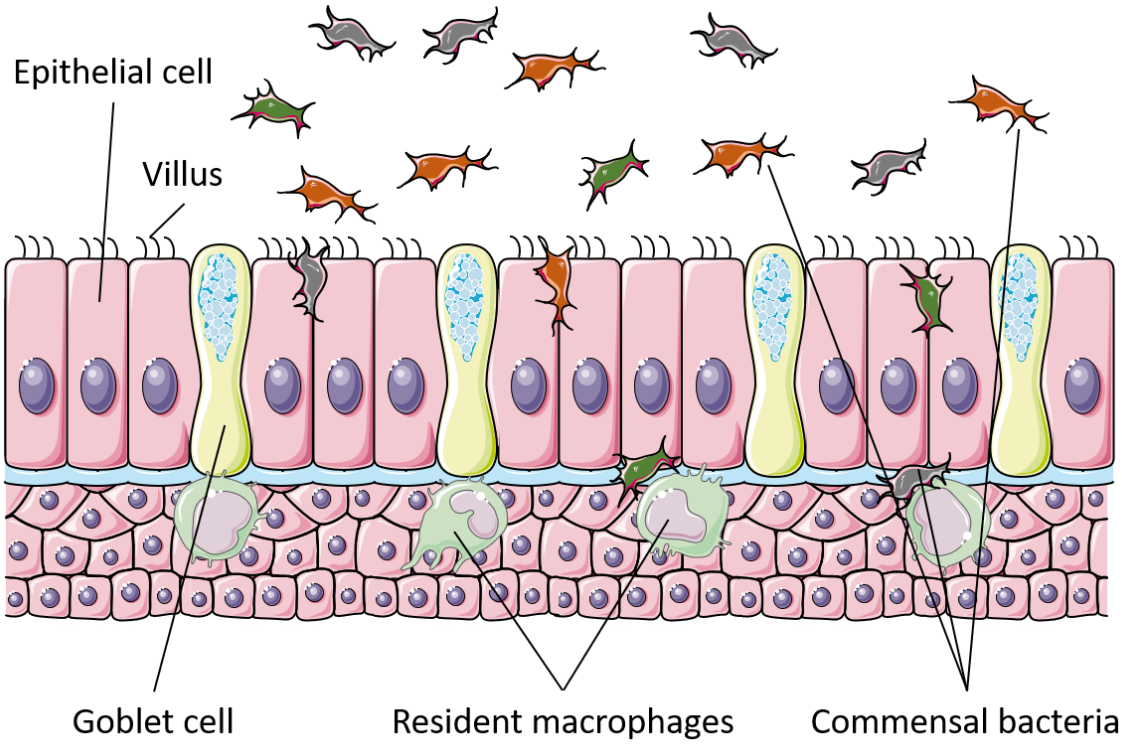

Fig. 3 Epithelial homeostasis in the colon. The physiological condition under which the colon epithelial interacts with resident flora. Some organisms are harmless to the epithelium and tolerated by it to a certain degree. Adapted with kind permission from Medical Art by Servier (Servier 2018).

1.3.3. Inflammation and Pathogenesis of UC

UC is one entity of inflammatory bowels disease (IBD) and shows the typical properties of an inflammatory event. These features, namely redness (*rubor*), pain (*dolor*), warmth (*calor*), swelling (*tumor*), and impaired function (*functio laesa*) are universal and, although not always seen or noticed, reliable clinical indicators for inflammatory processes (Laroux and Grisham 2001).

At the cellular level, several processes occur simultaneously under inflammatory conditions such as UC (Fig. 4). Individuals with genetic predisposition and structurally compromised

colonic epithelium are thought to be more vulnerable to invasive and virulent germs. Upon contact, these germs have a stress effect on IECs. If a bacterium penetrates the mucin layer, which is the first barrier of the mucosa, pathogen-associated molecular patterns (PAMPs) of the bacterium can be recognized and bound by TLRs located on the luminal surface of the IECs (Abreu 2010). This binding leads to an intracellular activation of nuclear factor of kappa-light chain-enhancer of activated B-Cells (NF-κB) and the mitogen-activated protein kinase (MAPK) pathway, which in turn leads to the generation of pro-inflammatory and apoptotic signals (Lawrence 2009).

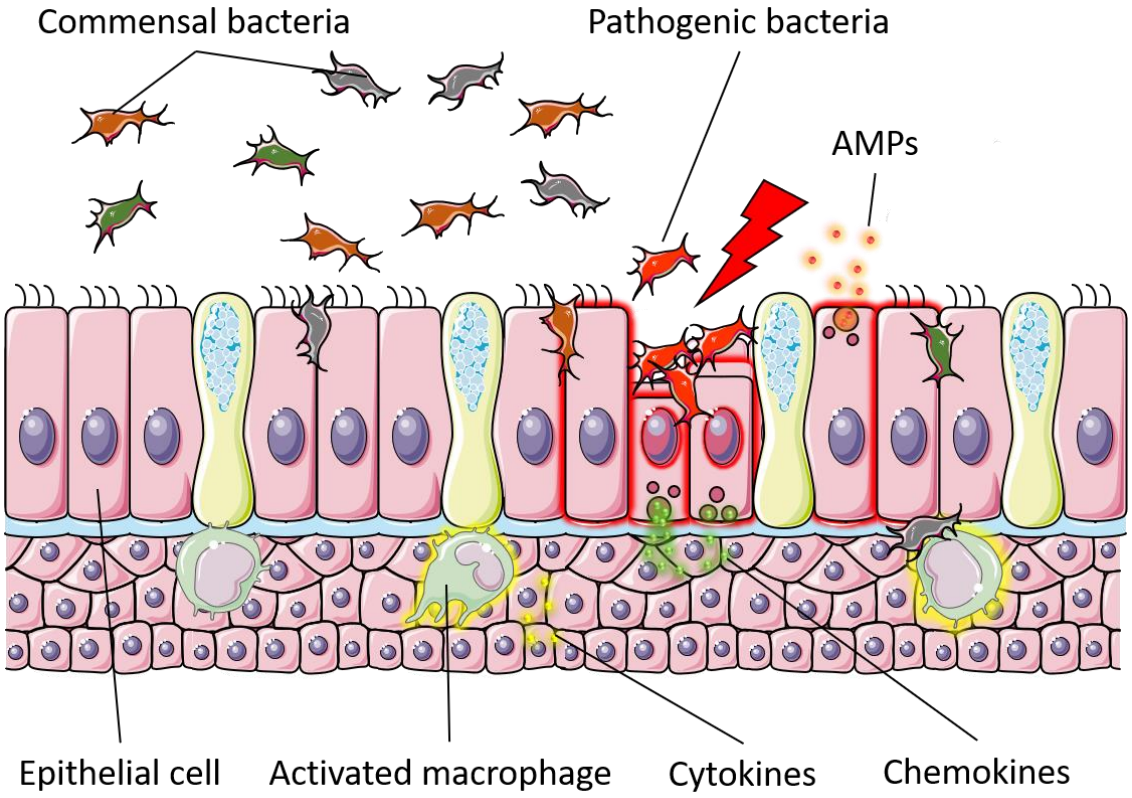

Fig. 4 Epithelium under stress. Invasive organisms, for example pathogenic bacteria, exert stress on IECs. These IECs in turn disburse AMPs to parry these bacteria directly and release chemokines to attract macrophages. These macrophages in turn release cytokines to provoke an immune response mediated by T cells. Adapted with kind permission from Medical Art by Servier (Servier 2018).

As a result, IECs produce antimicrobial peptides (AMP) that can be used to directly attenuate pathogens (Bevins and Salzman 2011). Simultaneously, IECs secrete chemokines such as C-X-C motif ligand 1 and 5 (CXCL1 and 5) Monocyte chemotactic protein 1 (MCP1/CCL2) thereby activates resident and attract circulating neutrophiles and macrophages (Kagnoff 2014). Depending on their polarization, these macrophages secrete pro-inflammatory cytokines such as Interleukin 1β and 6, (IL-1β and IL-6,) and Tumor-Necrosis-Factor α (TNF-α), or anti-inflammatory cytokines as IL-10, which again promote a plethora of

cellular responses including cell differentiation, proliferation and apoptosis (Danese and Fiocchi 2011).

As an alternative to the described pathway via IECs, invasive bacteria can directly get into contact with antigen-presenting cells, such as the dendritic cells (DCs) or macrophages, and thus activate an immune response (Fig. 5). DCs are able to bypass the tight barrier of IECs with their pseudopodia and, upon contact, recognize and directly phagocyte bacteria via their pattern-recognition-receptors (PRRs) (Mason et al. 2008).

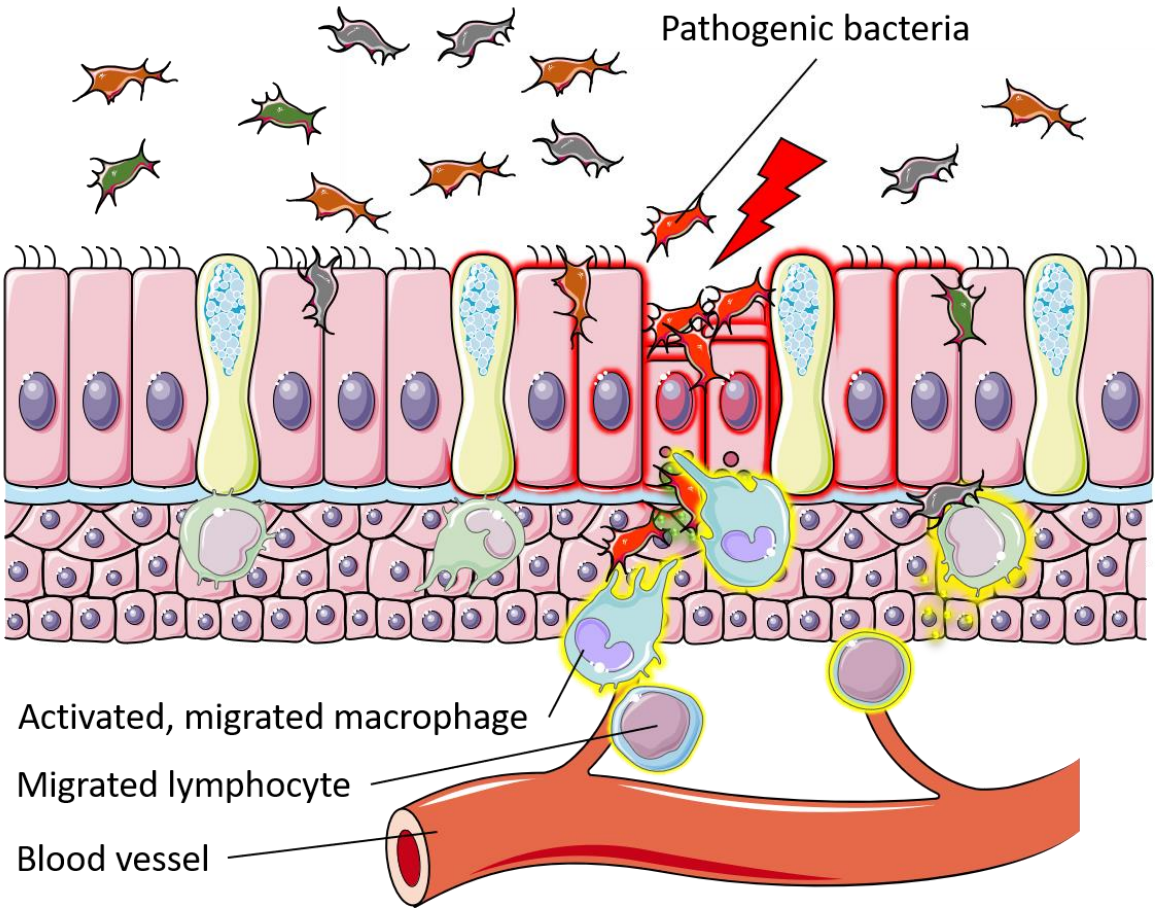

Fig. 5 Immune Response. After a short period of time, activated macrophages and lymphocytes migrate to the site of inflammation, attracted by the concentration gradient of chemokines. They soon identify foreign organisms, start defense mechanisms, and activate CD4$^+$ T cells via MHC class II. Adapted with kind permission from Medical Art by Servier (Servier 2018).

Macrophages, neutrophils, and DCs belong to the MHC (major histocompatibility complex) class II expressing cells and are able to present components of phagocytized bacteria to CD4$^+$ T helper 2 cells (Th2) and subsequently activate them (Buettner and Bode 2012). Resident or immigrating CD8$^+$ cytotoxic T cells (CTL) can be activated by macrophages as well and thereby initiate pathogen elimination. In addition, macrophages are able to decrease the amount of inflammation by expressing scavenger receptors such as CD163, which is able to

remove pro-inflammatory agents such as haptoglobin/hemoglobin complexes (Etzerodt and Moestrup 2013).

In contrast to CD, T cells in UC belong mainly to the subgroup of Th2 cells (Danese and Fiocchi 2011), which serve to activate immunoglobulin producing B cells located for instance in Peyer's patches (Newberry and Lorenz 2005). These Th2 cells release IL-13 but also TNF-α which causes epithelial barrier dysfunction by promoting apoptosis and cytotoxicity and thus closing a self-perpetuating circle of pro-inflammatory activity (Heller et al. 2005; Van Hauwermeiren et al. 2015). This dynamic interplay of IECs with cells of the innate and adaptive immune systems demonstrates the complexity of the immune response to mucosal damage and germ invasion.

1.3.4. Diagnosis of UC

After recognizing clinical signs of UC, such as diarrhea, bloody stools and tenesmus, the primary and most accurate diagnostic tool is a colonoscopy with biopsies (German S3-Guideline Ulcerative Colitis 2020). Other tests such as radiologic imaging, ultrasound or blood tests are not specific enough to diagnose UC beyond doubt (Stange et al. 2008). Nonetheless, laboratory tests on stool and blood samples can help assessing the severity of a colitis by quantifying levels of calprotectin or lactoferrin (Rahier et al. 2009; Lin et al. 2014). A colon within an acute colitis features typical signs of erythematous, granular erosions and ulcerations, and severe forms of colitis can show deep ulcerations and even spontaneous bleeding (Goldstein and Dulai 2006).

1.3.5. Therapy of UC

UC therapy can be divided into surgical and medical treatment options. First therapeutic measures are changes in lifestyle and nutrition. If these options prove to be insufficient, pharmaceutical measures should be considered. 5-amino-salicyl-acid (5-ASA) agents such as sulfasalazine are commonly used as a mainstay therapy and can be administered over a long period of time. It is assumed, that the therapeutic action of 5-ASA is mediated by the peroxisome-proliferator activated receptor γ (PPAR-γ), thereby decreasing the binding of NFκB to its promoting region (Dignass et al. 2009). Supposedly, this inhibition of NFκB will reduce its pro-inflammatory effect on the level of transcription (Lawrence 2009). If these agents are not tolerated due to side effects, or do not result in a satisfactory level of

effectiveness, therapy options can be escalated to azathioprine (AZA) and its metabolite 6-mercaptopurine (6-MP), both serving as purine analogues and by their structure inhibiting the purine ribonucleotide synthesis. The subsequent inhibition of the cell cycle leads to an attenuation of the immune response. AZA and 6-MP can contribute to a GC-free disease management and thus reduce the occurrence of iatrogenically induced Cushing symptoms (Longo 2012). GCs are commonly used in acute settings when an escalation of mainstay therapy does not suffice to cope with disease peaks. In addition, also long-term low-dose GC therapies must often be accepted. In these cases, different GC derivatives are used, such as intravenous (i. v.) prednisolone and methylprednisolone or budesonide foam, which is administered rectally (Pithadia and Jain 2011). GC should not be administered longer than necessary due to their major side effects such as osteoporosis, hyperglycemia, hypertonia, hyperlipidemia, abdominal striae, cataracts, secondary adrenal insufficiency on withdrawal and secondary iatrogenic immunodeficiency (Longo 2012; Pivonello et al. 2016). All above-described symptoms can occur during longer periods of GC administration and are subsumed by the term of iatrogenic Cushing syndrome. In cases of GC-refractory UC, calcineurin inhibitors such as cyclosporine A (CSA) or Tacrolimus can be considered. Both of them reduce the activation of nuclear factors of activated T cells (NFAT) by forming a complex with cyclophilin A and thus reduce the activity of T cells (Murphy and Weaver 2018). The use of sirolimus/rapamycin as an inhibitor of the mechanistic target of rapamycin (mTOR) is currently investigated in clinical trials and is called for by some authors as a complementary therapy but has not yet found its way into the guidelines (Mutalib et al. 2014). Lately, the treatment options were complemented by anti-TNF-α biologicals like infliximab or adalimumab. Both aim for the potent pro-inflammatory cytokine TNF-α, which induces an immune response mediated by Th1 cells (Pithadia and Jain 2011). Etanercept is an example for a recombinant fusion protein, containing the p75 subunit of the TNF-α receptor (TNFR) and the Fc-part of immunoglobulins. Both types of biologicals reduce the immune response by inhibiting the cytokine signaling pathway (German S3-Guideline Ulcerative Colitis 2020). The common goal of all treatment options is to suppress the immune response and thereby reduce inflammatory events and successive damages. Patients and physicians aim for a long-term and disease-free maintenance of remission.

In cases of colitis that are refractory to the named remedies, surgical options are a reasonable next step. Depending on the extent, a partial colectomy or even total proctocolectomy can be performed (German S3-Guideline Ulcerative Colitis 2020).

1.4. Colorectal Carcinoma

1.4.1. Epidemiology of Colorectal Carcinoma

The colorectal carcinoma (CRC) belongs to the most frequently found malignancies of GIT. According to the most recent *Report on Cancer* of the Robert-Koch-Institute, the 10 years prevalence of CRC in Germany is estimated to 351,520 cases (RKI Report on Cancer 2016). The incidence, which indicates newly diagnosed people per year, is estimated to 62,410 diagnoses. In general, men show a higher incidence and prevalence than women. As most cancer entities, colorectal carcinoma is found predominantly in the population of over 40 years of age and from there on shows a steep increase of incidence. The 5-year survival rate amongst men is estimated to 62.8 % and amongst women to 63.2 %. During the year 2008, costs of hospitalization in Germany added up to 1.73 billion Euro (RKI Report on Cancer 2016).

1.4.2. Development of CRC

The development of CRC strongly depends on the sub-entity, age, sex and ethnic group of the diseased subject. Among the German population 75 % of CRC cases are assumed to be sporadic, while only about 20 % are inherited e. g. through mutations of the APC-gene (adenomatous polyposis coli), which causes familial adenomatous polyposis (FAP), or microsatellite instability through mutations of e. g. MLH-1 (MutL homolog 1) or MSH-2 (MutS homolog 2), which can lead to hereditary nonpolyposis colorectal cancer (HNPCC) (Tanaka 2009). About 1 – 2 % of CRC cases are estimated to be caused by or related to UC, which equates to 600 – 1,200 cases per year in Germany. Similar to UC, CRC occurrence is connected to a certain diet and lifestyle. Smoking, frequent alcohol consumption, red meat, low fiber, low vitamins, high fat and low levels of exercise correlate with the development of CRC (Kumar et al. 2016).

1.4.3. Staging of CRC

Like most carcinomas, CRC is staged according to the Union for International Cancer Control (UICC) using the tumor-nodes-metastasis (TNM) classification. Considering the tumor size and its invasiveness, the affection of local lymph nodes and the occurrence of metastasis, CRC can be categorized and its prognosis can be determined with a considerable precision (Brierley et al. 2016). Four stages named I – IV (Table 1) are currently used to

stratify the therapeutic options, where stage I correlates with a better prognosis while Stage IV is the least favorable one (German S3-Guideline Colorectal Cancer 2019). As shown in Fig. 6, the T-classification refers to the extent of infiltration of the tumor into the tissues.

Table 1 UICC Classification of CRC Stages. T = tumor, N = lymph node, M = metastasis. Adapted from *Evidenced-Based Guideline for Colorectal Cancer* (German S3-Guideline Colorectal Cancer 2019).

UICC Stage	Primary Tumor	Lymph nodes	Metastasis
0	Tis	N0	M0
I	T1, T2	N0	M0
II a - c	T3 – 4b	N0	M0
III a - c	T1 – 4b	N1 – 2b	M0
IV a - c	Every T	Every N	M1 a - c

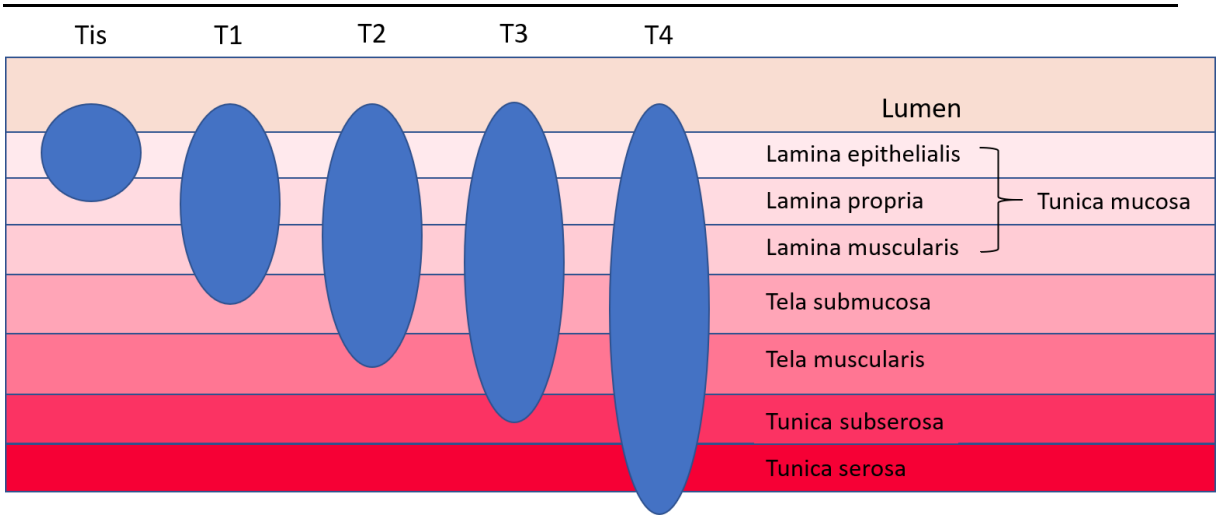

Fig. 6 Classification of tumors. The tumors invasiveness is defined by its infiltration into the wall of the colon. T0 shows no evidence of a tumor. This equals a carcinoma-in-situ that extends only to the lamina propria. T1 tumors have grown into submucosa, T2 into muscularis propria, T3 extend to the subserosa while T4 tumors have grown to the surface of the peritoneum or even affect other organs. Tx is used for tumors that cannot be evaluated. Adapted from Pathologic Basics of Disease, Robin et al., 2016 (Kumar et al. 2016).

1.4.4. Pathogenesis of Colitis-Associated CRC

Regardless of its cause, whether sporadic, inherited or induced by inflammatory events, most cases of CRC result in a similar outcome. Through a chronic activation of NF-κB, a higher cell turnover and the generation of reactive oxygen and nitrogen species (RONS), DNA damage is increased (Tanaka 2009). After a critical number of mutations in predisposing genes like APC, KRAS, TP53, MSH 2 or MLH 1 have occurred in the epithelial layer of the colonic tissue, the mutated cells enter an adenoma-carcinoma-sequence (Leslie et al. 2002; Kumar et al. 2016). These mutations can lead to so-called aberrant crypt foci (ACF), which

are altered stem cells at the basis of the crypts (Tanaka 2009). A subsequent growth stimulus then provokes an exophytic growth of macroscopic polyps into the lumen of the colon, containing parts of epithelium showing a high-grade dysplasia. This tubular adenoma subsequently turns into an invasive carcinoma by infiltrating the underlying layers of the tissue. Alternatively, endophytic and ulcerative growth, or a diffuse-infiltrative growth can be observed. Like in most tissues, chronic inflammation of the colon increases the likelihood of neoplastic growth. Frequency, duration, extensiveness, and severity of the inflammation seem to be directly linked to cancer development in the case of colitis. An onset of disease at a young age and an existing primary sclerosing cholangitis also predispose for CRC development (Rex 2010). Thus, the risk of patients with UC to grow a CRC on an initial dysplasia is estimated to be 20 to 30 times higher compared to control groups (Böcker et al. 2012).

1.4.5. Therapy of CRC

The aims and measures of CRC therapy are highly dependent on its stage. In almost every case of stage I – III, a surgical resection is the first step, often followed by chemotherapy. The mainstay chemotherapy persists of Fluoropyrimidines (FP) such as Capecitabin (Cap) and 5-Fluorouracil (5-FU), Platin-derivatives such as Oxaliplatin (Ox) and topoisomerase inhibitors like Irinotecan. Additionally, antibodies against the Epidermal Growth Factor Receptor (EGFR) like Cetuximab and antibodies against the Vascular Endothelial Growth Factor (VEGF) like Bevacizumab are in use. Stage IV patients either get an extended therapy regimen with more frequent and extensive surgeries and chemotherapy or will be treated with best supportive care in a palliative setting (German S3-Guideline Colorectal Cancer 2019).

1.5. Glucocorticoids

GCs such as cortisol in humans or corticosterone in rodents, are highly potent and almost ubiquitously active hormones (Fig. 7). They play an important role in many physiological systems and parts of the organism e.g., metabolism, constant sympathetic activity and in immunological events (Cain and Cidlowski 2017). Most of the human cortisol is produced in the fascicular zone of the adrenal cortex, which is part of the hypothalamic-pituitary-adrenal (HPA) axis (Fig. 8).

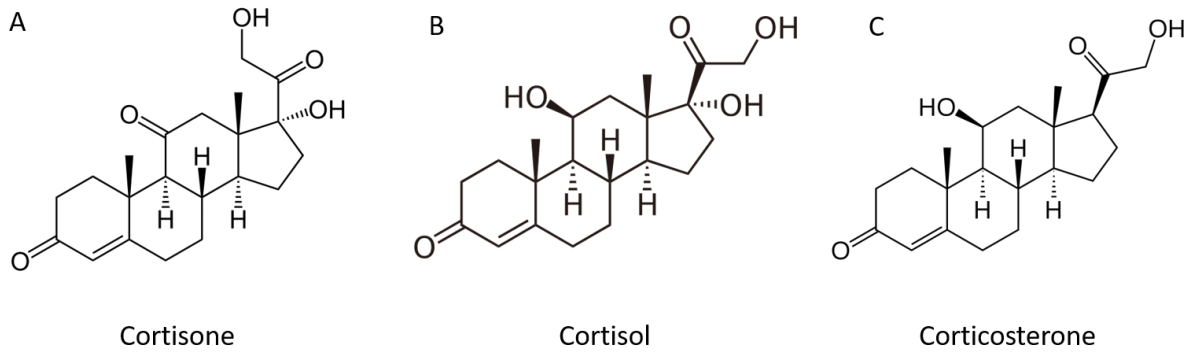

Fig. 7 Glucocorticoids. Depicted in (A) and (B) human GCs. Cortisone gets hydroxylated to Cortisol which is 1.25 x more active. (Berg et al. 2013) Corticosterone (C) is mainly found in rodents.

Influenced by many factors such as the day-night circadian cycle, levels of other hormones or neuro-psychological stimuli such as social, psychological, or physiological stress, the hypothalamus secrets corticotropin-releasing-hormone (CRH), which on its part provokes the production of adrenocorticotropin (ACTH) in the anterior pituitary (Sapolsky et al. 2000).

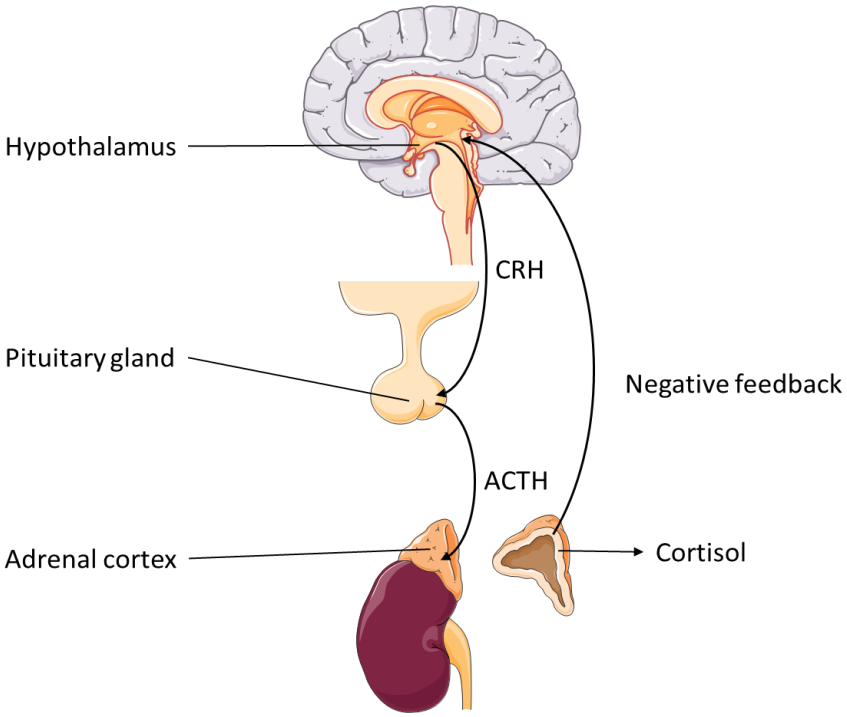

Fig. 8 The Hypothalamic-Pituitary-Adrenal axis. The regulatory feedback mechanism of the physiological cortisol production depends mainly on CRH made by the hypothalamus, which induces ACTH production, which again induces cortisol production in the fascicular zone of the adrenal gland. Adapted with kind permission from Medical Art by Servier (Servier 2018).

Once released into the blood stream, ACTH reaches the adrenal gland and stimulates the production of cortisol. Higher levels of cortisol on the other hand are able to reduce CRH secretion and in this manner form a negative feedback. Hence, the HPA axis can be identified as a regulatory circuit (Chrousos 1995).

Cortisol and its even stronger synthetic derivatives such as prednisolone and dexamethasone (DEX) show a potent attenuating effect on inflammatory processes (Adcock and Mumby 2017). This knowledge has been used quite successfully for many decades in medical routine in order to treat inflammatory diseases and process. GCs belong to the most widely prescribed medications and are also used in most cases of severe UC (Van Staa et al. 2000; Grandt et al. 2018; German S3-Guideline Ulcerative Colitis 2020).

1.6. Glucocorticoid Receptor

For a balanced homeostasis in the colon, in which there are no excessive immune reactions, the activity of GCs is crucial. Especially in cells directly affected by contact to microbiota such as epithelial cells, but also cells of the immune system, e. g. macrophages and T cells, this ability is of high importance (Artis 2008). To understand the effect of GCs on cells in an immunologically active state, one has to understand the interaction of the GR with its ligands and furthermore its interaction with different other cellular compounds.

According to our current knowledge, the GR consists of 4 domains, the N- terminal domain (NTD), the DNA-binding domain (DBD), a hinge-region and a ligand-binding domain (LBD) (Busillo and Cidlowski 2013; Oakley and Cidlowski 2013). In the cytoplasm, the monomeric GRs forms a complex with a variety of other proteins in the cytoplasm, such as heatshock-protein 90 (HSP90) or 70 (HSP70) and immunophilins (Cruz-Topete and Cidlowski 2015). GCs are highly lipophilic and therefore able to easily pass the cell membrane. Once in the cytoplasm, GCs bind to the ligand-binding domain of the GR which causes the GR-protein complex to disintegrate (Vandevyver et al. 2013). The GR with the bound GC will subsequently translocate into the nucleus with the help of importins and exert its effects via two major mechanisms.

In the DNA-binding dependent mechanism, the GR binds to GC-responsive-elements (GREs) in a dimerized form and activates transcription by allowing RNA polymerase II complexes to bind to DNA (Fig. 9). Alternatively, dimerized GRs bind to negative GREs (nGRE), which represses transcription (Surjit et al. 2011). Also, the DNA-binding dependent mechanism is possible with GR monomers linked to co-factors, so-called "composite GREs" (So et al. 2007). Depending on the co-factors, either activation or repression through binding to repressing elements (RE) on the DNA, not allowing the RNA polymerase II complex to properly connect to the DNA are characterized (Uhlenhaut et al. 2013).

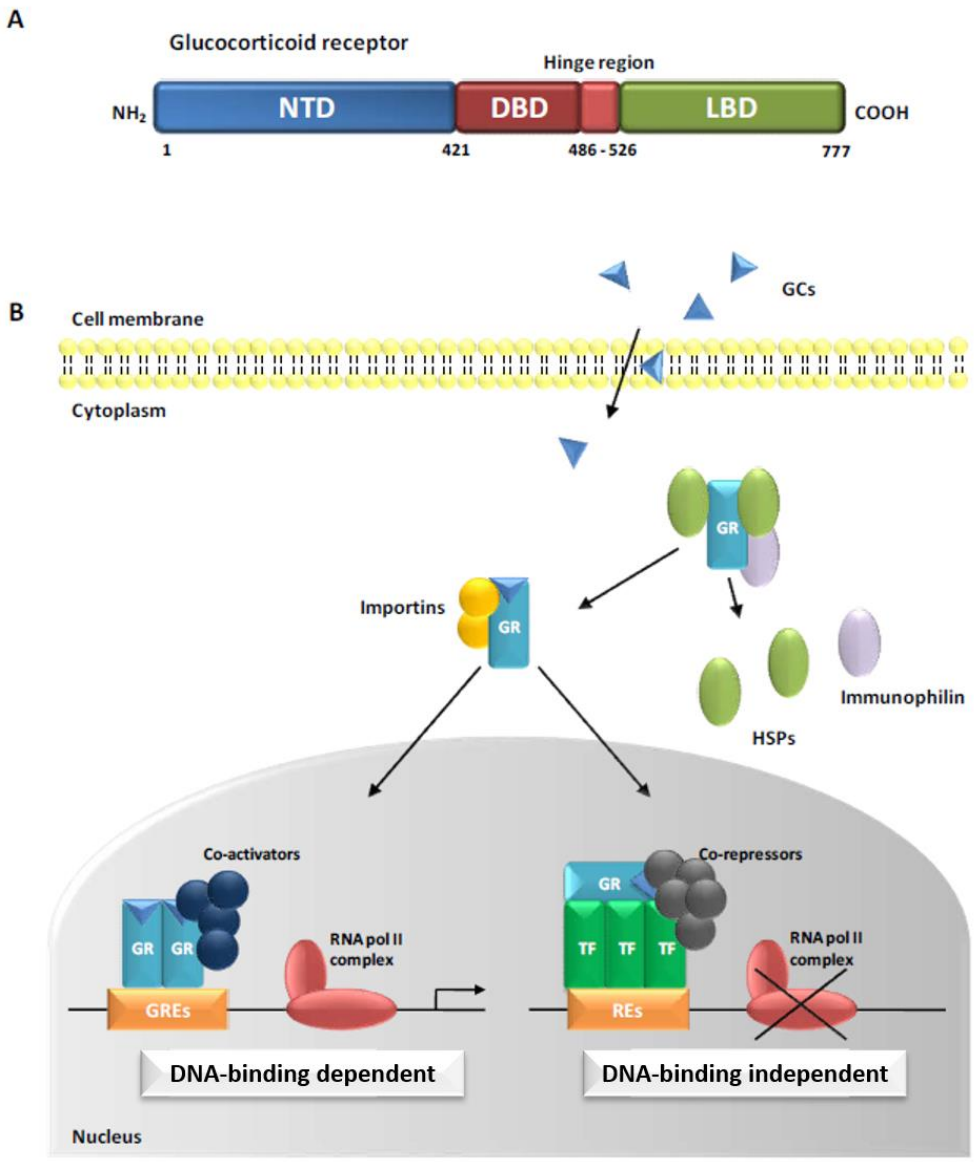

Fig. 9 The GR and its cellular interactions. The primary structure of the GR amino acid sequence with the N-terminal domain, the DNA- binding domain, the hinge-region and a ligand binding domain is shown in (A). After passing the cell membrane, GCs bind to dimerized or monomeric GR and thus promote the DNA-binding dependent or DNA-binding independent pathway (B). Adapted from Carina Klaßen (Klaßen 2016).

The DNA-binding dependent mechanism is opposed by the DNA-binding independent mechanism. In case of "tethering", in which monomeric GRs physically interact with co-factors, both activation and repression of transcription are possible, whereas it is assumed that in the case of "sequestration" and "competition" by monomeric GRs, only repression occurs (Vandevyver et al. 2013).

1.7. Murine Models of UC and CRC

1.7.1. DSS-Induced Colitis

Dextran Sodium Sulfate (DSS) is a complex branched poly-glucoside-polymer with linked sodium sulfate salts. Its size can vary between 5 and 500 kDa (kilodalton), depending on the number of branches (Perše and Cerar 2012). The ability to induce colitis in mice by oral administration of DSS was first described by Okayasu et al. (Okayasu et al. 1990). Even though its exact effects on the colon remain unclear, it serves as a reliable model to induce colitis. Most groups such as Melgar and colleagues propose an interplay of several mechanism (Melgar et al. 2005)(Melgar et al. 2005). Besides toxic effects of DSS on the epithelium, destruction of the mucin and modified functioning of macrophages are presumed. As Kitajima could show, DSS can be found in resident macrophages as well as in spleen and kidney briefly after treatment (Kitajima et al. 1998). Interestingly, in order to induce DSS colitis, the adaptive immune system is not required, as Dieleman and colleagues could illustrate by treating mice with combined immunodeficiency (Dieleman et al. 1994). Additionally, the presence of the resident microbiota seems to play an important role in the development of the disease (Säemann et al. 2000). Mice held under germ-free conditions do either develop a much less severe colitis or do not develop any colitis at all (Hudcovic et al. 2001; Kitajima and Morimoto 2001). It is being discussed whether the availability of medium-chain-length fatty acids produced by commensal bacteria is a crucial premise for the effect of DSS to be displayed (Laroui et al. 2012). Beside the conditions mentioned above, sex, mouse strain and breeding conditions seem to affect the susceptibility of DSS colitis to a large degree as well. In contrast to a normal dosage of 2 % (w/v) DSS in tap water, certain strains require a higher concentration. Male mice seem to have an increased susceptibility compared to females, while inbred mice demonstrated to be less responsive to DSS (Mähler et al. 1998).

In order to initiate the murine colitis model, DSS has to be administered to mice via drinking water. Apart from the achievement of a reliable model of acute colitis, a chronic colitis model has been established (Melgar et al. 2005). In both cases, the size of the DSS molecules play an important role. To obtain a severe colitis with the subsequent potential to proceed to cancer with the help of e. g. Azoxymethane (AOM), the treatment with 40 kDa DSS seems to bring the best results (Kitajima et al. 2000).

1.7.2. AOM/DSS-Induced CRC

In order to establish a reliable colitis-dependent carcinogenesis model, the group of Tanaka and colleagues developed a protocol on top of the DSS induced colitis, using AOM (Tanaka et al. 2003). AOM is a genotoxic colonic carcinogen, which needs to be activated enzymatically before it can exert its DNA-altering effect. Once converted, AOM serves as an electrophile, which can either react with free electron pairs, or bind to and react with the negatively charged parts of the DNA (Tanaka 2009). It is assumed, that the cumulative DNA-changing reactions cause various mutations within the DNA, which either get corrected by DNA-repairing enzymes, or transferred into daughter cells where the mutations can lead to aberrant cell growth. However, Suzuki and colleagues could show that AOM on its own does not induce CRC but rather depends on additional stimuli such as DSS to display its effect (Suzuki et al. 2005). After first injecting AOM intraperitoneally, the mice receive DSS for a period of at least 7 days, via the drinking water. Within the subsequent weeks, tumor growth is observed by colonoscopy and expected to peak around the 14th week after AOM injection. In this model, however, successful tumorigenesis required a minimum concentrations of 10 mg/kg body weight AOM and 2 % (w/v) DSS. The degree of tumor development depends on the dosage of the DSS administration (Suzuki et al. 2005; Snider et al. 2016).

1.7.3. Insights from Mouse Models

The DSS colitis murine model is a well-accepted disease model of UC in mice ever since it was implemented by Okayasu and colleagues in 1990 (Okayasu et al. 1990). Early on, immune cells and their role within inflammation but also potential pharmaceutical targets such as cytokines or the GR came into scientific focus. For example, in 1997, Kojouharoff and colleagues were able to show that monoclonal antibodies against TNF-α, but not against IL-1β, could reduce disease burden in mice (Kojouharoff et al. 1997). This observation is consistent with current clinical practice, where TNF-α antagonists such as Infliximab have been common therapy since 2006 (Rutgeerts et al. 2005; German S3-Guideline Ulcerative Colitis 2020). However, in contrast to observations in humans, Kojouharoff also described an exacerbation of acute colitis when DEX was administered, a finding that has not been well explained until now.

In 2011, Crielaard's group analyzed the role of macrophages polarization. It was assumed, that classically activated M1 macrophages have a pro-inflammatory activity, while

alternatively activated M2 macrophages rather regulate and resolve inflammatory events (Mosser and Edwards 2008; Mills 2012; van Dalen et al. 2018). However, Crielaard`s group could show, that macrophages being polarized into the M2 type were associated with exacerbated DSS colitis (Crielaard et al. 2011). This observation is in stark contrast to other inflammatory mouse models, such as the experimental autoimmune encephalitis model, in which this M2 polarization is beneficial. Contrary to expectations, it was observed that application of long-circulating liposomes with included DEX did not improve the disease but rather worsened it.

In 2018, Reichardt, Meers and colleagues demonstrated in mice with GR-deficient macrophages that the absence of the GR did not lead to a more severe disease burden but rather delayed disease resolution and impaired the recovery from colitis in mice. In addition, a higher numbers of macrophages was detected in inflammatory infiltrates (Meers et al. 2018).

Most recently, Zhang and colleagues revisited the paradoxical colitis observation of colitis exacerbation after DEX treatment, which arose in 1997. Here, they analyzed the effects of mTOR on the disease course of colitis and tumor burden of CRC in a DSS colitis and in a DSS/AOM CA-CRC model. They again demonstrated that the treatment with DEX both exacerbated colitis and increased the tumor burden in CRC. In contrast, deletion of mTOR in IECs attenuated the course of colitis and tumor burden (Zhang et al. 2020).

In order to assess the role of the GR in the development of colitis and CRC *in vivo*, it is crucial to be able to control its cell-type specificity and time point of deletion. Namely, it has been shown by Cole and colleagues, that a GR deficiency *in toto* is lethal to its subjects (Cole et al. 1995). Therefore, either the location of GR deficiency has to be reduced to the organ of interest using tissue-specific promoters as done by Reichardt S. and colleagues and Klaßen and colleagues (Reichardt et al. 2012; Klaßen et al. 2017). Or, alternatively, the GR itself has to be changed in a structural way, that allows a general disease-free survival of the organism until any experiment as done by Reichardt H. and colleagues (Reichardt et al. 1998). Once deleted or modified, the effects of the absent or modified GR on the course of colitis and CA-CRC can be analyzed.

Since IECs play a central role in the development of colitis and CA-CRC, $GR^{villinCreERT2}$ mice allow a targeted deletion of the GR exclusively in IECs of the colon and are therefore an ideal target for intervention. GR^{dim} mice exhibit a ubiquitous and constitutional inhibition of

GR dimerization and thus prevent the activating signaling cascade via binding to GREs, or a repressing signaling cascade via binding with to nGREs. These effects, being present in all nucleated cells of the organism, are less specific to one cell type but are no less interesting. Both models, $GR^{villinCreERT2}$ mice and GR^{dim} mice are promising candidates for assessing the role of the GR in inflammation and consecutive carcinogenesis.

1.8. Objectives

GCs are frequently used to treat UC and the development of colorectal carcinoma seems to be directly linked to the prevalence of UC. It is also known that the occurrence of CRC correlates with the severity and duration of UC which leads to the assumption, that early treatment of UC is strikingly important for the prevention of CA-CRC in affected patients in order to reduce the probability of tumor development.

In order to assess the role of the GR for the development and severity of UC and CRC *in vivo*, it is therefore crucial to be able to control its presence and features within the organism itself. The disease models described above allow controlling structure or availability of the GR and are therefore promising candidates to bring new perspectives and answers to the following three questions:

I. Which effects does a GR-deficiency in IECs have on the course of colitis in $GR^{villinCreERT2}$ mice?

II. Which effects does a GR-deficiency in IECs have on the course of CA-CRC in $GR^{villinCreERT2}$ mice?

III. Which effects does an impaired dimerization of the GR in all nucleated cells have on the course of colitis in GR^{dim} mice?

In the course of this study, these three questions were investigated and embedded into the current scientific discussion.

2. Material and Methods

2.1. Material

2.1.1. General Equipment

Table 2 General Equipment

Instrument	Model	Manufacturer
Anesthetic Machine	Perseus A500	Drägerwerk AG, Lübeck, Germany
Centrifuges:	Centrifuge 5804-R Centrifuge 2-5 Microfuge 5417R Minifuge Rotilabo Multifuge 4KR	Eppendorf, Hamburg Germany Sigma Laborzentrifugen, Osterode am Harz, Germany Eppendorf, Hamburg, Germany Intas, Göttingen Heraeus, Hanau Germany
Coloscope	HOPKINS multi-purpose rigid endoscope	Karl Storz, Tuttlingen, Germany
Electrophoresis Chamber Systems	40-1214	PEQLab Biotechnologie GmbH, Erlangen, Germany
Electrophoresis Power Supplies	EPS 301	Amersham Biosciences Europe GmbH, Freiburg, Germany
Gel Imager	UV system camera and gel imager	Intas GmbH, Göttingen, Germany
Immunowash	Nunc Immuno Wash 12	Thermo Scientific, Wilmington, DE, USA
Incubator	Hera Cell 240	Heraeus, Hanau Germany
Magnet	DynaMag 2	Life Technologies, Oslo, Norway
Microplate Reader	Spectrophotmeter Power Wave 340	BioTek Instruments, Bad Friedrichshall, Germany
Microscope	Light Microscope Primo Star Axio Scope A1	Carl Zeiss Microscope GmbH, Göttingen, Germany
Microtome	Leica SM2000R	Leica Biosystems, Wetzlar, Germany
Photometer	Nanodrop 2000	Peqlab Biotechnology, Erlangen, Germany
Pipettes:	Micropipette 0.1-2.5 µl, 2-20 µl, 20-200 µl and 200-1000 µl Research Multichannel Pipette S-12 20-200 µl	Eppendorf, Hamburg, Germany Brand, Wertheim, Germany
Real-Time PCR System	7500 Real-Time PCR	Applied Biosystems, Foster City, CA, USA
Scales:	Acculab ALC-3100.2 MC1 RC6011	Sartorius, Göttingen, Germany Sartorius, Göttingen, Germany
Shaker	GFL 3006	Gesellschaft für Labortechnik, Burgwedel, Göttingen
Sterile Bench	Hera Safe	Heraeus, Hanau, Germany
Thermocycler	Mastercycler EP Gradient	Eppendorf, Hamburg, Germany
Thermomixer	Comfort	Eppendorf, Hamburg, Germany
Tissue Embedding System	EG 1160	Leica Biosystems, Wetzlar, Germany
Tissue Processor	Excelsior ES	Thermo Scientific, Wilmington, DE, USA
Vaporizer	Dräger Vapor 2000	Drägerwerk AG, Lübeck, Germany
Vortex	Genie-2	Scientific Industries, Bohemia, NY, USA
Water Bath	W12	Labortechnik Medingen, Dresden, Germany
Water Purification System	Arium Pro	Sartorius, Göttingen, Germany

2.1.2. Consumables

Table 3 List of Consumables

Instrument	Model	Manufacturer
96-well Optical Reaction Plates		Applied Biosystems, Foster City, CA, USA
Cell Culture Plates	6-well, 24-well, 48-well flat bottom	Greiner bio-one GmbH, Frickenhausen, Germany
ELISA plates	Nunc Maxisorb flat bottom 96 well plate	eBioscience, San Diego, USA
Haemoccult Test		Beckman Coulter GmbH, Krefeld, Germany
Microscope slides	SuperFrost Plus	Menzel Glaeser, Braunschweig
Needles	24G 1”, 20G 1½”, 27G¾”, 25G 1”	B. Braun Melsungen AG, Melsungen, Germany
Optical adhesive covers		Applied Biosystems, Foster City, California, USA
Pasteur pipettes	3 ml	Th. Geyer GmbH, Renningen, Germany
Pipette tips	10 µL, 200 µL, 1000 µL	Greiner bio-one GmbH, Frickenhausen, Germany
Reaction tubes	PCR Tubes Multiply-µStrip Pro 8-Strip	Sarstedt, Nümbrecht , Germany
	1.5 ml, 2 ml, Safe-Lock	Greiner bio-one GmbH, Frickenhausen
	15 ml, 50 ml	Greiner bio-one GmbH, Frickenhausen
	12 ml Round Bottom	Greiner bio-one GmbH, Frickenhausen
	1,8 ml Cryotube Vials	Thermo Scientific, Copenhagen, Denmark
Syringes	1 ml	Henke Sass Wolf, Tuttlingen, Germany
	2 ml, 5 ml, 60 ml	BD Biosciences, Heidelberg, Germany
Serum separation tubes	STT BD Microtainer	BD Biosciences, Franklin Lakes, USA
Tissue cassettes	MacrOFlow	Microm International, Waldorf

2.1.3. Chemicals and Reagents

Table 4 Chemicals and Reagents

Chemical/Reagent	Manufacturer
5x Phusion Reaction Buffer HF with 7.5 mM Magnesium Chloride	Genaxxon Biosciences, Ulm, Germany
Agarose Ultrapure	Invitrogen, Carlsbad, CA, USA
Azoxymethan	Sigma-Aldrich, Taufkirchen, Germany
Chloroform	Sigma-Aldrich, Taufkirchen, Germany
Dexamethasone (Dex) Dexa-Ratiopharm Injection Solution	Ratiopharm, Ulm, Germany
Dextran Sulfate Sodium Salt 36 – 50 kDa	MP Biomedicals, LLC, Illkirch, France
dNTP Mix PCR	Genaxxon Biosciences, Ulm, Germany
Ethanol	Carl Roth, Karlsruhe, Germany
Ethidium Bromide Solution	Carl Roth, Karlsruhe, Germany
Fetal Bovine Serum (FBS)	Invitrogen, Carlsbad, CA, USA
Generuler DNA Ladder 1 kb	Fermentas, St.-Leon-Rot, Germany
Glycerol	Carl Roth, Karlsruhe, Germany
Hemalum Solution Acid acc. to Mayer	Carl Roth, Karlsruhe, Germany
Hydrogen Peroxide 30%	Carl Roth, Karlsruhe, Germany
Orange G Sodium Salt	Sigma-Aldrich, Taufkirchen, Germany
Paraffin Wax for Histology	Sigma-Aldrich, Taufkirchen, Germany

Chemical/Reagent	Manufacturer
PfuS DNA Polymerase	own Production
Protease Inhibitor Cocktail	Sigma-Aldrich, Taufkirchen, Germany
Proteinase K	AppliChem, Darmstadt, Germany
Qiazol lysis reagent	Qiagen, Hilden, Germany
Sulfuric Acid	Merck, Darmstadt, Germany
Tamoxifen Free Base	Sigma-Aldrich, Taufkirchen, Germany
Tween-20	Carl Roth, Karlsruhe, Germany
Wash Buffer EnVision Flex	Agilent, Santa Clara, CA, USA
Sevofluran	AbbVie Deutschland GmbH, Ludwigshafen, Germany

2.1.4. Commercial Assays

Table 5 Commercial Assays

Assay	Manufacturer
iScript cDNA Synthesis Kit	BioRad, München, Germany
Mouse IL-1b ELISA MAX Standard Set	BioLegend, San Diego, CA, USA
Mouse IL-6 ELISA MAX Standard Set	BioLegend, San Diego, CA, USA
Mouse TNF-α ELISA MAX Standard Set	BioLegend, San Diego, CA, USA
Power SYBR-Green PCR Mastermix	Applied Biosystems, Foster City, CA, USA
RNeasy Plus Universal Kit	Qiagen, Hilden, Germany
Poly A Dynabeads mRNA direct kit	Thermo Scientific, Vilnius, Lithuania

2.1.5. List of Antibodies for ELISA

Table 6 List of Antibodies for Immunohistochemistry

Specificity	Clone	Isotype	Manufacturer
CD3	SP7	Rabbit IgG	Abcam
CD68	FA-11	Rat IgG2a	Abcam
GR1	Ly-6G / Ly-6C	Rat IgG2b, κ	BD Biosciences
GR	M-20	Rabbit IgG	Santa Cruz Biotechnology

2.1.6. Oligonucleotides

Table 7 List of Oligonucleotides

Target Gene		Sequence
HPRT	Fwd	5’ GTC CTG TGG CCA TCT GCC TA 3’
	Rev	5’ GGG ACG CAG CAA CTG ACA TT 3’
TNF-α	Fwd	5’ ATG GCC TCC CTC TCA TCA 3’
	Rev	5’ CTT GGT GGT TTG CTA CGA 3’
IL-1b	Fwd	5’ CTC ATC TGG GAT CCT CTC CA 3’
	Rev	5’ AAG CAG CCC TTC ATC TTT TG 3’
IL-6	Fwd	5’ AGT TGC CTT CTT GGG ACT GA 3’
	Rev	5’ CAG AAT TGC CAT TGC ACA AC 3’
CD-163	Fwd	5’ GAA GCC CAC AAA GAA AGC TG 3’
	Rev	5’ TGC ACA CGA TCT ACC CAC AT 3’

Target Gene		Sequence
IL-10	Fwd	5' AGG CAG AGA AGC ATG GCC CAG 3'
	Rev	5' CGG GAG AAA TCG ATG ACA GCG CC 3'
F4/80	Fwd	5' ACC CTC CAG CAC ATC CAG 3'
	Rev	5' TCA CAG CCC GAG GGT GTC 3'
CXCL-1	Fwd	5' ACC GAA GTC ATA GCC ACA GTC 3'
	Rev	5' CTC CGT TAC TTG GGG ACA CC 3'
CXCL-3	Fwd	5' CTT CAT CAT GGT GAG GGG CTT 3'
	Rev	5' CCA GAC AGA AGT CAT AGC CAC 3'
CXCL-5	Fwd	5' TGC CCT ACG GTG GAA GTC AT 3'
	Rev	3' AGC TTT CTT TTT GTC ACT GCC C 3'
CCL-2/MCP-1	Fwd	5' AGC TGT AGT TTT TGT CAC CAA GC 3'
	Rev	5' GAC CTT AGG GCA GAT GAT GCA GT 3'

2.1.7. Software

Table 8 Software

Software	Developer
GraphPad Prism for Windows v5.04	GraphPad Software, La Jolla, CA, USA
ImageJ 1.52n	Wayne Rasband Nat. Inst. Of Health, USA
analySIS	Olympus, Tokio, Japan
Gen 5 1.09.8	BioTek Instruments, Bad Friedrichshall, Germany
Primer-Blast Software	http://www.ncbi.nlm.nih.gov/tools/primerblast/
Microsoft Office 2007 and 2010	Microsoft, Redmond, WA, USA
Nanodrop 2000 Software	Thermo Scientific, Wilmington, DE, USA
Mendeley Desktop 1.17.8	Mendeley Ltd., Oxford, UK
Coloscope	Karl Storz, Tuttlingen, Germany
7500 System SDS Software 1.4.0.25	Applied Biosystems, Foster City, CA, USA
OlyVIA 2.4	Olympus, Tokio, Japan
Ilastik 1.3.2	Niels Buwen, Christopher Decker, Kemal Eren

2.1.8. Buffers and Solutions

Table 9 Buffers and solutions

Buffer or solution	Composition	
ELISA Assay Diluent	10 % FCS	In PBS
ELISA Carbonate coating buffer pH 9,5	0,1 M Na_2CO_3	In ddH_2O
ELISA Substrate Buffer	0,1 M Citric Acid	
	0,2 M Na_2PO_4	In ddH_2O
ELISA Developing Solution	Substrate Buffer 1 % TMB in DMSO 0,2% H_2O_2	
Phosphate Buffer Saline pH 7,4 (PBS)	137 mM NaCl 2,7 mM KCl 10 µM Na_2PO_4 2,0 mM KH_2PO_4	In ddH_2O
PBS/BSA	0,1 % BSA	In PBS
PBS/Tween	0.1% Tween 20	in PBS

Buffer or solution	Composition	
Tris-buffered saline pH 7,2 (TBS)	150 mM NaCl 10 mM Tris 1 mM HCl	In ddH_2O
TBS-Tween	0,1% Tween 20	In TBS

2.1.9. Media

Table 10 Media

Media	Composition
RPMI 1640	
RPMI 1640^{++}	10 % FBS 1 % Penicillin/Streptomycin 500 ml RPMI

2.2. Methods

2.2.1. Animal Experimentation

All experiments were performed according to the German Animal Welfare Act and approved by the Lower Saxony State Office for Consumer Protection and Food Safety (LAVES). All mice were held and bred under pathogen-free (SPF) conditions at the central animal facility at Göttingen University Medical Center (ZTE). They were housed in individually ventilated cages (IVC) with a 12 hour day/night cycle with water and feed at free disposition. The age of mice used for experiments was at least 10 weeks.

2.2.2. Mouse Strains

The DSS-induced UC model was established in two different mouse strains. GR^{dim} mice provide a model for a sterically modified GR while $GR^{villinCreERT2}$ mice provide a model for the lack of the GR in epithelial cells. The latter was also used as a model for colitis-associated CRC.

2.2.3. GR^{dim} Mice

$Nr3c1^{tm3GSc}$ mice on a BALB/c background, in the following denominated as GR^{dim} mice, are genetically modified and characterized by a single point mutation in the DBD of the GR gene. This mutation has been inserted by homologous recombination of murine embryonic stem cells (Reichardt et al. 1998). The mutation constitutively compromises dimerization of

the GR by replacing alanine with threonine (A458T) in the D-loop of the second Zinc-finger (Fig. 10). Consequently, dimerization and DNA-binding are impaired. The GR^{dim} mutation is present in all somatic and germ cells of the mice. GR^{wt} (Nr3c1) mice were used as controls.

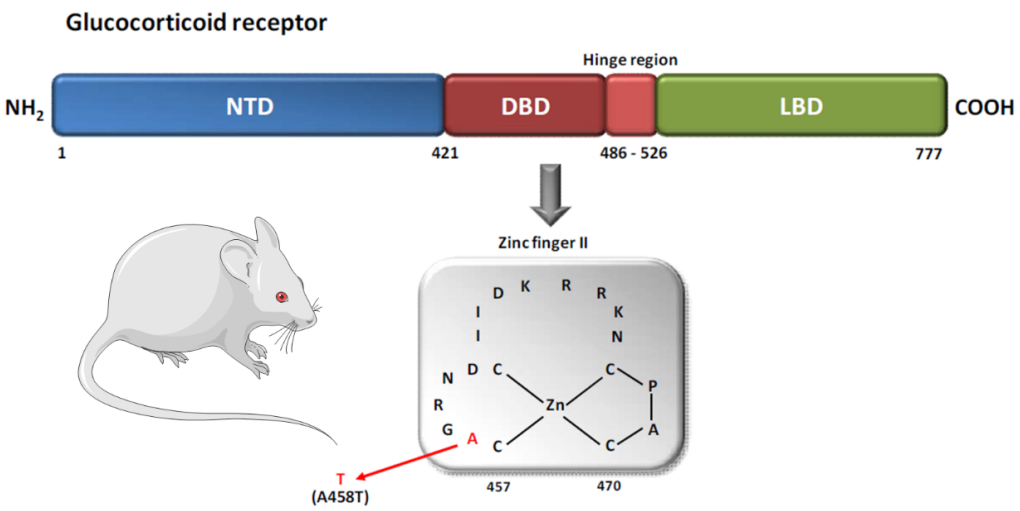

Fig. 10 Modified GR in GR^{dim} mice. By replacing alanine with threonine at position 458, the GR in GR^{dim} mice is altered in its tertiary structure and therefore promotes the transrepressing pathway instead of the transactivation pathway. Adapted from Holger Reichardt with images from Servier Medical Art. (Servier 2018) and (Reichardt et al. 1998).

2.2.4. $GR^{villinCreERT2}$ Mice

In order to obtain $GR^{villinCreERT2}$ mice, Villin-Cre^{ERT2} mice (Tg(Vil1-cre/ERT2)23Syr) and GR^{flox} ($Nr3c1^{tm2GSc}$) mice on a C57BL/6 background were intercrossed. This cross-breeding educed $GR^{villinCreERT2}$ mice ((Nr3c1tm2GSc;Tg(Vil1-cre/ERT2)23Syr) und GR^{flox} mice as littermate controls (el Marjou et al. 2004). The $GR^{villinCreERT2}$ mouse model allows the specific deletion of the GR in IECs through a tamoxifen-inducible Cre/loxP recombination system (Tronche et al. 1999). The villin gene is predominantly expressed in the epithelial cells of the gut and colon. In Villin-Cre^{ERT2} mice a Cre-recombinase is expressed under the control of the villin promoter. Thus, GR deletion is limited to these specific cells (Fig. 11) (Reichardt et al. 2012; Stremmel et al. 2017). Mice of both sexes, at the age of 10 – 12 weeks were included in the experiments.

2.2.5. Induction of Recombination by Tamoxifen Treatment

Prior to any colitis experiments performed with $GR^{villinCreERT2}$ mice, they were treated with tamoxifen. Tamoxifen powder dissolved in ethanol 70 % (w/w) was subsequently stirred and warmed to 37 °C in a 1:30 ratio in sunflower seed oil. A dosage of 150 µl tamoxifen-oil dispersion at a concentration of 20 mg/ml was administered to each mouse by oral gavage ten, seven and four days before the start of the experiment.

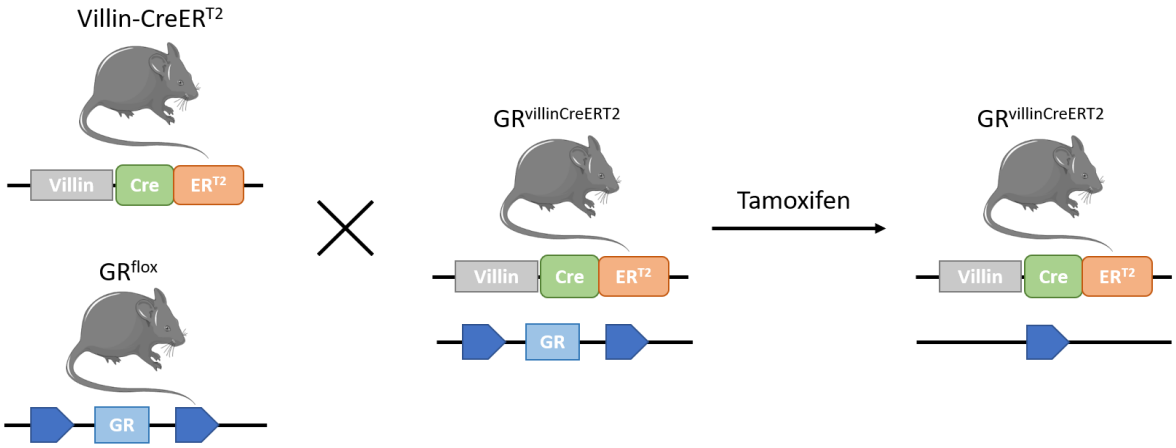

Fig. 11 Induction of recombination by tamoxifen treatment. By inter-crossing Villin-CreER^{T2} with GR^{flox} mice, the offspring provided a tamoxifen-inducible, villin-dependent Cre-recombinase system that specifically allows deleting the GR gene in IECs. Thus, expression of the GR in epithelial cells is impeded. Adapted from Carina Klaßen with pictures of Servier Medical Art (Klaßen 2016; Stremmel et al. 2017; Servier 2018).

2.2.6. Clinical Scoring of DSS-Colitis

To simulate human colitis, a murine model first described by Okayasu and colleagues (1990) was used. Colitis was induced with Dextran-Sodium-Sulfate (DSS), a polysaccharide with a molecular weight between 5 kDa and 500 kDa (Perše and Cerar 2012). Throughout every experiment, the progression of the acute DSS-induced colitis had to be monitored in every mouse. For that purpose, the Disease Activity Index (DAI) score was implemented. The DAI is a standardized rating score, used by many groups working with murine DSS colitis models (Vagnerová et al. 2006; Hunter et al. 2010; Hamers et al. 2015). It includes body weight loss, a haemoccult score and stool consistency as shown in table 11.

Table 11 DAI Score

Weight/ initial weight (%)	score
100 – 99	0
99 – 95	1
95 – 90	2
90 – 80	3
80 – 70	4

Blood appearance	score
No haemoccult reaction	0
Mild/green reaction	1
Strong/blue reaction	2
Visible blood in stool	3
Visible blood in stool and anus	4

Consistency	score
Normal	0
Soft	1
Liquid/ diarrhoeic	2

Every parameter was measured daily and added up to receive the total DAI score. Individuals with a weight loss exceeding 20 % of their initial weight had to be removed and sacrificed due to ethical standards defined by LAVES.

2.2.7. DSS Colitis in GR^{villinCreERT2} Mice

To induce DSS-colitis in GR^{villinCreERT2} mice, 1.2 % (w/v) DSS was added to the drinking water for eight days and changed every other day. During a subsequent recovery time of four days, mice received pure tap water (Fig. 12). To eliminate the GR in IECs of GR^{villinCreERT2} mice using tamoxifen-induced gene recombination, all mice including the GR^{flox} mice that served as a control group had to be treated with tamoxifen prior to the experiment as described above. All mice were evaluated with the DAI score on a daily basis, starting on the third day.

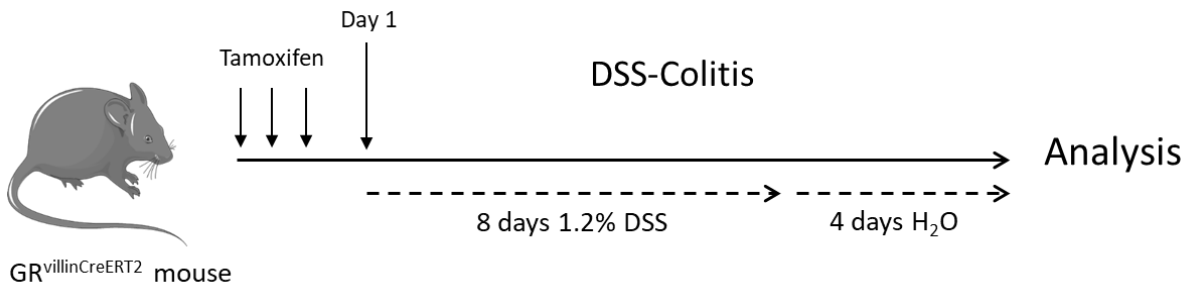

Fig. 12 Protocol illustrating the induction of DSS-colitis in GR^{villinCreERT2} mice. After the induction of recombination by tamoxifen treatment by oral gavage at day 10, 7 and 4 prior to the experiment, eight days of 1.2 % DSS followed by four days of normal tap water was performed. Mice were then sacrificed and analyzed. Own image with pictures of Servier Medical Art (Servier 2018).

2.2.8. DSS Colitis in GR^{dim} Mice

DSS-colitis in GR^{dim} mice was induced similarly to GR^{villinCreERT2} with the difference, that no tamoxifen treatment was necessary. Furthermore, GR^{dim} mice coped far better with the DSS-treatment for which reason a higher DSS concentration (3.5 % w/v) was required for disease development. After eight days of DSS treatment and continuous weighing and scoring, the DSS drinking water was exchanged by normal tap water (Fig. 13). The mice were sacrificed on day 10 after 2 days of recovery.

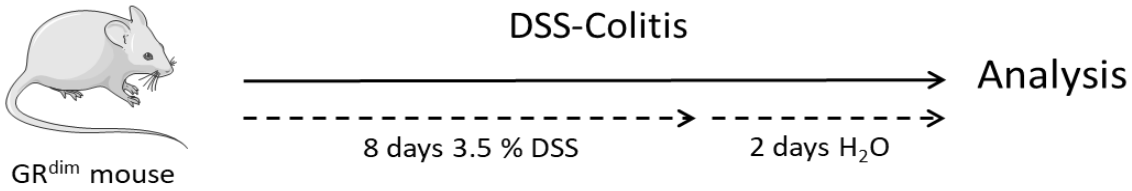

Fig. 13 Protocol illustrating the induction of DSS-colitis in GR^{dim} mice. The experiment was performed by providing eight days of 3.5 % (w/v) DSS drinking water followed by two days of DSS-free tap water. The mice were subsequently sacrificed and analyzed. Own image with pictures of Servier Medical Art (Servier 2018).

2.2.9. Induction of AOM-Induced Colorectal Carcinoma

The development of colorectal cancer in the murine model was achieved by performing the standard DSS-colitis protocol plus an intraperitoneal injection of 10 mg/kg AOM at day 1 (Fig. 14). Beginning at week 6, a weekly colonoscopy was conducted in order to monitor the tumor growth.

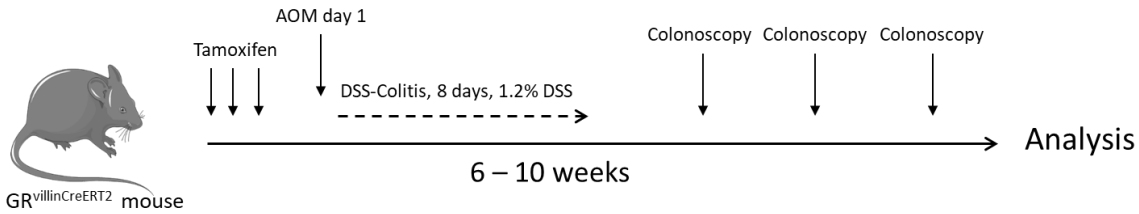

Fig. 14 DSS-induced colitis and AOM-induced Colorectal Carcinoma. After the induction of recombination by tamoxifen-treatment by oral gavage at day 10, 7 and 4 prior to the experiment, an initial intraperitoneal AOM injection followed by eight days of 1.2 % DSS was performed. After the acute phase of colitis, colonoscopy was performed beginning at week 6. Mice were sacrificed as soon as they showed S 3 tumors. Own image with pictures of Servier Medical Art (Servier 2018).

2.2.10. Anesthesia

Before performing the controlling colonoscopy, all mice were anaesthetized with volatile Sevoflurane, which was applied through addition to the oxygen-flow with the help of a vaporisator. After a pre-anesthesia at a dosage of 5 Vol-% Sevoflur in a casket, each mouse was anaesthetized through a snout mask at 2.5 Vol-% during colonoscopy.

2.2.11. Colonoscopy

Colonoscopy was performed in order to monitor the tumor growth between week 6 and 8 after AOM injection. The aim was to find the time point at which the mice had sufficiently grown tumors, while preventing excessive size or even the occurrence of an obstructive ileus leading to the death of a mouse. The mouse to be examined was fastened on its back while its snout remained in the anesthesia mask. Before examination, the rectum of the mouse was flushed with H_2O to remove potential stool residues. The colonoscope, 10 cm in length, 1.9 mm in diameter was moistened with H_2O. A continuous air flow allowed an unobstructed view on the colon mucosa, by slightly inflating the colon. With this technique, respecting natural peristalsis, the whole descending colon up to the left flexure could be inspected and checked upon tumors. Tumors were then categorized by their size, depending on how many quadrants of the colon intersection they occupied. As shown in Figs. 15 and 16, tumors of individual mice with a positive finding were categorized into five different stages (S1 - S5).

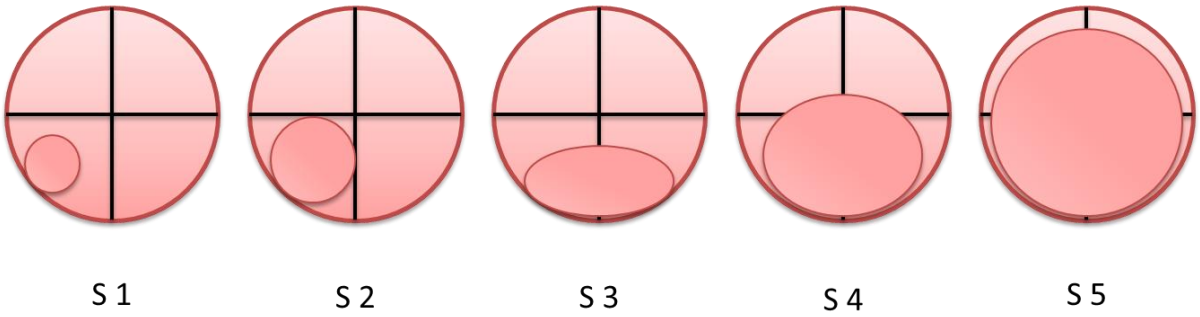

Fig. 15 Schematic representation of the different stages of Tumor Progression. Findings were divided into 5 different stages. S 1 corresponds to small but visible polyp in one quadrant, S 2 fills a whole quadrant, while S 3 extends over 2 quadrants. S 4 reaches over all quadrants and S 5 occludes the colon. Own images.

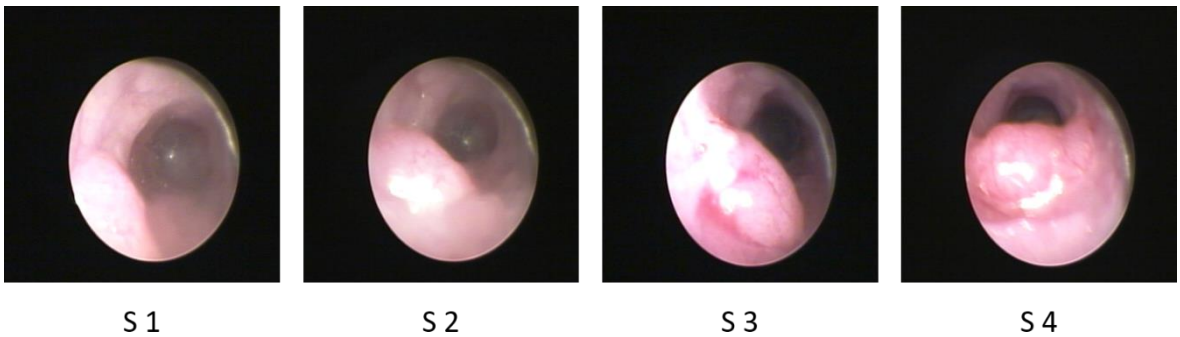

Fig. 16 Stages of Tumor Progression identified by Colonoscopy. Picture taken during colonoscopy of tumor stages 1 to 4. Own Images.

A S 1 category indicates that less than one quadrant was affected while S 2 rated tumors fill a whole quadrant. S 3 rated tumors span two quadrants while S 4 rated tumors can bridge

three or more quadrants. S 5 rated tumors occlude most of the lumen. All mice were sacrificed when tumors of the category S 3 were detected by colonoscopy in at least one animal.

2.2.12. Sample Collection

During colitis, the colon is the organ providing the most valuable information. Besides that, blood can be analyzed for chemokine and cytokine concentrations during inflammatory events. Both organs were collected and analyzed concerning their levels of pro- and anti-inflammatory markers. The colon was additionally macro- and microscopically examined with respect to oncogenic events.

2.2.13. Blood Preparation

Mice were sacrificed by CO_2 inhalation. Blood was collected by heart puncture and transferred immediately to serum separation tubes (Microtainer) containing EDTA to prevent coagulation. After 30 min of rest, the tubes were centrifuged at 20,000 rcf for 2 min. The supernatant was then transferred to 1.5 ml reaction tubes and stored at -20° C until further analysis.

2.2.14. Isolation of the Colon

Mice were sacrificed by CO_2 inhalation and the colon of each mouse was then removed. In order to conserve an intact colon, the rectum was removed generously including the exterior sphincter around the circum-perineal region. From there up to the ileocecal valve the colon was isolated, measured in length and immediately perfused with approximately 10 ml PBS to remove remaining feces. The colon was then further prepared either for gene expression analysis by quantitative reverse transcription polymerase chain reaction (qRT-PCR), cytokine quantification via enzyme-linked immunosorbent assay (ELISA) or histological evaluation. For subsequent analysis by qRT-PCR, three additional pieces of the colon, each 5 mm in length, were obtained per colon section and preserved in 2 ml tubes at -80 °C until further processing.

2.2.15. Colon Preparation for ELISA Analysis

To obtain samples for cytokine analysis, the clean colon was dissected into 3 equal parts. Each part, proximal, medial, and rectal, provided one piece of approximately 5 mm length. The pieces were placed into 48-well plates each well containing 500 µl of RPMI/FCS pen/strep media (Fig. 17). After a 24 h incubation time, all pieces and remnants were removed from the wells and left to dry for 24 h at 37 °C. The media left in the wells was used for ELISA analysis or stored at -20 °C. All dried pieces were weighed to be able to refer the cytokine levels to the weight of the tissue of origin.

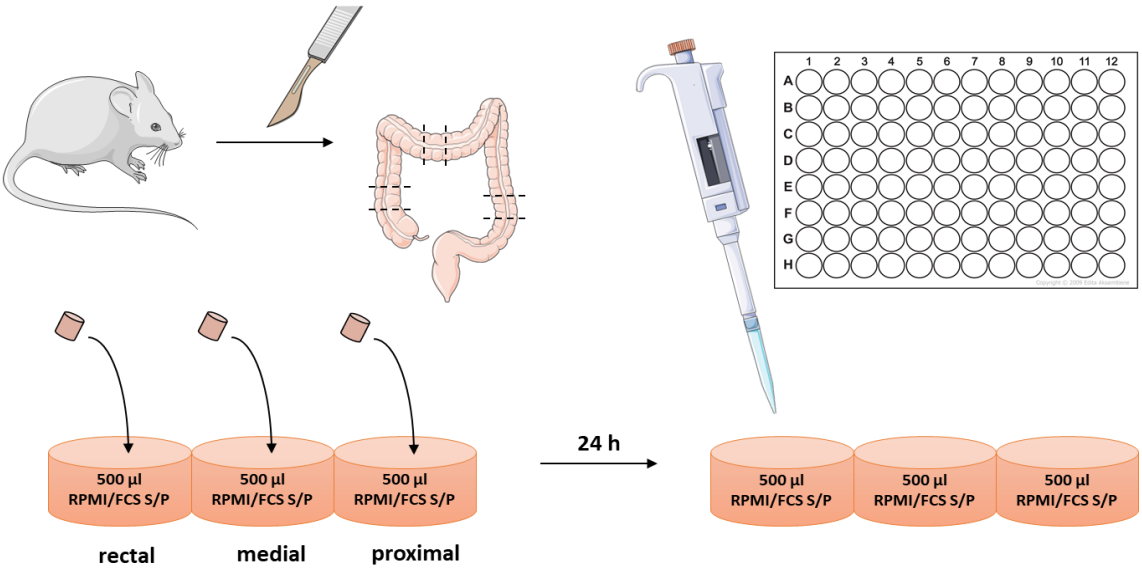

Fig. 17 Sample preparation of the colon. After dissection of the colon, one piece of the rectal, medial, and proximal part each was put into media and incubated for 24 h at 37 °C. The media was subsequently used for ELISA analysis. Own image with pictures of Servier Medical Art (Servier 2018).

2.2.16. Histological Examination using Swiss-roles

For histological examination, a technique called "Swiss-role" was performed. The whole colon was opened longitudinally, fixed on a moistened Whatman paper and subsequently rolled up from the rectal to the proximal end as tightly as possible. The role was then put into a tissue cassette and left for fixation in 4 % PFA for 24 h. In order to retrace certain positions of the tumors, a standard orientation had to be maintained by putting the colon role onto its left edge.

2.2.17. Enzyme-Linked Immunosorbent Assay (ELISA)

To quantify the secretion of certain cytokines such as TNF-α, IL-1β or IL-6, a standard ELISA was performed, using commercial kits and following the manufacturer's instructions. Flat-bottomed 96-well optical plates were coated over night with 100 µl capturing antibodies (1:200 dilution in coating buffer) at 4° C. The next day all wells were washed several times with PBS/Tween and blocked using 200 µl Assay Diluent (AD) for 1 h at room temperature (RT) on a shaker. After a second washing step, 100 µl of a serial dilution standard, provided with the kit, and samples were loaded in triplicates and duplicates, respectively, and incubated for 2 h at RT on a shaker. The third washing step was followed by the addition of the detection antibodies (1:200 in AD) and an incubation of 1 h at RT on a shaker. After the fourth washing step, Horse Radish Peroxidase (HRP, 1:1,000 in AD) was added and the solution incubated for another 30 min at RT on a shaker. Finally, after the last washing step, 100 µl of TMB substrate solution were added. The plate was left in the dark for 20 min until the color of the solution changed from transparent to blue. The reaction was stopped using 100 µl of 2N H_2SO_4. Subsequently, the absorbance was measured at 450 nm and 570 nm using a spectrophotometer. Finally, the concentration of the cytokines could be calculated by interpolation of the absorbance values of the standard dilutions.

2.2.18. RNA Isolation

The RNA from colon samples was isolated using the RNeasy plus Universal Kit (Quiagen) by homogenizing the tissue in 900 µl of Quiazol with an Ultra Turrax mixer. Afterwards, 100 µl of DNA Eliminator and 180 µl of chloroform were added, thoroughly vortexed and centrifuged at 20,000 rcf at 4° C for 15 min. 600 µl of the upper phase were then mixed with the same amount of 70 % EtOH and filled into an RNA separation column. After centrifuging for 20 s at RT, 700 µl of RWT buffer were added and the reaction tubes were centrifuged again for 20 s. This process was repeated with 500 µl of RPE buffer at 20,000 rcf for 2 min. After a dry spin, the RNA was eluted by adding 70 µl of RNase free water and centrifuging for 1 min at 20,000 rcf. Subsequently, the RNA concentration was measured with the Nanodrop device and its purity confirmed by running the RNA preparations on a 1 % agarose gel. The RNA was then used for further processing or stored at -20° C.

2.2.19. PolyA mRNA Isolation

This step of isolating mRNA has been added to the standard procedure in order to eliminate any remaining DSS from the RNA preparations. DSS interferes with DNA polymerase and therefore must be removed before performing any quantitative reverse transcription PCR (qRT-PCR) analysis (Kerr et al. 2012). This can be achieved using the Dynabeads mRNA Purification Kit. 75 µg total RNA was adjusted with DEPC-treated water to a volume of 100 µl, heated at 65° C for 2 min before adding 100 µl of calibrated Dynabeads in binding buffer. The RNA/Dynabeads suspension was then left for annealing on a shaker for 10 min. Subsequently, the reaction tubes were placed on a magnet, where the supernatant got removed and the mRNA-bead complex washed 3 times with 200 µl. After discarding the remaining liquid, 20 µl of Tris-HCL, pH 7.5 were finally added. To elute the mRNA, the suspension was heated at 80 °C and placed on the magnet immediately. The eluted mRNA was transferred to an RNase-free tube. Its concentration was measured with the Nanodrop device. The mRNA was used for reverse transcription or stored at -20 °C.

2.2.20. Synthesis of cDNA

The previously isolated mRNA was reverse transcribed into cDNA for qRT-PCR with the help of the iScript kit. 5 µl of mRNA were mixed with 0.25 µl Reverse Transcriptase, 4 µl of iScript buffer were added and the volume adjusted to 20 µl. The synthesis of the cDNA was achieved with a 3-step incubation program in a thermomixer:

Table 12 Synthesis of cDNA, Protocol

Time	Temperature	Action
5 min	RT	Annealing
30 min	42 °C	Reverse Transcription
5 min	85 °C	Denaturation of Reverse Transcriptase

2.2.21. Polymerase Chain Reaction (PCR)

To verify successful cDNA synthesis, a test PCR was conducted. 4 µl of High-Fidelity buffer, 1 µl dNTPs, 1 µl of 10 µM reverse and forward Primer Mix of the housekeeping gene hypoxanthine phosphoribosyl transferase (*Hprt*), 1 µl of PfuS polymerase, and 1 µl of the template were mixed and filled up to 20 µl with ddH_2O. The amplification product was visualized by performing a gel electrophoresis using a 1.5 % agarose gel. The product

appeared as a definable band while ddH_2O was used as negative control to exclude contaminations.

Table 13 PCR Program

Time	Temperature	Action	
1 min	98.5 °C	Activation	
20 s	98.5 °C	Denaturation	30 X
15 s	64 °C	Annealing	
20 s	72 °C	Elongation	
2 min	72 °C		

2.2.22. Quantitative Reverse-Transcription PCR

A qRT-PCR reaction was performed in order to quantify expression levels of certain mRNAs using the Power SYBR Green Kit (Applied Biosciences).

qRT-PCR reaction mix:

1 µl cDNA
12.5 µl SYBR Green
11 µl ddH_2O
0.5 µl of 10 µM Primer mix

Table 14 Quantitative reverse transcription PCR Program

Time	Temperature	Action	
2 min	50 °C	Activation	
10 min	95 °C	Denaturation	
15 s	95 °C	Denaturation	40 X
1 min	60 °C	Annealing + Elongation	
15 s	95 °C		
1 min	60 °C	Dissociation stage	
15 s	95 °C		

Gene expression was calculated with the method of relative quantification by referring the expression level of the target gene to the expression level of the housekeeping gene *Hprt* as an endogenous control. The ΔΔCt method was used for data analysis.

2.2.23. Histology

All histological analyses were carried out in collaboration with Dr. Hanibal Bohnenberger at the Institute for Pathology of the University Medical Center Göttingen.

2.2.24. Isolation and Fixation of Colon "Swiss-role"

Dehydration of the fixated specimens was performed using a Thermo Scientific Excelsior ES system with the following steps:

Table 15 Histological dehydration

Reagent	Time
4 % PFA	1:15 h
Ethanol 70 %	0:30 h; 0:45 h
Ethanol 96 %	1:00 h; 1:15 h
Ethanol 100 %	1:10 h; 1:30 h
Xylol	0:20 h; 0:30 h; 1:00 h
Paraffin	0:30 h; 0:45 h; 1:30 h

The dehydrated and fixed Swiss-roles of the colon were embedded in paraffin maintaining their left-edge-down orientation. 2 µm sections of the desired regions were cut with help of a microtome for subsequent staining and immunohistochemistry. In case of proving a tumor free specimen, 2 µm sections were cut in 200 µm steps throughout the whole colon role.

2.2.25. Hematoxylin and Eosin Staining of Colon Tissue

For a broad overview of the sections, a Hematoxylin and Eosin (HE-) staining was performed following these steps:

Table 16 HE-staining, Protocol

Reagent	Time
Drying	10:00 min
Xylol	2:30 min; 2:30 min
Ethanol 100 %	1:00 min
Ethanol 95 %	1:00 min
Ethanol 70 %	1:00 min
ddH_2O	1:00 min
Hematoxylin (Meyer's)	6:00 min
HCl Ethanol	0:05 min
ddH_2O	8:00 min
Eosin	3:00 min
ddH_2O	0:15 min
Ethanol 70 %	0:30 min
Ethanol 95%	1:30 min
Ethanol 100 %	2:00 min
Xylol	2:00 min

Hematoxylin stains acid components of the cell such as the nucleus displaying a violet color (Fig. 18A). Eosin stains alkaline components of the cell, mostly the cytoplasm in red color.

2.2.26. Periodic acid-Schiff (PAS) Staining of Colon Tissue

PAS Staining was used to depict degraded colon mucosa after DSS colitis (Fig. 18B). The staining visualizes mucopolysaccharides found in the glycocalyx and mucus of the mucosa. Particularly goblet cells can be clearly identified with this method. The staining protocol was performed with the following steps:

Table 17 PAS-staining, Protocol

Reagent	Time
Drying	10:00 min
Xylol	2:30 min; 2:30 min
Ethanol 100 %	1:00 min
Ethanol 95 %	1:00 min
Ethanol 70 %	1:00 min
ddH_2O	1:00 min
Periodic Acid	5:00 min
ddH_2O	1:00 min
Schiff's	15:00 min
ddH_2O	5:00 min
Hematoxylin (Meyer's)	3:00 min
ddH_2O	5:00 min
Ethanol 70 %	0:30 min
Ethanol 95 %	1:30 min
Ethanol 100 %	2:00 min
Xylol	2:00 min

2.2.27. Masson's Trichrome Staining of the Colon Tissue

Masson's Trichrome Staining was performed to illustrate and differentiate immunological infiltrations and plaques (Fig. 18C). The recipe colors muscle fibers and keratin red, collagen and bone green, whereas the cytoplasm is colored pink and the cell nuclei colored dark. The protocol was performed in the following steps:

Table 18 Masson's Trichrome staining, Protocol

Reagent	Time
Drying	10:00 min
Xylol	2:30 min; 2:30 min
Ethanol 100 %	1:00 min
Ethanol 95 %	1:00 min

Reagent	Time
Ethanol 70 %	1:00 min
ddH_2O	1:00 min
Weigert's B solution	10:00 min
ddH_2O	1:00 min
Hematoxylin solution	10:00 min
ddH_2O	1:00 min
Beibrich scarlet-acid fuchsin	2:00 min
ddH_2O	1:00 min
Phosphomolybdic acid	12:30 min
ddH_2O	1:00 min
Aniline blue	10:00 min
ddH_2O	1:00 min
Ethanol 70 %	0:30 min
Ethanol 95 %	1:30 min
Ethanol 100 %	2:00 min
Xylol	2:00 min

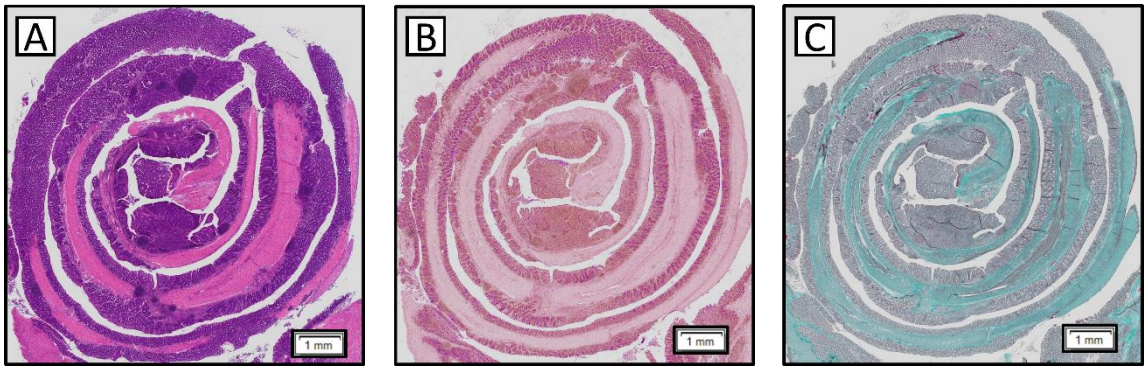

Fig. 18 Histological stainings for qualitative tumor analysis. In order to analyze the histological features regarding tumor growth and cell infiltration, three different stainings were performed. HE staining (A) shows the acidic nucleus in violet and alkaline components in pink, PAS staining (B) visualizes mucopolysaccharides, especially goblet cells, and Masson's trichrome staining (C) dyes collagen in green and muscle fibers in red.

2.2.28. Immunohistochemistry (IHC)

IHC was performed in order to stain certain proteins and thus visualizing desired cells or cell components within a specimen (Fig. 19) using monoclonal or polyclonal antibodies (AB) obtained from host organisms such as rabbits, goats or hybridoma cells (Hanly et al. 1995; Tomita and Tsumoto 2011). Both types of ABs bind specifically with their Fab part (antigen binding fragment) to the desired epitope. A second AB from a different host species then binds to the Fc part (crystallizable fragment) of the first AB. Horseradish peroxidase (HRP) attached to the Fc part of the second AB then converts a substrate such as diaminobenzidine (DAB) into a chromatic, alcohol insoluble precipitate (Magaki et al. 2019). The staining protocol was conducted in the following way:

Table 19 IHC, Protocol

Step	Reagent	Time
Antigen Retrieval	Citric acid, 0,05 % Tween 20	10:00 min
Endogenous Enzyme Block	H_2O_2 3 %	10:00 min
Protein Block	Horse Serum	30:00 min
Primary Antibody	αCD3; αCD68; αGR; αGR1	30:00 min
Secondary Antibody	ImmPRESS Goat/Rabbit	30:00 min
Substrate-Chromogen	DAB	5:00 min
Counterstaining	F-Hematoxylin	8:00 min
Rinse	ddH_2O	5:00 min

Each step was intermitted by 5 min of TBS/T (Tris-buffered-saline-Tween) buffer rinsing. To examine a specimen concerning its specific immunological activity, different primary ABs were applied to visualize different targets:

αCD3 - T cells
αCD68 - Macrophages
αGR1 - Neutrophils
αGR - Glucocorticoid Receptor

2.2.29. Histological Image Analysis

Stained specimens were fixed with coverslips and afterwards scanned by first using a Leica Axio A1 Microscope and ZEN light 2012 picturing software for a broad overview in 10x magnification, and secondly using an OLYMPUS VS-ASW 2.9 slide scanner with a 20x magnification. For cell counting, pictures were viewed using OlyVIA version 2.4 software and subsequently edited using ImageJ version 1.52i. In order to quantify IHC stained T cells and macrophages, two different methods were applied.

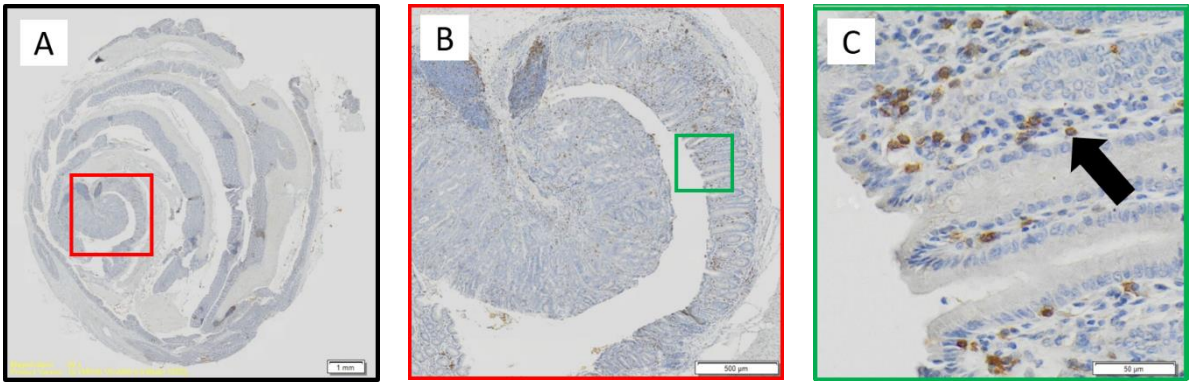

Fig. 19 Image analysis. The IHC-stained specimens were scanned at 20x magnification and could be analyzed using OlyVIA or ImageJ software. Cells stained with DAB could be recognized by the brown color (arrow in C).

2.2.30. Manual Cell Counting

To quantify T cells and macrophages in tumors, the stained cells were first counted manually. To do so, pictures of IHC-stained specimens were cropped to the region of interest using ImageJ (Image → Crop) and subsequently analyzed with the enclosed cell counting feature (Plugins → Analyze → Cell Counter) (Fig. 20A). The Cell Counter function allows a manual marking of the cells and provides a count of set marks (Fig. 20B, C). Tissue of tumor, its shaft and surrounding healthy appearing mucosa were discriminated using micromorphological features such as intact crypts, intact and plenty goblet cells, general dystrophic versus eutrophic tissue architecture and cell morphology. Subsequently, stained cells were counted, and the area of interest was measured (Analyze → Measure). The number of cells was then divided by the area of interest to obtain the cells per area ratio. This ratio was compared within tumor, shaft and mucosa.

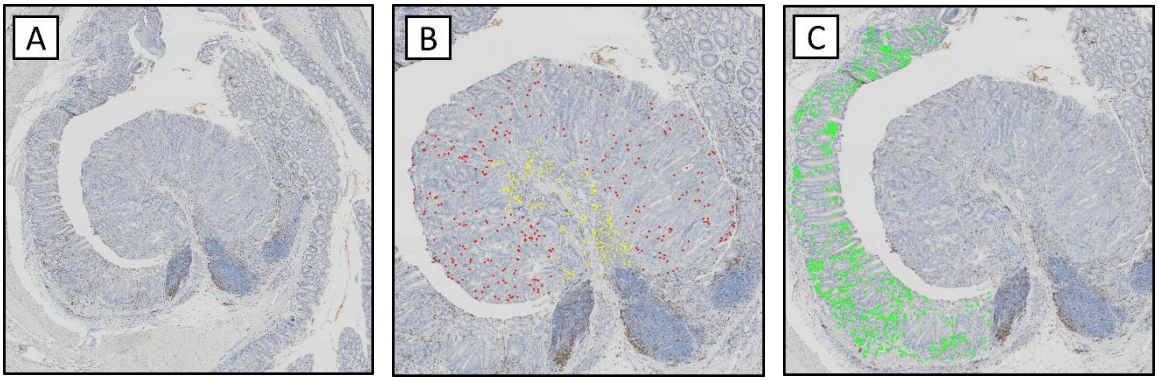

Fig. 20 Example for manual cell counting. Shown is a tumor of a $GR^{villinCreERT2}$ mouse with an IHC-staining of $CD3^{+}$ T cells. After identifying the tumor with its shaft and healthy mucosa (A), the T cells of the tumor tissue (red) and shaft (yellow) were spotted and counted. Subsequently, T cells in a comparable area of healthy mucosa were spotted (green) and counted.

2.2.31. Automated Iterative Cell Classification and Counting with Ilastik Version 1.3.2

As a complementary method to manual cell counting, an automated cell classification was performed. First, pictures of IHC-stained specimens were cropped to the region of interest using ImageJ (Image → Crop). Then, the cropped pictures were uploaded and analyzed with Ilastik Pixel Classification mode (Fig. 21A), training Ilastik with a random forest classifier as done by Berg and colleagues (Berg et al. 2019). Six different Gauss distributions were applied to each of three categories: “Color”, “Edge” and “Texture”. Pixel classification was performed on pre-calculated image features. Features comprise color edge and texture features of varying length scales obtained by using different filter kernel sizes. The random

forest classifier was trained and used for subsequent segmentation (Fig. 21B). After training the random forest classifier with all available samples with the same staining, images were segmented into these categories (Fig. 21C), exported, and the class appearance characterized with respect to total area by performing a histogram analysis using ImageJ. The area of identified stained cells was subsequently divided by the total area of interest, thus obtaining the ratio of cell area per total area.

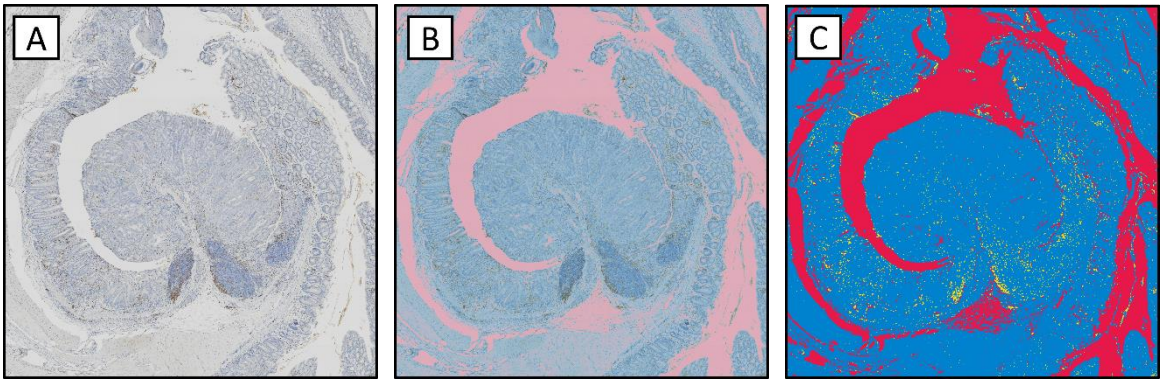

Fig. 21 Automated cell classification and counting. After training the Ilastik software with the original picture (A), it calculates the probability (B) of the different types of tissue and cells and subsequently puts out the segmentation (C) in different channels. The relative area of each color can then be calculated.

Both methods were tested for their comparability. Equal samples were then counted using manual and automated iterative cell classification and results were compared, concluding that the automatic cell classification indeed provides almost the same results.

2.2.32. Statistical Analyses

Statistical analyses were performed using GraphPad Prism software version 5.01 and Microsoft Excel 2010. Curve analysis (weight curves and DAI score curves) was performed by one-way ANOVA with Bonferroni's post-hoc test comparing all groups to each other. Two statistical comparisons (chemokine concentration and relative mRNA expression levels) were analyzed using a two-tailed, unpaired Student's t-test with confidence intervals of 95 %. Results were visualized with p-values showing statistical significance: $p < 0.05$ (*), $p \leq 0.01$ (**), $p < 0{,}001$ (***). Error bars correspond to the standard error of the mean (SEM) for N = 3 independent experiments.

3. Results

3.1. Influence of GR Expression in IECs on the Course of DSS Colitis and CA-CRC

3.1.1. Clinical Course of DSS Colitis

Body weight and health condition of mice treated with 1.2 % (w/v) DSS for a period of twelve days were compared. A significant difference in weight loss between $GR^{villinCreERT2}$ and GR^{flox} could be shown between day 9 and day 12. $GR^{villinCreERT2}$ mice had a higher weight loss within the last four days compared to GR^{flox} mice. Focusing on the DAI score, which includes stool consistency, the hemoccult score and weight loss, a significant difference between $GR^{villinCreERT2}$ and GR^{flox} could be shown within the last five days. The condition of $GR^{villinCreERT2}$ mice deteriorated significantly stronger than the condition of $GR^{flox/flox}$ mice.

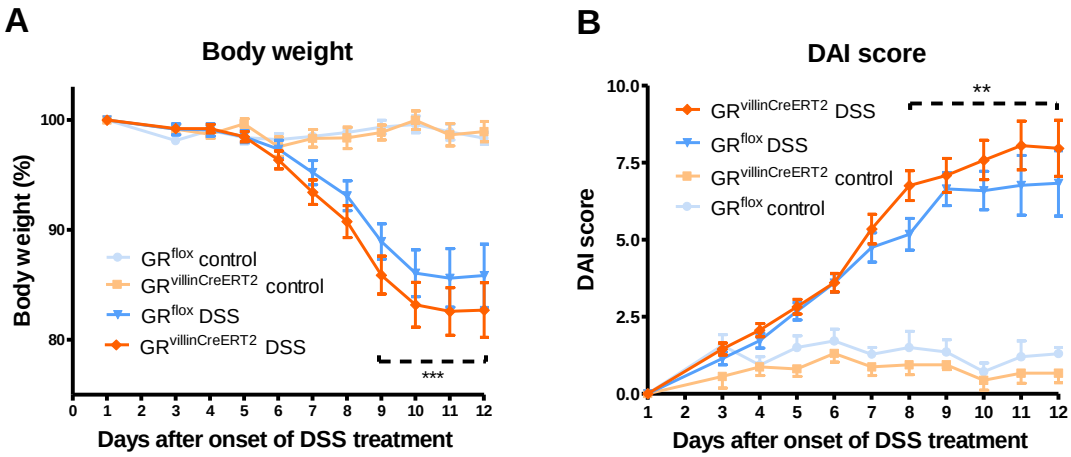

Fig. 22 Body weight and DAI score of $GR^{villinCreERT2}$ mice. Pooled data from short-term (DSS) and long-term (DSS/AOM) experiments. Mice were treated with 1.2 % (w/v) DSS in the drinking water for 8 days and then let to recover for 4 days. They were sacrificed after day 10 and day 12, respectively. $GR^{villinCreERT2}$ DSS mice: N = 22. GR^{flox} DSS mice: N = 14. $GR^{villinCreERT2}$ control: N = 8. GR^{flox} control: N = 7. (A) The body weight is depicted relative to the weight measured at day 0. (B) The DAI score was calculated based on stool consistence, intestinal bleeding, and weight loss. Statistical analysis was performed by one-way-ANOVA followed by Bonferroni's post-hoc test with a (***) significant difference in between day 9 and day 12 between $GR^{villinCreERT2}$ mice and GR^{flox} mice receiving DSS (A). A (**) significant difference between day 8 and day 12 between $GR^{villinCreERT2}$ mice and GR^{flox} mice receiving DSS was observed for the DAI score (B).

Comparing the lengths of the colon, no significant differences between $GR^{villinCreERT2}$ and GR^{flox} could be shown, neither between those under DSS administration nor within the control groups (Fig. 23).

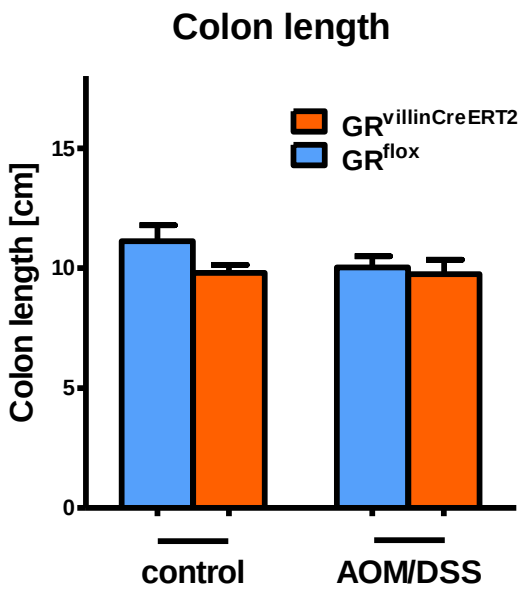

Fig. 23 Colon length after DSS treatment. $GR^{villinCreERT2}$ DSS mice: N = 9. GR^{flox} DSS mice: N = 8. $GR^{villinCreERT2}$ control: N = 4. GR^{flox} control: N = 5. Mice were treated with 1.2 % (w/v) DSS in the drinking water for 8 days and then let to recover for 4 days. Mice were sacrificed after day 10 and day 12, respectively. The colons were removed and compared in length.

3.1.2. Gene Expression of Cytokines and Chemokines

In order to assess differences in gene expression of pro-inflammatory cytokines and chemokines, qRT-PCR analysis of colon samples was performed. To do so, RNA was isolated from small pieces of the colon and after subsequent reverse transcription into cDNA, qRT-PCR was performed. Expression levels were quantified and compared by normalizing to *Hprt* as an endogenous control. The pro-inflammatory cytokines TNF-α, IL-1β and IL-6 were selected as indicators of inflammatory events. Additionally, the chemokines *Cxcl1*, *Cxcl5* and *Ccl2* were analyzed concerning differences in gene expression. CXCL1, CXCL5 CCL2 are inflammation-promoting chemokines. They are secreted by IECs and attract monocytes/macrophages to the site of inflammation. Although not statistically significant, gene expression of all analyzed cytokines as well as chemokines were lower in the $GR^{villinCreERT2}$ mice than in the GR^{flox} mice (Fig. 24). These results are consistent with those later obtained by ELISA analysis. It is possible that the lack of the GR in $GR^{villinCreERT2}$ mice reduces the recruitment of macrophages to the inflammatory site.

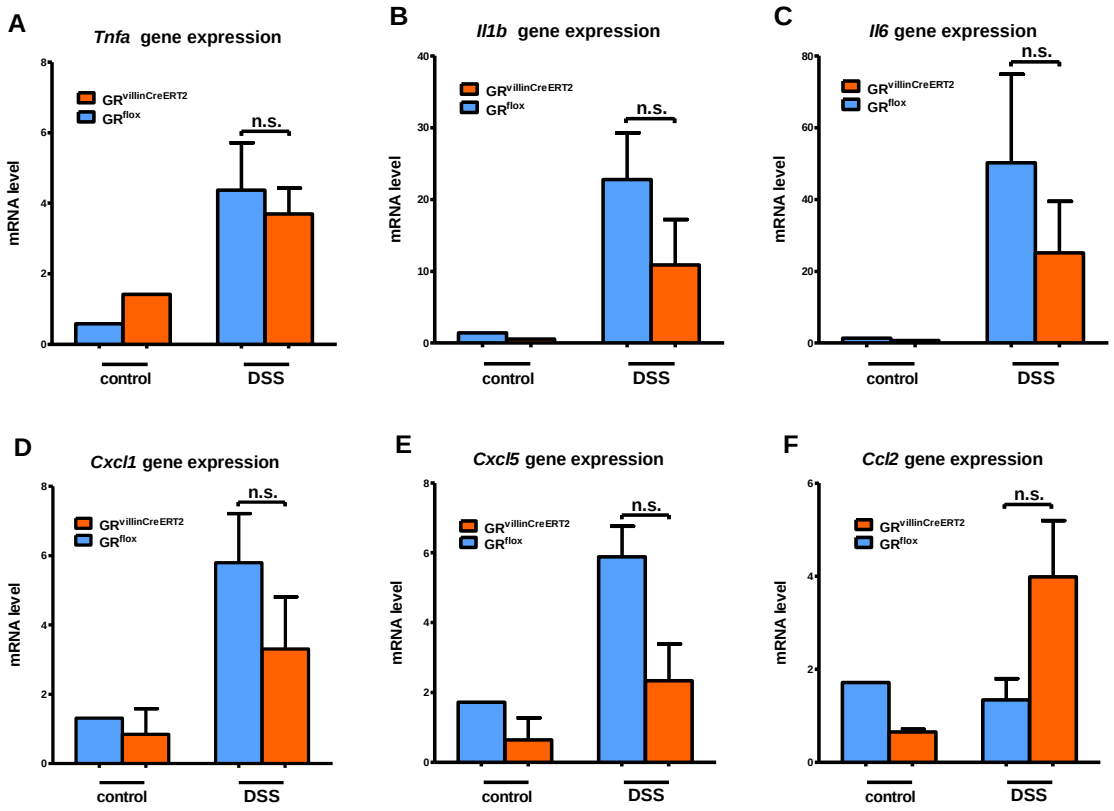

Fig. 24 Levels of cytokine and chemokine mRNA. $GR^{villinCreERT2}$ DSS mice: N = 6. $GR^{flox/flox}$ DSS mice: N = 5. $GR^{villinCreERT2}$ control: N = 2. GR^{flox} control: N = 2. Mice were treated with 1.2 % (w/v) DSS in the drinking water for 8 days and then let to recover for 4 days. They were sacrificed after day 10 and day 12, respectively. The colon was dissected, mRNA isolated and qRT-PCR performed. Relative mRNA levels of *Tnfa* (A), *Il1b* (B), *Il6* (C), *Cxcl1* (D), *Cxcl5* (E) and *Ccl2* (F) were determined by normalization to the housekeeping gene *Hprt*.

3.1.3. Protein Levels of Cytokines and Chemokines

Postulating that increased gene expression of cytokines is associated with an increased production of the respective proteins, pro-inflammatory cytokines TNF-α, IL-1β and IL-6 were measured with ELISA. After sacrificing the mice, the colon was dissected, and pieces of 5 mm length were incubated o/n in medium. Cytokines released by the inflamed tissue transgressed into the medium and could subsequently be analyzed by ELISA and compared in corresponding groups. While there was a significant cytokine elevation within the mice under DSS administration, which indicates an inflammatory process on a molecular level, no significant differences between $GR^{villinCreERT2}$ mice and GR^{flox} mice could be shown (Fig. 25).

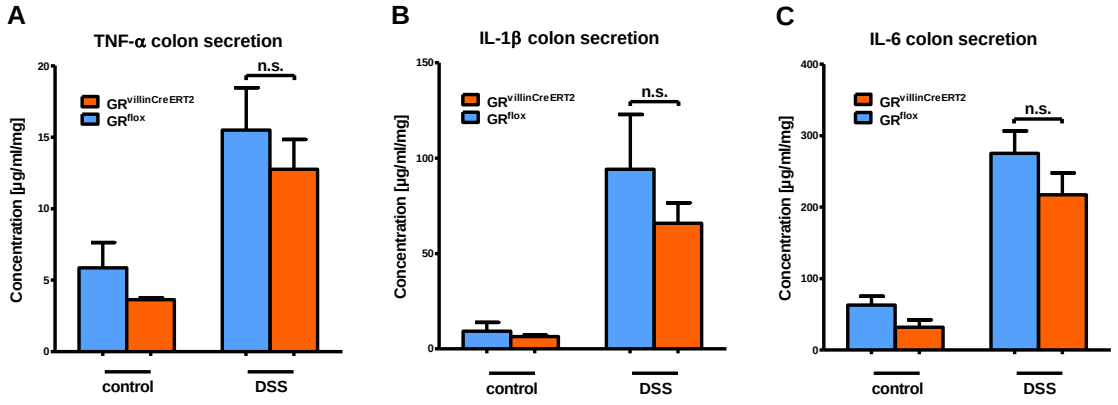

Fig. 25 Levels of pro-inflammatory cytokines. $GR^{villinCreERT2}$ DSS mice: N = 6. GR^{flox} DSS mice: N = 5. $GR^{villinCreERT2}$ control: N = 2. GR^{flox} control: N = 2. Mice were treated with 1.2 % (w/v) DSS in the drinking water for 8 days and then let to recover for 4 days and were sacrificed after day 10 and 12, respectively. After sacrificing $GR^{villinCreERT2}$ and GR^{flox} mice with DSS treatment and controls, dissecting the colon, and incubating pieces of 5 mm length o/n in medium, ELISA analysis was performed. Concentrations of TNF-α (A), IL-1β (B) and IL-6 (C) were measured.

Considering the fact, that UC in humans typically does not evenly affect the whole colon, but is rather located in certain, predominantly rectal areas, it was necessary to analyze and compare different sections of the colon. To do so, specimens of an oral, medial and rectal part of the colon were dissected and subsequently incubated in medium. As shown in Fig. 26, concentrations of TNF-α, IL-1β and IL-6 were then measured and compared between all groups of mice. Interestingly, both $GR^{villinCreERT2}$ and GR^{flox} mice under DSS administration showed strong differences of cytokine concentrations within the colon. It appears, that mice of both genotypes featured a concentration peak in the medial part, followed by the rectal and oral part. However, no statistical differences between $GR^{villinCreERT2}$ and $GR^{flox/}$ mice could be shown, even though, a tendency to lower cytokine concentrations in $GR^{villinCreERT2}$ mice was observed.

In Fig. 26, the concentration of TNF-α (A), IL-1β (B) and IL-6 (C) is itemized by localization within the colon. The concentration patterns of each cytokine appear quite similar as the medial part turns out to be the most inflammatory active part. However, respecting each cytokine, within one group of mice, rectal, and oral concentrations were varying considerably in relation to the medial concentration. This effect could be explained through different half-time periods of the analyzed cytokines.

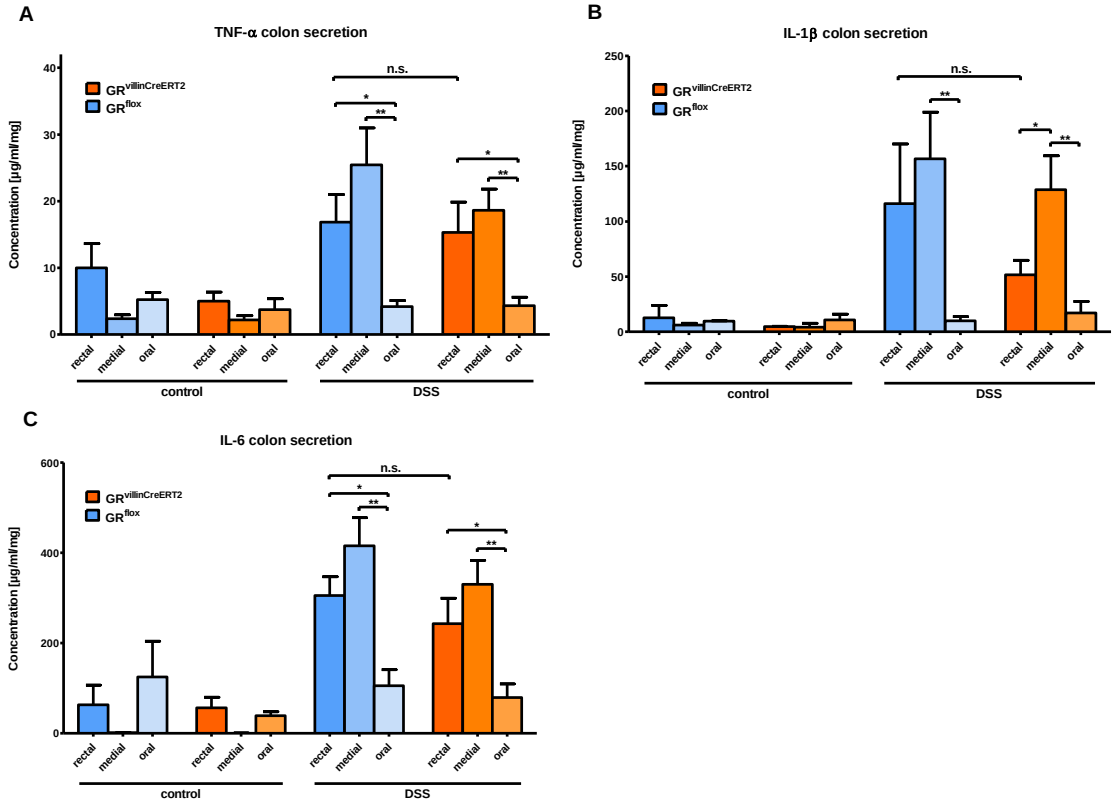

Fig. 26 Concentrations of pro-inflammatory cytokines dependent on the localization within the colon. $GR^{villinCreERT2}$ DSS mice: N = 6. GR^{flox} DSS mice: N = 5. $GR^{villinCreERT2}$ control: N = 2. GR^{flox} control: N = 2. Mice were treated with 1.2 % (w/v) DSS in the drinking water for 8 days and then let to recover for 4 days and were sacrificed after day 10 and 12, respectively. After DSS treatment, the mice were sacrificed, and the dissected colon was divided into 3 parts, namely a rectal, medial, and oral part. Each part was incubated o/n in medium and levels of TNF-α (A), IL-1β (B) and IL-6 (C) were compared using ELISA analysis.

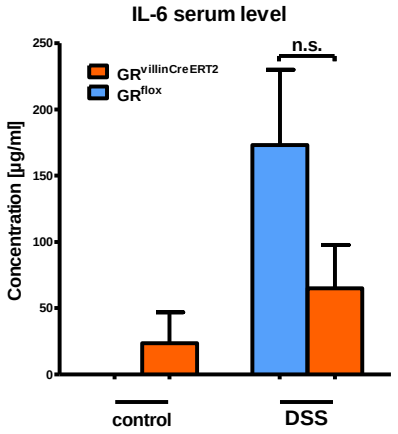

Fig. 27 Concentration of IL-6 in the serum. $GR^{villinCreERT2}$ DSS mice: N = 6. GR^{flox} DSS mice: N = 5. $GR^{villinCreERT2}$ control: N = 2. GR^{flox} control: N = 2. Mice were treated with 1.2 % (w/v) DSS in the drinking water for 8 days and then let to recover for 4 days and were sacrificed after day 10 and 12, respectively. After sacrificing the mice, blood was collected by heart puncture. The concentration of IL-6 in the serum was then analyzed by ELISA.

Considering possible differences between local and systemic cytokine production, IL-6 levels were measured in the serum (Fig. 27). Although lower concentrations were observed in $GR^{villinCreERT2}$ mice, the difference was not statistically significant.

3.1.4. Quantitative Tumor Analysis of CA-CRC after DSS Colitis

In order to quantify the tumor burden of mice treated with DSS and AOM, the number and size of tumors in the colon were analyzed. Starting in week 6, colonoscopy was performed to monitor tumor development. When tumors of category S 3 were detected in at least one animal, all mice were sacrificed and dissected. The colon was cut open longitudinally from their rectal to the oral part, and tumors were then macroscopically identified and counted, starting at the rectal part (Figs. 28 and 29B). The number of tumors in $GR^{villinCreERT2}$ mice was significantly higher than in GR^{flox} mice, indicating that the onset of tumorigenesis was earlier and/or its development faster. To prove the absence of tumors in the control group, Swiss-roles of every colon belonging to the control group were prepared and histological cuts were made in perpendicular cross sections to the transverse axis of 200 µm thickness and subsequently microscopically controlled upon tumors. However, no tumors were found (Fig. 29B).

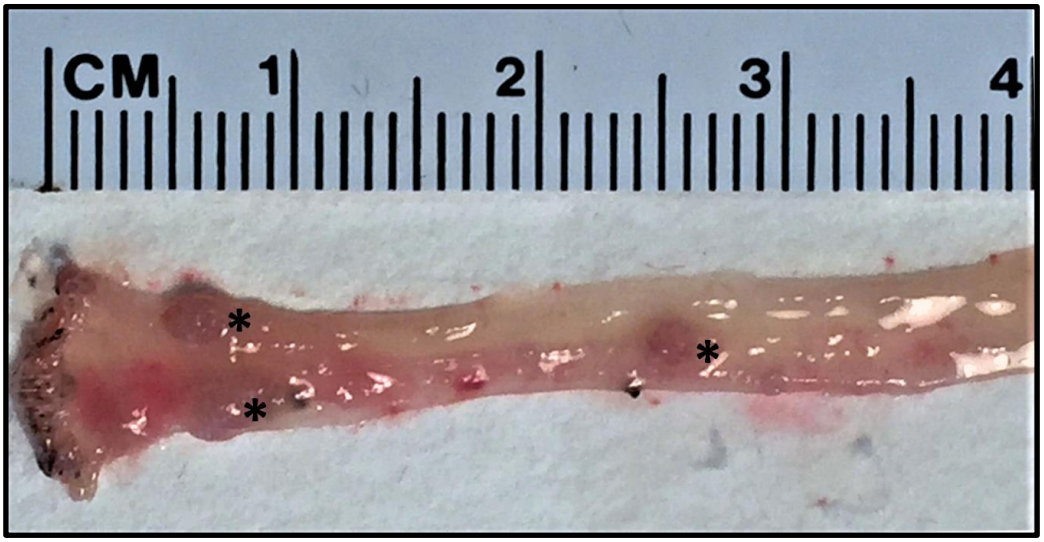

Fig. 28 Macroscopic inspection of the Colon. After injecting AOM and inducing DSS colitis for 8 days, follow up colonoscopies were performed beginning in week 6. When tumors of category S 3 were detected by colonoscopy in at least one animal, all mice were sacrificed and dissected. To quantify the tumor burden, every colon was dissected longitudinally, and the number and size of the macroscopically visible tumors were subsequently counted and measured. The colon shown above contains 3 different tumors, marked with asterisks (*). Own images.

Identified tumors were measured in size (Fig. 29A). The tumor burden was calculated by multiplying the mean tumor size with the tumor number (Fig. 29B,C). All three values were significantly increased in $GR^{villinCreERT2}$ compared to GR^{flox} mice.

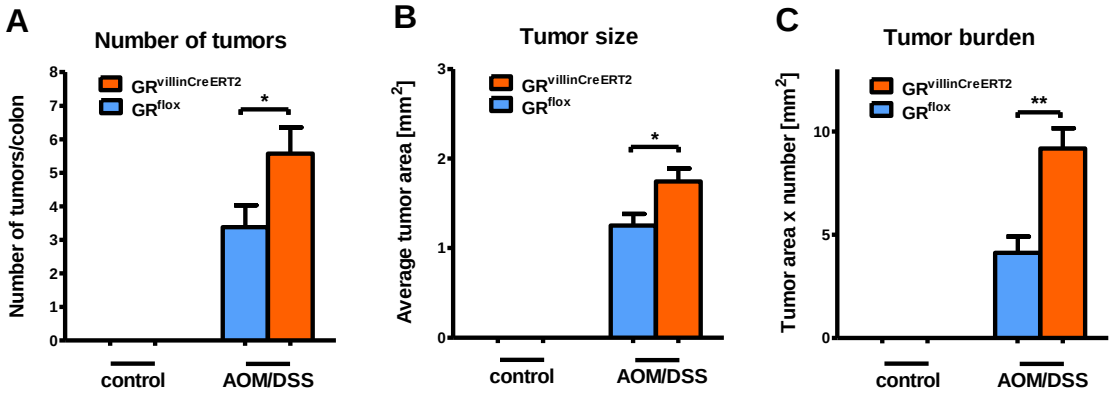

Fig. 29 Quantitative tumor analysis. $GR^{villinCreERT2}$ DSS/AOM mice: N = 5. GR^{flox} DSS/AOM mice: N = 5. $GR^{villinCreERT2}$ control: N = 1. GR^{flox} control: N = 3. After injecting AOM and inducing DSS colitis for 8 days, follow up colonoscopies were performed beginning in week 6. When tumors of the category S 3 were detected by colonoscopy in at least one animal, all mice were sacrificed and dissected. The colon was then cut up longitudinally and all tumors were counted (A) and the tumor area was calculated according to the formula $[(\text{length} + \text{width}) \times 0.5]^2$ (B). By multiplying the tumor area and its number, the tumor burden (C) was calculated.

3.1.5. Histological Tumor Analysis

For a qualitative comparison of tumors, sections of Swiss-roles of $GR^{villinCreERT2}$ and GR^{flox} mice treated with DSS and AOM were analyzed using different staining protocols:

1. Hematoxylin and Eosin (HE) Staining
2. Periodic acid-Schiff (PAS) Staining
3. Masson's Trichrome Staining

Each protocol has specific advantages in its staining properties. HE stainings highlight the nucleus within the epithelial cells and stromal cells of the mucosa, strongly demarcating them from the submucosa and muscularis. The dysmorphic tissue architecture within the tumors is thus well accentuated (Fig. 30B,D). PAS stainings allow good visualization of the mucin-producing goblet cells. Fig. 30E shows that goblet cells in intact crypts are evenly distributed in the mucosa, whereas they are hardly present in the tumor tissue (F). Here, only disorganized mucus inclusions can be seen. Masson`s trichrome stainings color the submucosa in turquoise and the muscularis particularly in red (Fig. 30G). In panel H, there is hardly any submucosa or muscularis visible in the tumor tissue.

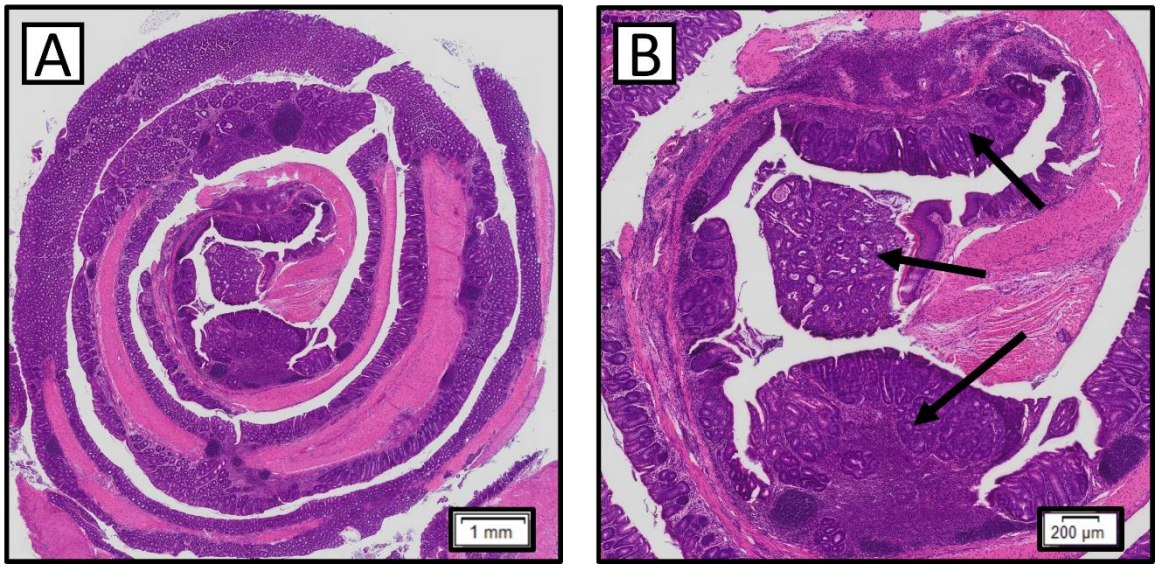
A
1 mm
B
200 µm

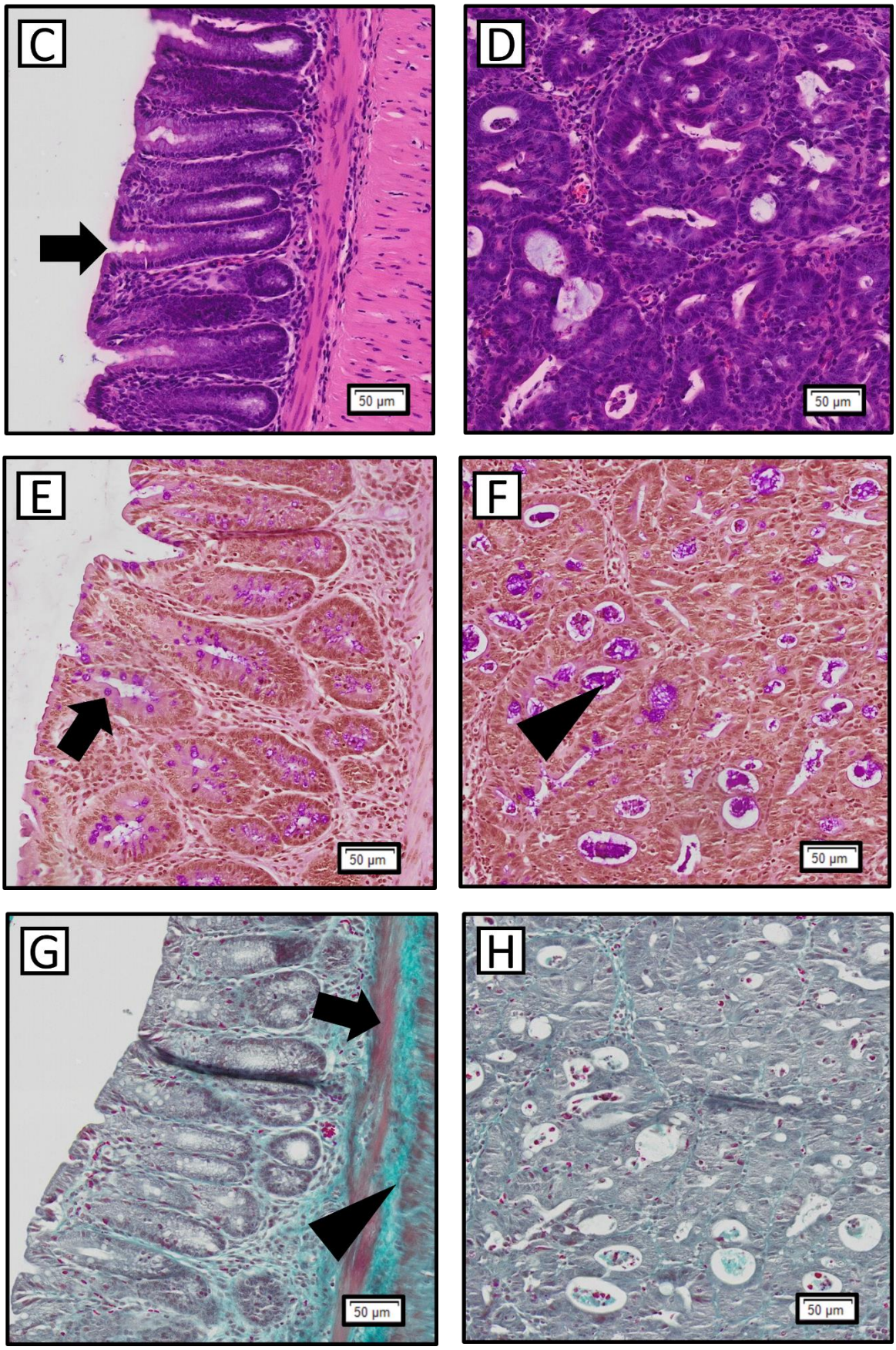

Fig. 30 Histological stainings of Swiss-roles from one exemplary GR^{flox} mouse (A,C,E,G) and one GR^{villinCreERT2} mouse (B,D,F,H) After injecting AOM and inducing DSS colitis for eight days, follow up colonoscopies were performed beginning in week 6. When tumors of the category S 3 were detected by colonoscopy in at least one animal, all mice were sacrificed and dissected. (A-D) HE stainings show the whole Swiss-role in a macro view. In

panel B, three tumors with exophytic growth can be seen (narrow arrows). Panel C shows a healthy mucosa with intact crypts (broad arrow, whereas panel D depicts the typical dysmorphic structure of the tumor tissue with unorganized growth of the remaining crypts (dart). (E,F) PAS staining of the colon of a GR^{flox} mouse (8E) show a healthy mucosa with intact crypts and an abundance of goblet cells (broad arrow), dyed in violet. Panel F depicts the typical dysmorphic structure of tumor tissue from a GR^{villinCreERT2}mouse with an unorganized growth of the remaining crypts and enclosed mucus bodies dyed in violet (dart). (G,H) Masson's trichrome stainings show a healthy mucosa, the collagen of the submucosa in turquoise and the muscularis in red of a healthy colon (G) and the typical dysmorphic structure of the tumor tissue (H) with unorganized growth of the remaining crypts. The tumor features low amounts of submucosa and almost no muscularis.

The typical features of cancerous growth, such as dysmorphic, disorganized, and invasive tissue with visible loss of function of exocrine activity allow the designation of tumors in the colon and can reliably be assessed using the described stainings (Jass 2007; Brenner et al. 2014). All studied tumors depicted these typical features of the adenoma-carcinoma-sequence type observed in most cases of human CRCs (Leslie et al. 2002). Therefore, most of them showed exophytic growth with a shaft, originating from submucosa. Unambiguous classification of tumors as invasive carcinomas based on these characteristics is a necessary prerequisite to designate the CA-CRC mouse model as such. Differentiation from tumors of other genesis, such as edema or adenomas, is therefore required (Bürtin et al. 2020).

3.1.6. Quantification of Inflammatory Cell Infiltration by IHC

Additionally, IHC was performed using different antibodies. To prove the successful deletion of the GR through tamoxifen induced gene recombination, colon tissue from GR^{villinCreERT2} and GR^{flox} mice was stained with an anti-GR antibody. Both, in sections of tumor tissue and neighboring tumor free tissue, staining of the GR in the epithelium of GR^{villinCreERT2} mice was absent while it was clearly detectable in GR^{flox} mice (Fig. 31A,B). By contrast, in the underlying lamina propria GR positive cells were detected in the colon of mice in both genotypes (Fig. 31C,D), thus confirming the selective deletion of the GR in IECs.

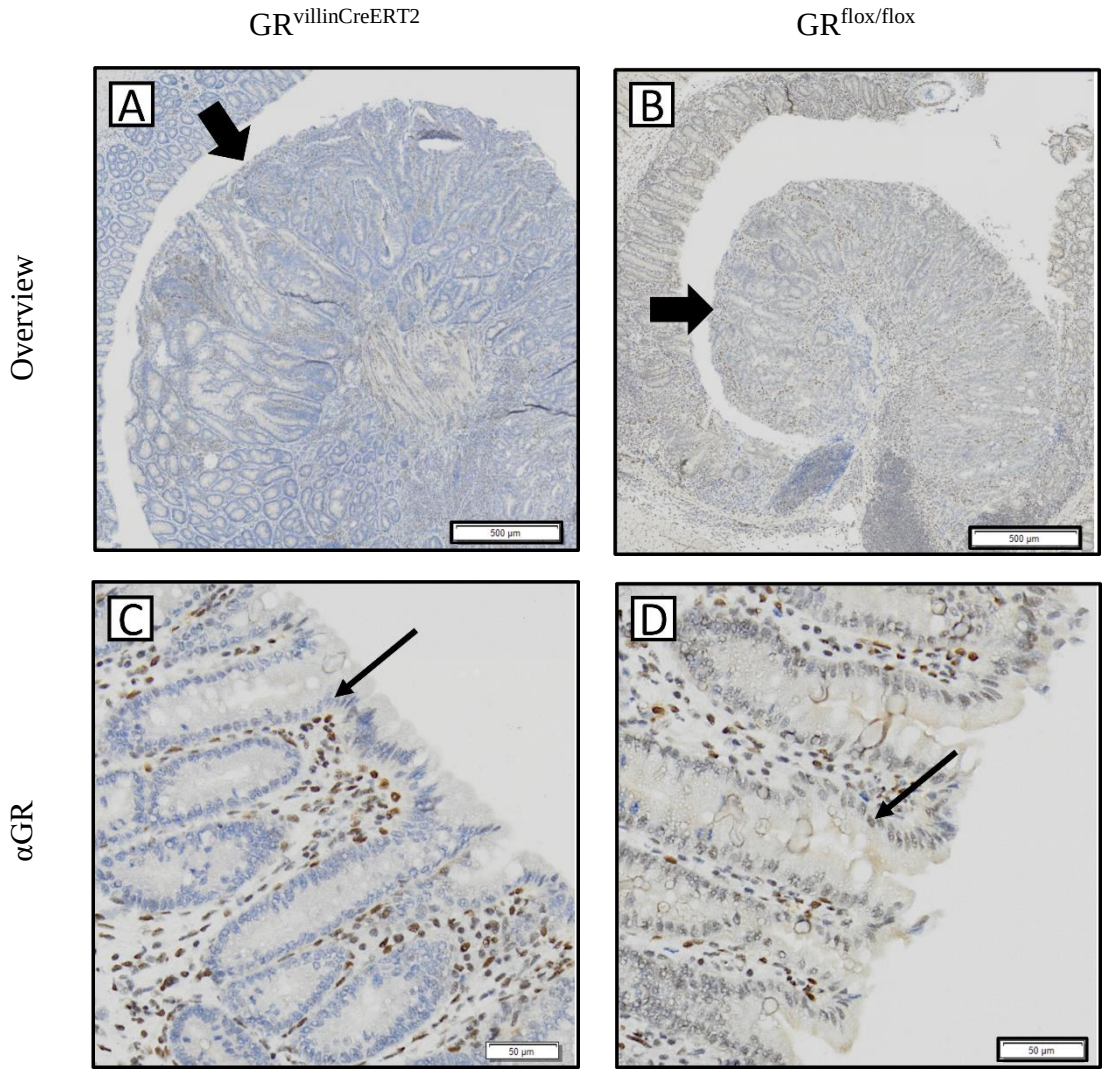

Fig. 31 Validation of GR deletion in IECs of GR^{villinCreERT2} mice by IHC. After injecting AOM and inducing DSS colitis for eight days, follow up colonoscopies were performed beginning in week 6. When tumors of the category S 3 were detected by colonoscopy in at least one animal, all mice were sacrificed and dissected. Comparing tissue sections of GR^{villinCreERT2} mice (A) and GR^{flox} mice (B), tumors are marked by broad arrow. To confirm deletion, of the GR, it was stained in both samples. IECs in GR^{villinCreERT2} mice (C) don't show any dye, while IECs in GR^{flox} mice (D) show dye admittance (narrow arrow).

To quantify inflammatory cell infiltration, anti-CD3 and anti-CD68 antibodies were used to identify T cells (Fig. 32A,B) and macrophages (Fig. 32C,D) respectively. Quantification was performed by manual cell classification with ImageJ and by statistical learning-based image segmentation with ImageJ and Ilastik, as described in the Materials and Methods section (3.2.32).

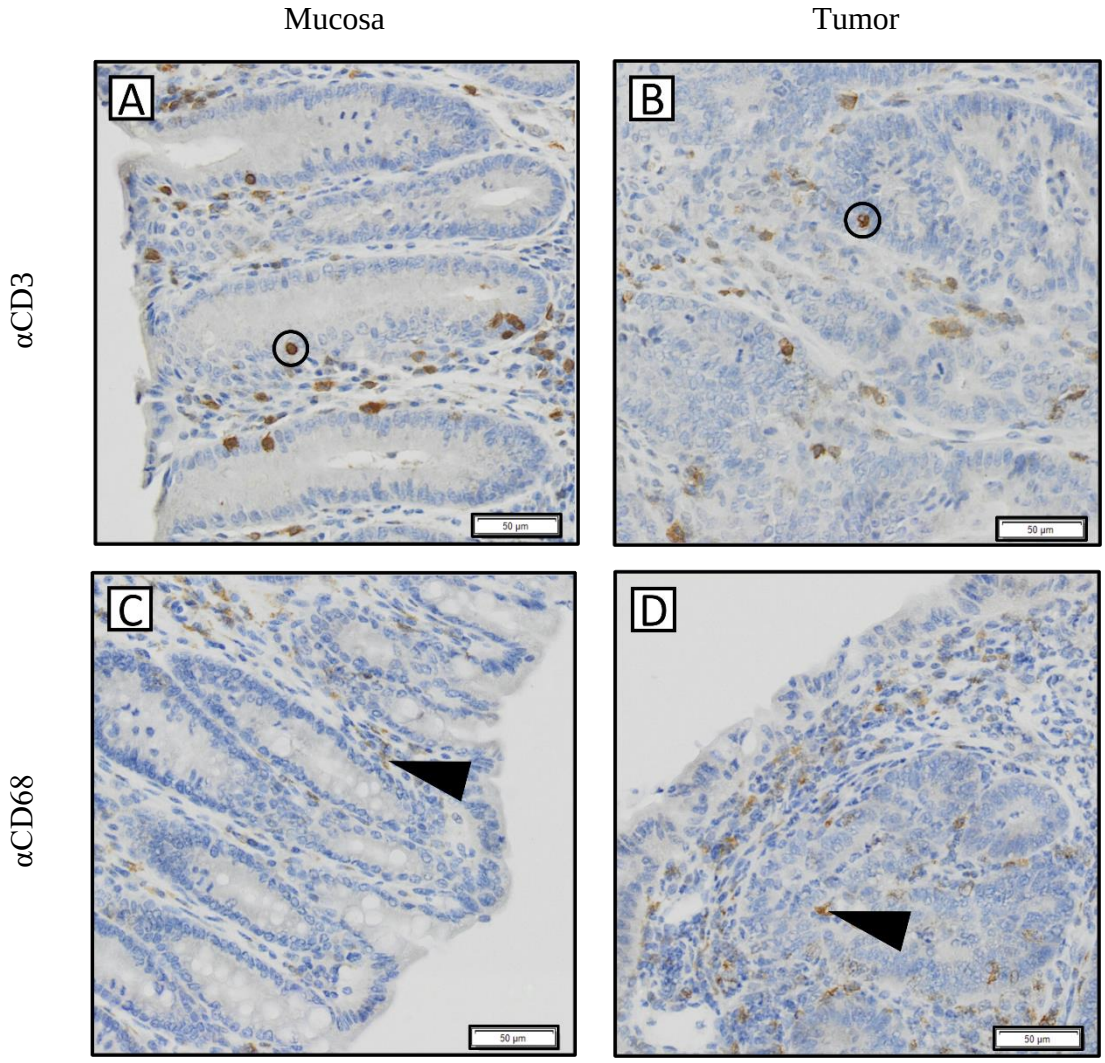

Fig. 32 IHC stainings of T cells and macrophages. After injecting AOM and inducing DSS colitis for eight days, follow up colonoscopies were performed beginning in week 6. When tumors of the category S 3 were detected by colonoscopy in at least one animal, all mice were sacrificed and dissected. To quantify inflammatory cell infiltration, $CD3^+$ T cells and $CD68^+$ macrophages were stained using specific antibodies. In tumor samples from both genotypes $CD3^+$ T cells (A,B) could be identified (circle) and showed a clear delimitation against other cells. $CD68^+$ macrophages (G,H), marked with darts, were also present in tumors of mice of both genotypes and appear to be more diffuse due to their many pseudopodia.

Within all tumor samples, three different areas were observed (Fig. 33). At first, an area of healthy appearing mucosa in local proximity to the tumor was defined and cells were counted. Cells within the whole tumor, as well as the shaft and rest of tumor tissue were analyzed to preserve differences of cell numbers due to tumor evasion mechanisms.

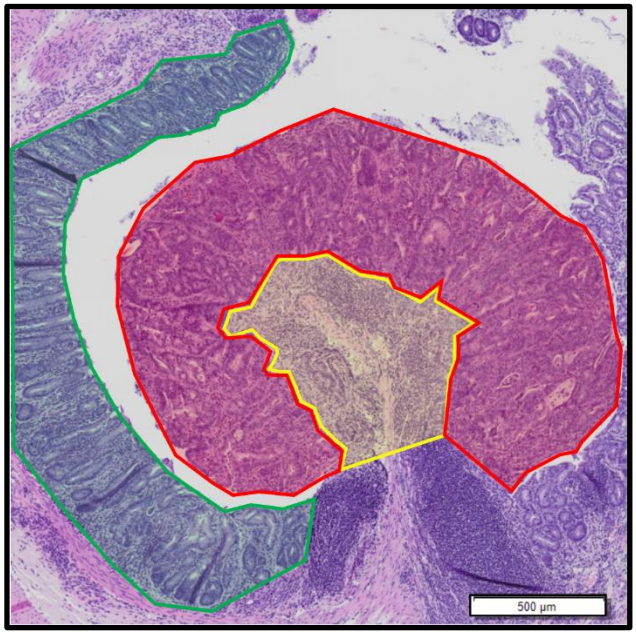

Fig. 33 Segmentation of an HE stained tumor section. After injecting AOM and inducing DSS colitis for eight days, follow up colonoscopies were performed beginning in week 6. When tumors of the category S 3 were detected by colonoscopy in at least one animal, all mice were sacrificed and dissected. An HE stain of an exemplary section is depicted. Before quantification, the specimens were classified into tumor (red), shaft (yellow) and mucosa (green).

As shown in Fig. 34, enumeration of $CD3^+$ T cells (A) and $CD68^+$ macrophages (B) was first done manually using ImageJ. The same samples were subsequently analyzed by statistical learning-based image segmentation with ImageJ and Ilastik as explained in the Material and Methods section (3.2.32). Both methods showed a very similar picture regarding both cells of interest (Fig. 34C,D). This observation suggests a high comparability between both methods and an internal validity of the statistical learning-based image segmentation with ImageJ and Ilastik.

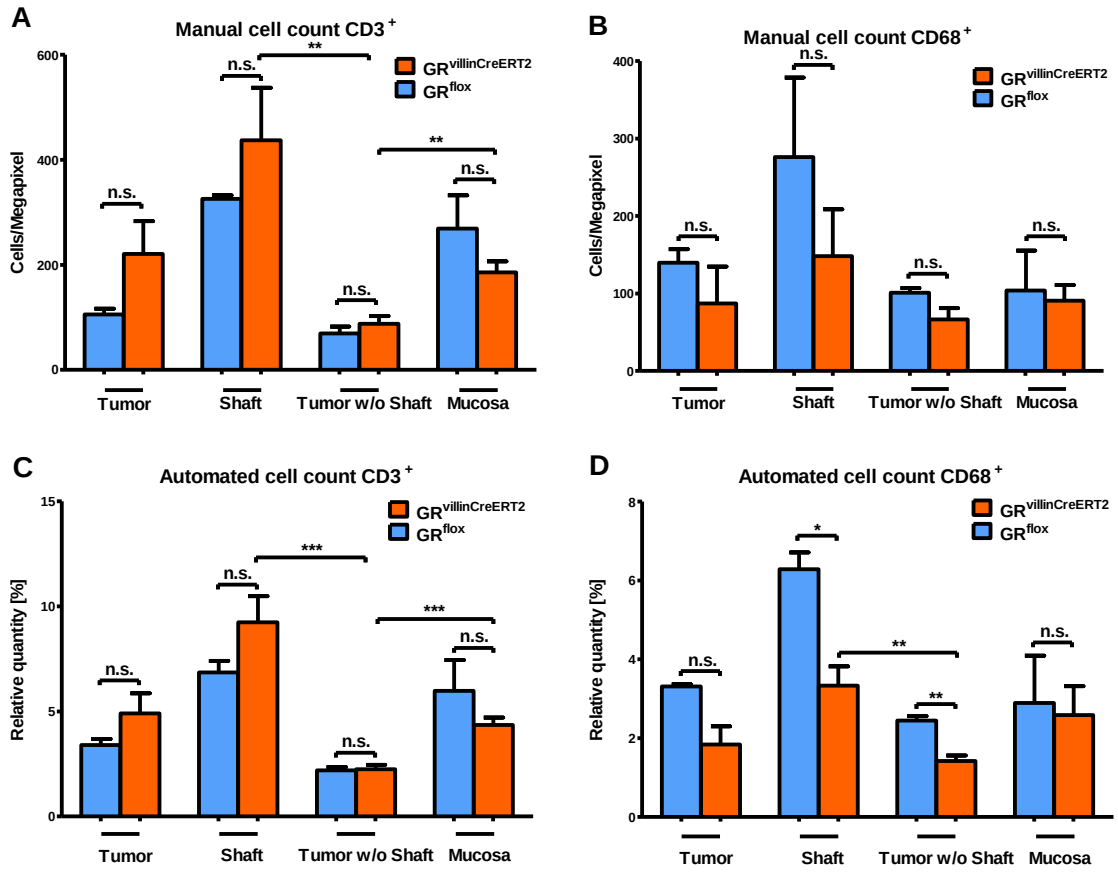

Fig. 34 Cell counts of CD3+ and CD68+ cells in tumors and mucosa. GR^{villinCreERT2} mice: N = 5. GR$^{flox/flox}$ mice: N = 5. After injecting AOM and inducing DSS colitis for eight days, follow up colonoscopies were performed beginning in week 6. When tumors of the category S 3 were detected by colonoscopy in at least one animal, all mice were sacrificed and dissected. IHC was performed to visualize CD3+ T cells (A,C) and CD68+ macrophages (B,D). Subsequently, the cells were counted manually using only ImageJ (A,B) or automatically using ImageJ and Ilastik (C,D). The count is displayed in relation to a defined area. The numbers of CD3+ and CD68+ cells per area were compared between different localizations and between GR^{villinCreERT2} and GR^{flox} mice.

The results of both methods were compared between GR^{villinCreERT2} and GR^{flox} mice and within each group. CD3+ T cells (Fig. 34A,C) are found in a higher density in the shafts of tumors in GR^{villinCreERT2} mice than in the shafts of tumors in GR^{flox} mice. Even within both mouse groups, there is an increased density of T cells in shafts compared to the mucosa. An inverse observation was made for CD68+ macrophages (Fig. 34B,D). Macrophages in the shaft of tumors in GR^{villinCreERT2} mice are significantly less frequent than in those of GR^{flox} mice. Also, in the other localizations of the analyzed tissues, the density of macrophages in GR^{villinCreERT2} mice is consistently lower than the density of macrophages in GR^{flox}. This observation might be explained through lower chemokine levels and thus macrophage attraction by IECs in GR^{villinCreERT2} mice, as shown by qRT-PCR analysis in section 4.1.2.

The higher significance level of automatic counting can possibly be explained by the method which calculates areas in Ilastik quantification rather than using a dichotomous counting

method. Cell components not considered in a manual counting method, such as pseudopodia, are thus included in the calculation and contribute to reducing standard errors.

When comparing the number of T cells between shaft and tumor and mucosa and tumor in $GR^{villinCreERT2}$ mice (Fig. 34A,C), significant differences were observed. The same observation was made regarding the density of macrophages in (Fig. 34D). This finding could indicate tumor evasion mechanisms.

3.2. Influence of Impaired GR Dimerization on the Course of DSS Colitis

3.2.1. Clinical Course of DSS Colitis

GR^{dim} mice and GR^{wt} control mice treated with 3.5 % (w/v) DSS for ten days were compared concerning body weight and DAI score. No significant differences regarding both parameters could be demonstrated (Fig. 35).

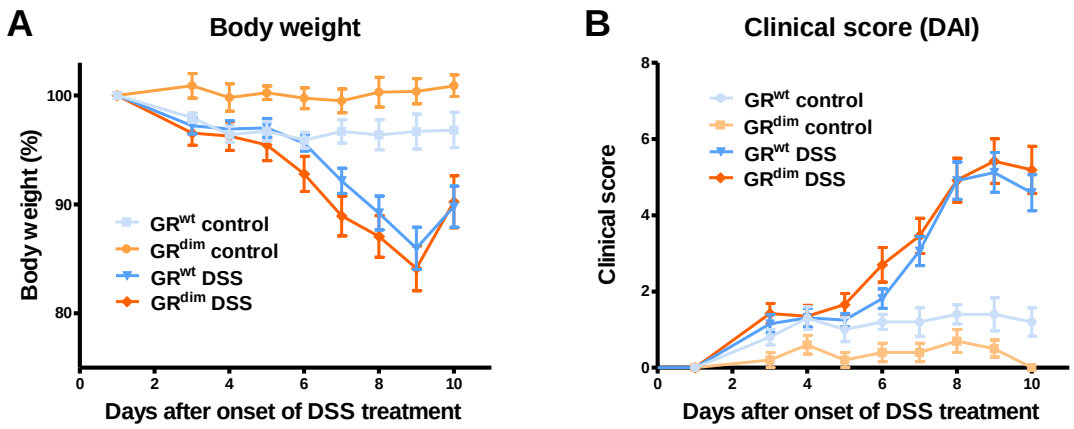

Fig. 35 Body weight and DAI score of GR^{dim} mice during DSS colitis. Mice were treated with 3.5 % (w/v) DSS in the drinking water for eight days and then let to recover for two days. Control mice were left untreated. All mice were sacrificed after ten days. GR^{dim} DSS mice: N = 13. GR^{wt} DSS mice: N = 16. GR^{dim} control: N = 5. GR^{wt} control: N = 5. The body weight is depicted relative to the weight measured at day 0 (A). The DAI score was calculated based on stool consistence, intestinal bleeding, and weight loss (B). Statistical analysis was performed by one-way-ANOVA followed by Bonferroni's post-test.

Also, the lengths of the colon were compared between GR^{dim} and GR^{wt} mice under DSS administration. However, no significant difference could be shown between both groups (Fig. 36).

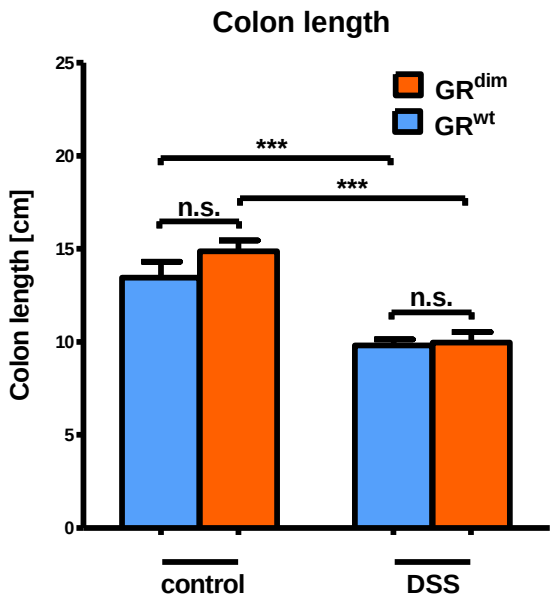

Fig. 36 Colon length after DSS treatment. Mice were treated with 3.5 % (w/v) DSS in the drinking water for eight days and then let to recover for two days. Control mice were left untreated. All mice were sacrificed after ten days. GR^{dim} DSS mice: N = 13. GR^{wt} DSS mice: N = 16. GR^{dim} control: N = 5. GR^{wt} control: N = 5. After dissecting the mice, the colons were cut open longitudinally and compared in length.

3.2.2. Gene Expression of Cytokines and Chemokines

To analyze an influence of GR dimerization on macrophage polarization, we analyzed the pro-inflammatory cytokines TNF-α, IL1β and IL-6. These cytokines are secreted by macrophages with M1 polarization and foster inflammatory activity. Additionally, the anti-inflammatory cytokine IL-10 and the anti-inflammatory macrophage scavenger receptor CD163 served as surrogate for an M2 polarization of macrophages. All cytokines were analyzed concerning differences between mRNA levels to determine whether inhibition of GR dimerization had any effects on macrophage polarization and the expression of anti-inflammatory signals. Therefore, colon tissue was collected, RNA isolated and after subsequent reverse transcription into cDNA a qRT-PCR was performed. Expression levels of mRNA were quantified and compared by normalizing to *Hprt* as endogenous control. Neither pro- nor anti-inflammatory cytokine mRNA levels showed significant differences. Also, CD163 mRNA levels were similar (Fig. 37D).

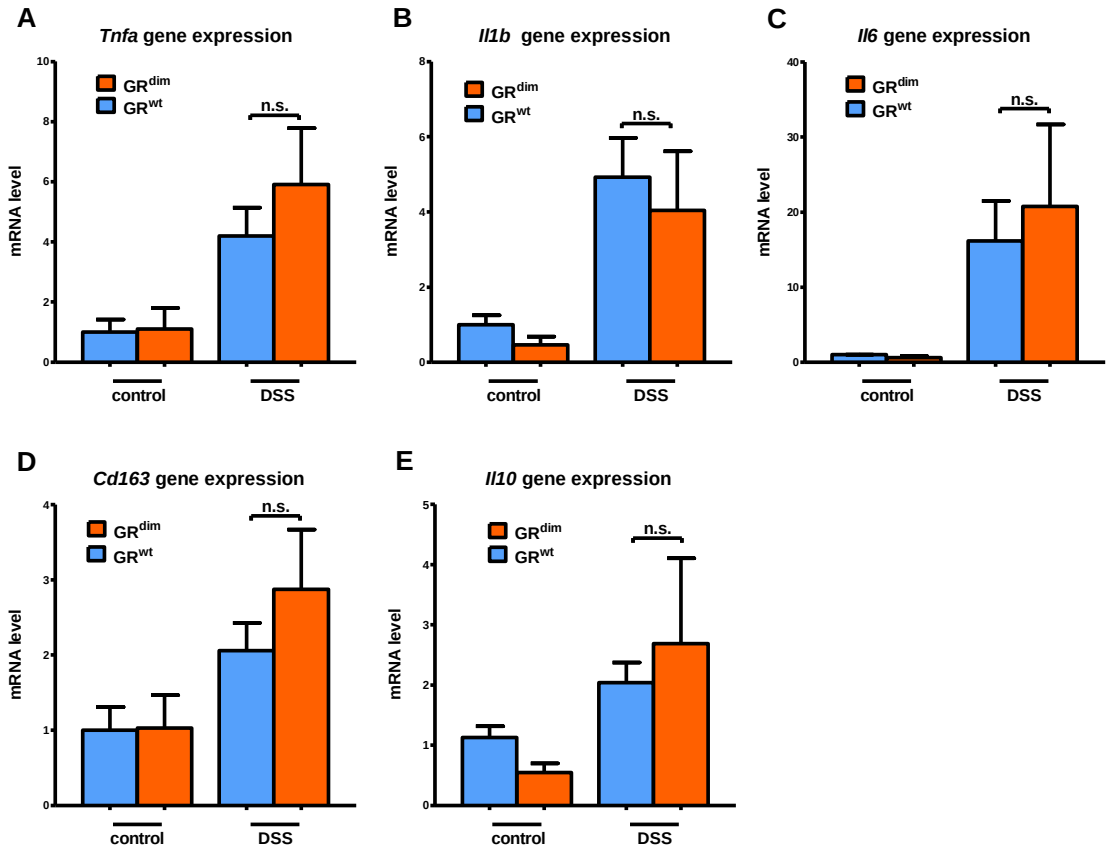

Fig. 37 Levels of of cytokine and CD163 mRNAs. Mice were treated with 3.5 % (w/v) DSS in the drinking water for eight days and then let to recover for two days. Control mice were left untreated. All mice were sacrificed after ten days. GR^{dim} DSS mice: N = 13. GR^{wt} DSS mice: N = 16. GR^{dim} control: N = 5. GR^{wt} control: N = 5. After sacrificing the mice, the colons were dissected, mRNA isolated and an qRT-PCR analysis performed. The mRNA levels of *Tnfa* (A), *Il1b* (B), *Il6* (C), *IL10* (E) and *Cd163* (D) were determined and compared between corresponding groups.

3.2.3. Protein Levels of Cytokines and chemokines

To investigate changes in cytokine secretion on the protein level, serum concentrations of the pro-inflammatory cytokines TNF-α, IL-1β and IL-6 were measured by ELISA. After sacrificing the mice and dissecting the colon, pieces of 5 mm length were incubated o/n in medium. Cytokines released by the inflamed tissue transgressed into the medium and could be subsequently analyzed by ELISA and compared between corresponding groups (Fig. 38). While there was a significant elevation of cytokine levels within mice under DSS administration, which proved an inflammatory process on a molecular level, no significant differences between GR^{dim} mice and GR^{wt} mice could be shown.

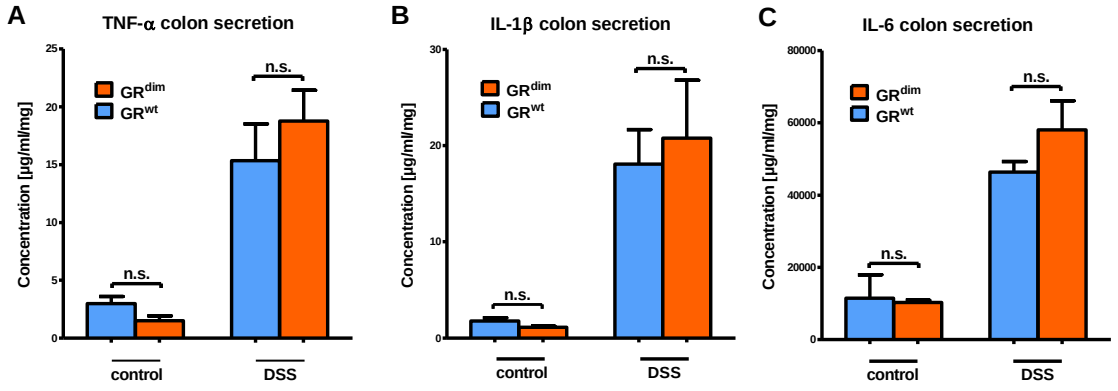

Fig. 38 Concentrations of pro-inflammatory cytokines in colon culture supernatants. Mice were treated with 3.5 % (w/v) DSS in the drinking water for eight days and then let to recover for two days. Control mice were left untreated. All mice were sacrificed after ten days. GR^{dim} DSS mice: N = 13. GR^{wt} DSS mice: N = 16. GR^{dim} control: N = 5. GR^{wt} control: N = 5. After sacrificing the mice and dissecting the colon, pieces of 5 mm length were incubated o/n in medium. ELISA analysis was performed for GR^{dim} mice and GR^{wt}mice with DSS treatment and controls. Concentrations of TNF-α (A), IL-1β (B) and IL-6 (C) were measured and compared between corresponding groups.

In contrast to the cytokine secretion detected in the supernatants of colon cultures, IL-6 concentrations in the serum of GR^{dim} mice were significantly higher than in the serum of GR^{wt} mice, indicating a stronger inflammatory response in GR^{dim} mice compared to the GR^{wt} mice (Fig. 39).

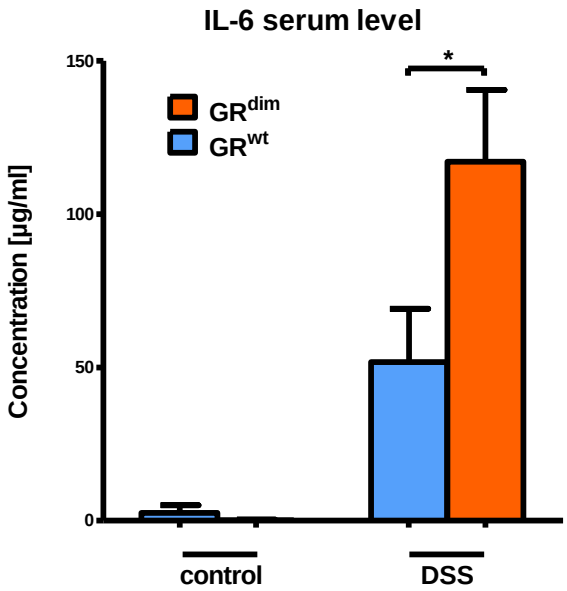

Fig. 39 Concentration of IL-6 in the serum. Mice were treated with 3.5 % (w/v) DSS in the drinking water for eight days and then let to recover for two days. Control mice were left untreated. All mice were sacrificed after ten days. GR^{dim} DSS mice: N = 13. GR^{wt} DSS mice: N = 16. GR^{dim} control: N = 5. GR^{wt} control: N = 5. After sacrificing the mice, blood was collected by heart puncture. The serum was then analyzed for IL-6 concentrations with ELISA and corresponding groups were compared.

The differences between cytokine levels in the supernatant of colon cultures and serum could be explained by different systemic or local cytokine secretion. Alternatively, these differences could be explained by a systemic latency in cytokine concentrations, while local cytokine production already declined.

Considering the fact, that UC is typically not evenly affecting the whole colon, but rather located in certain, predominantly rectal areas, pieces of an oral, medial, and rectal part of the colon were dissected and subsequently incubated o/n in medium. The data from the analysis of TNF-α are shown as an example in Fig. 40. It is striking that the GR^{dim} group treated with DSS seems to have its inflammatory maximum in the rectal section in contrast to the GR^{wt} group and the data obtained for $GR^{villinCreERT2}$ mice, which have their inflammatory maximum in the medial part of the colon.

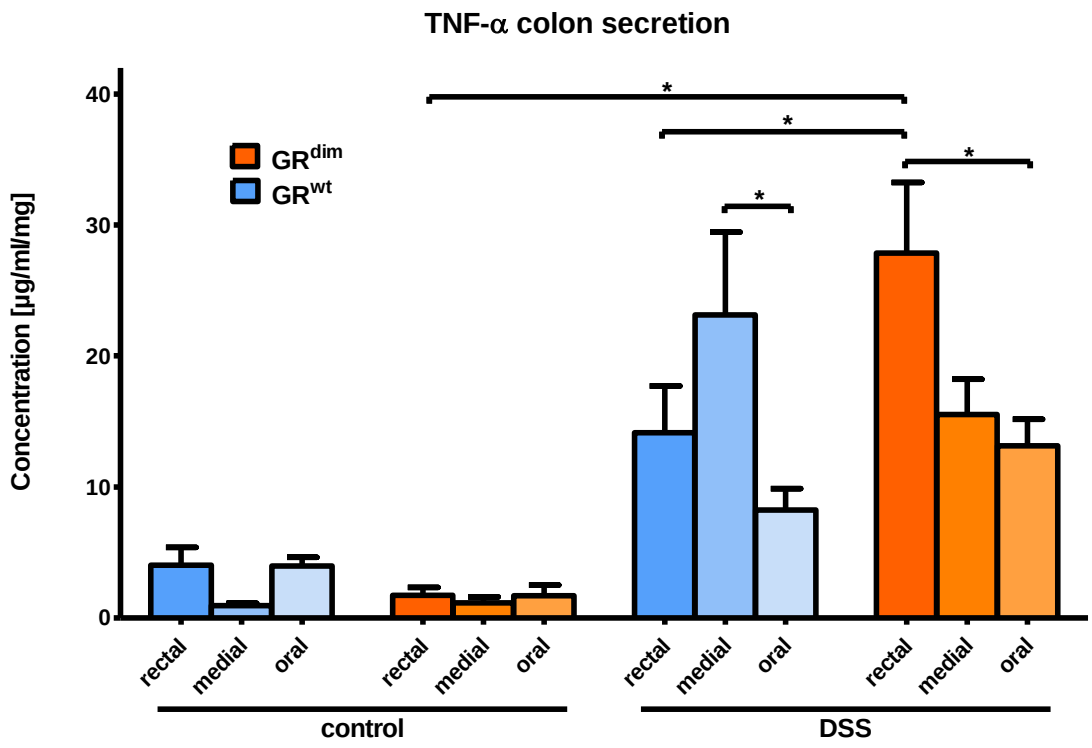

Fig. 40 Concentrations of TNF- α by localization. Mice were treated with 3.5 % (w/v) DSS drinking water for eight days and then let to recover for two days. Control mice were left untreated. All mice were sacrificed after ten days. GR^{dim} DSS mice: N = 7/6. GR^{wt} DSS mice: N = 8/8. After sacrificing the mice, dissecting the colon, and incubating pieces of 5 mm length o/n in media, ELISA analysis was performed on GR^{dim} mice and GR^{wt}mice with DSS treatment and controls. Concentration of pro-inflammatory cytokines TNF-α (A), IL-1β (B) and IL-6 (C) within rectal, medial, and oral parts were compared within corresponding groups.

Concentrations of TNF-α, IL-1β and IL-6 were then measured in supernatants of the rectal part of the colon only and compared between all groups of mice. Interestingly, both GR^{dim}

mice and GR^{wt} mice under DSS administration showed remarkable differences of cytokine concentrations within the colon.

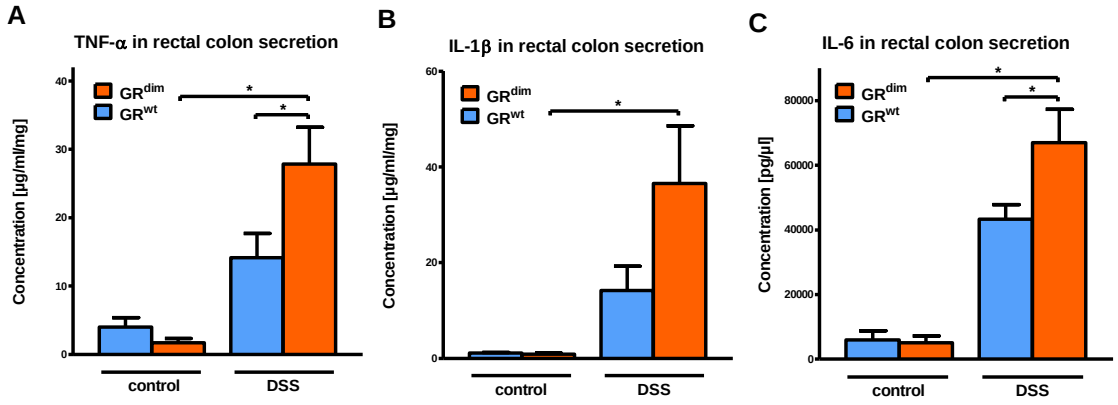

Fig. 41 Concentrations of cytokines in supernatants of rectal colon cultures. Mice were treated with 3.5 % (w/v) DSS in the drinking water for eight days and then let to recover for two days. Control mice were left untreated. All mice were sacrificed after ten days GR^{dim} DSS mice: N = 13. GR^{wt} DSS mice: N = 16. GR^{dim} control: N = 5. GR^{wt} control: N = 5. After sacrificing the mice and dissecting the colon, pieces of 5 mm length were incubated o/n in medium, ELISA analysis was performed for GR^{dim} mice and GR^{wt}mice with DSS treatment and controls. Concentrations of the pro-inflammatory cytokines TNF-α (A), IL-1β (B) and IL-6 (C) within the rectal parts of the colon were compared.

While GR^{dim} mice displayed a clear gradient from the rectal to the oral part, comparable to most entities in human, GR^{wt} mice featured a concentration peak in the medial part, followed by the rectal and oral part. Comparing GR^{dim} mice and GR^{wt} mice under DSS administration, TNF-α and IL-6 concentrations of the rectal part of GR^{dim} mice were significantly higher than rectal parts of GR^{wt} mice (Fig. 41A,C).

4. Discussion

4.1. Influence of the GR in IECs on DSS Colitis and CA-CRC

4.1.1. DSS Colitis in $GR^{villinCreERT2}$ Mice

In all inflammatory processes, GCs such as cortisol in humans and corticosterone in rodents play a central regulatory role. After tissue damage, for example by physical noxae such as heat or cold, by chemical noxae such as acids or bases, or by biological noxae such as toxins or infections by germs, a local inflammation and a systemic stress reaction are initially triggered. On the one hand, the amount of secreted cortisol is increased, and on the other hand, the GR is modified at the cellular level. It is assumed that in the first phase of the inflammatory response, the GR in pro-inflammatory mode modulates the cellular response (Surjit et al. 2011). As it progresses, the function of the GR then switches to an anti-inflammatory mode to support the resolution phase (Vandevyver et al. 2013). To evaluate the effects of the GR in the context of UC and CA-CRC, its depletion in IECs is a promising strategy.

I. GR expression in IECs prevents an exaggerated disease course in DSS colitis

In the $GR^{villinCreERT2}$ mouse model, it could be demonstrated that the GR in IECs is entirely depleted. Based on the DAI score and the loss of body weight, mice whose IECs in the colon no longer possess the GR, suffer an earlier and more severe inflammation than those mice with an intact GR. From day 8 on, their DAI was higher and their body weight lower than that of the control group. Therefore, it is fair to assume, that an intact GR in IECs is a prerequisite for a better endurance and recovery throughout the course of DSS colitis. This finding corresponds well to the current view and understanding of the effect of endogenous GCs on inflammation (Busillo and Cidlowski 2013; Adcock and Mumby 2017).

In the case of GR deletion in myeloid cells, it has already been shown that especially the recovery of mice from DSS colitis was compromised (Meers et al. 2018). In the case of GR deletion in IECs, however, the disease progression itself was initially aggravated. To show how the disease course and especially the recovery in $GR^{villinCreERT2}$ mice is affected, further studies could be considered, in which the disease course is monitored for a longer period. In addition, investigation of inflammatory parameters such as IL-6 in serum during the disease phase would be an interesting project. This would allow to evaluate the course of the disease

on the basis of systemic biochemical parameters without having to sacrifice the mice at an early stage. In future projects, it could also be considered to quantify fecal calprotectin as a biochemical parameter of intestinal inflammation as it is done in routine diagnostics in humans (German S3-Guideline Ulcerative Colitis 2020). Fecal calprotectin is obtained via the feces and, after quantification, allows conclusions to be drawn about the activity of granulocytes in the intestine (Rahier et al. 2009; Lin et al. 2014). It is also known that IECs themselves can produce GCs (Ahmed et al. 2019). A quantification of fecal GCs and ACTH in serum could indicate whether GR-deficient IECs produce more GCs as a compensatory response to the lack of the GR. Both markers can be obtained non-invasively and could complement the clinical DAI scoring and provide a quantifiable biochemical proof of inflammation.

Since only the GR within IECs is switched off in the $GR^{villinCreERT2}$ model, these cells are of foremost interest during the post-sacrifice analysis. It can be assumed that these IECs, in their role as a central communicative and regulatory instance of the inflammatory processes at the mucosa have a great influence on the behavior of many other cells of the mucosa and submucosa, especially on immune cells. Due to the cell specific deletion of the GR, alterations with respect to the measured cytokine and chemokine production can be directly associated with the absence of the GR in IECs and are expected predominantly within the epithelial layer of the colon. Because there is a risk that the concentrations of chemokines and cytokines in relation to the mass of tissue analyzed may be unintentionally falsified by the presence of irrelevant parenchymal cells, a more focused analysis of the relevant portions of mucosa and submucosa would be a useful next step. Distortion of the analyzed parameters due to edematization of the tissue also has to be considered. It is known that inflamed tissue also becomes edematous and thus the mass proportion shifts in favor of the parenchyma (Laroux and Grisham 2001). This would result in lower cytokine concentrations in relation to the mass in more inflamed intestinal sections. This effect could be counteracted by drying the intestinal parts and subsequently doing the analysis in relation to the dry mass. However, a method which completely prevents the co-analysis of the parenchyma should be preferred. In further studies the isolation of IECs, for example from the lamina propria using fluorescence-activated cell sorting (FACS), would be a logical next step to increase the significance of the qRT-PCR and ELISA analysis. This procedure has already been applied by Li D and colleagues and Li H and colleagues (Li D et al. 2019; Li H et al. 2019).

II. GR^{villinCreERT2} mice show a pattern of inflammation in DSS colitis which is different from the inflammation patterns in human UC

Selection and localization of the intestinal segment to be analyzed play an important role. Namely, the intestine was not found to be uniformly affected by the inflammation. In the case of GR^{villinCreERT2} and GR^{flox} mice, the concentration of cytokines peaked in the medial part of the colon, followed by the rectal part and then by the oral part. The selection of the correct location of tisue biopsies is therefore essential for representative results. In further investigations, prior staining of the intestine with e. g. methylene blue as done by and Kiesslich and colleagues in humans and Puthia and colleagues in mice could improve the selection of the intestinal segment of interest (Kiesslich et al. 2003; Puthia et al. 2014). Methylene blue allows a better identification of inflammatory or neoplastic lesions within the mucosa during CA-CRC. Due to impaired barrier functions of the mucosa during said events, methylene blue accumulates in the damaged tissue. A more precise selection of inflamed colon sections could make the results more accurate and valid. It is therefore a promising complementary method.

An interesting observation concerns the above-mentioned varying degrees of inflammation in the different bowel segments. Both, GR^{villinCreERT2} mice and their littermate GR^{flox} controls showed a peak in the cytokine concentrations of TNF-α, IL-1β and IL-6 in the medial part of the colon, followed by the rectal and subsequently oral part. This contrasts with the typical distribution pattern in humans, where inflammation gradients from rectal to oral dominate (Fumery et al. 2018). The fact that DSS reaches the bowel from its oral end could explain this observation. However, it is also possible that the composition or distribution of commensal bacteria has an influence on the inflammatory pattern. It is known that, at least in human, certain strains of bacteria are distributed differently in the gut (Gill et al. 2006; Donaldson et al. 2016). It was also shown that the presence of medium fatty acid chains is a prerequisite for the effect of DSS colitis (Laroui et al. 2012). Both observations can be plausible reasons for the different pattern of inflammation in mice, compared to humans.

4.1.2. CA-CRC in GR^{villinCreERT2} Mice

I. Mice lacking the GR in IECs have a higher tumor burden in DSS colitis-associated colorectal carcinoma

It is known that chronic inflammation of the colon, especially in UC, increases the risk of CRC (Kumar et al. 2016; German S3-Guideline Ulcerative Colitis 2020). In our studies on CA-CRC using the AOM/DSS mouse model, we could confirm this observation in GR^{villinCreERT2} mice. The number of tumors, their size and the tumor burden were significantly larger in GR^{villinCreERT2} mice than in the control group of GR^{flox} mice. There is much to suggest that the previously observed stronger inflammation in the GR^{villinCreERT2} mice facilitates tumor development. The fact that more frequent and stronger inflammatory events are associated with a higher rate of CRC was also observed in humans. It remains unclear whether the deletion of the GR directly leads to the formation of the tumors, or whether the preceding colitis, which was more pronounced in GR^{villinCreERT2} mice, is decisive for the development of the tumors. In order to clarify this question, a rescue experiment would be necessary in which the knockout in GR^{villinCreERT2} mice by tamoxifen administration would be performed only after resolution of DSS colitis. GR^{villinCreERT2} mice would presumably show a comparable disease course during DSS colitis as GR^{flox} mice as the GR in IECs would only be deleted after termination of colitis. The effects of further tumor development could thus be more clearly traced back to the deleted GR.

II. T cell and macrophage infiltration into the tumor is significantly lower than infiltration into the mucosa of GR^{villinCreERT2} mice

The histological analysis of the tumors left some questions unanswered. Already Page and colleagues described that immunosuppressed people develop tumors more often than immunocompetent people (Page et al. 1963). This correlation has also been described in mice (Girardi et al. 2001; Shankaran et al. 2001). Vinay and colleagues documented heterogeneous immune evasion mechanisms of different cancer entities (Vinay et al. 2015). It was therefore obvious to elucidate whether such evasion mechanisms can be demonstrated in the form of lower amounts of immune cells in the tumors of the analyzed mice. Manual quantification of CD3^{+} T cells and CD68^{+} macrophages did not show any significant differences between the tumors of GR^{villinCreERT2} mice and GR^{flox} mice. After quantifying

them by statistical learning-based image segmentation, however, a significantly lower amount of $CD68^+$ macrophages in tumor shafts of $GR^{villinCreERT2}$ mice was observed, suggesting a weaker immune response towards tumors in $GR^{villinCreERT2}$ mice. Noteworthy also significantly lower numbers of $CD3^+$ T cells in tumor tissue compared to mucosa in $GR^{villinCreERT2}$ mice were found. This could be interpreted as one of the immune evasion mechanisms mentioned above.

It should be noted that the intra- and inter-individual comparability of tumors is limited due to highly variable morphology and number of tumors. Furthermore, it is not clear whether tumors found in AOM/DSS-treated $GR^{villinCreERT2}$mice, which is considered to be a CRC model, displays indeed an invasive tumor in the sense of a carcinoma and not an exophytic, polypus adenoma. Although the dysmorphic, disorganized, and invasive growth of the tumors observed in this study suggests that these are indeed carcinomas, a conclusive assessment, though, can only be made with further histopathological IHC stainings and molecular biological analyses of oncogenes and markers such as APC and MSH, as done in routine diagnostics on human specimens, proving cellular aberrance (German S3-Guideline Colorectal Cancer 2019). In order to observe and evaluate any dominance of macrophages or T cells within the tumors found here, further analyses using FACS would be an interesting next step, although acquisition of these cells from the tumors can be expected to be challenging. Analysis of macrophage polarization via IHC staining would be easier to perform. M1 polarized macrophages are known to be tumor suppressive, while M2 polarized macrophages favor tumor growth (Mills 2012; van Dalen et al. 2018). Therefore, a higher amount of M2 polarized macrophages in tumors of $GR^{villinCreERT2}$ could be expected. For more robust results also in terms of reproducibility, further manual and automated analyses of tumors are necessary.

III. High-throughput analysis using iterative automated cell counting is a promising complementary quantification method

Further histological work via high-throughput analysis using iterative automated cell counting may allow for the possibility of more accurate tumor assessment. By using volumetric imaging, the two-dimensional image of tumors could be replaced by a quasi-three-dimensional image in which volume relations of cells of interest to the whole tumor

could show a more precise picture of the infiltration properties altered by GR modification, as done exemplarily by Bonda and colleagues (Bonda et al. 2020).

4.1.3. DSS Colitis in GR^{dim} Mice

In contrast to the $GR^{villinCreERT2}$ mice, GR^{dim} mice do not have a specific tissue in which the GR is selectively switched off. GR^{dim} mice rather have a constitutionally altered GR in all cells of the body (Reichardt et al. 1998). Since a complete GR elimination is a condition incompatible with life, this method is limited to preventing the dimerization of the GR and thus preventing GRE and nGRE dependent modes of transcriptional gene activation and repression (Vandevyver et al. 2013; Cruz-Topete and Cidlowski 2015; Louw 2019).

I. Impaired GR dimerization leads to a more severe course of DSS colitis and increased cytokine production

GR^{dim} mice, beginning at day 5, deteriorated earlier and more markedly than GR^{wt} mice, but at no time this reached statistical significance. Analyses of cytokine and chemokine concentrations released by incubated colon tissue after 10 days of DSS treatment also showed no statistically significant differences between the groups. However, the IL-6 concentration in serum was significantly higher in GR^{dim} mice than in GR^{wt} mice. The comparison between IL-6 levels in the supernatant of colon cultures and serum shows a plausible concordance of inflammatory activity suggesting that the systemic and local responses are homologous, but delayed. The selection of a proper time point of sacrifice seems to play an important role. Comparing local and systemic cytokine levels of IL-6, in future experiments an earlier sacrifice e. g. at day 8 would be conceivable. Possible further analyses of the cytokines TNF-α and IL-1β would also be desirable additions, but may be reduced in significance because of the much shorter half-life of these cytokines. (Hehlgans and Pfeffer 2005; Donnelly et al. 2009; Nielsen et al. 2016). Possibilities of an experiment-accompanying analysis of serum cytokines are limited by the animal welfare act, so that in further experiments non-invasive methods should be considered.

II. GR^{dim} mice show an inflammation pattern in DSS colitis which is similar to the inflammation patterns in human UC

Surprisingly, regarding the segmental analysis of the colon fragments, GR^{dim} mice showed an inflammatory gradient with similarity to the dominating appearance in humans, in whom

inflammation is primarily found in the rectal portions of the colon (Fumery et al. 2018). GR^{wt} mice on the other hand, showed a similar pattern as observed in $GR^{villinCreERT}$ mice, with an inflammation peak in the medial part of the colon. The observation made in GR^{dim} mice contradicts at first sight the hypothesis that the DSS concentration gradient along the colon is responsible for the distribution of inflammation. The contrast to the data obtained with the $GR^{villinCreERT}$ mice may possibly be explained by the methodology, in which a maximum of inflammation between rectal and medial sections would remain undetected. Alternatively, composition and distribution of the microbiota or even different disease susceptibilities within the mouse strains would be possible explanations for this phenomenon (Gill et al. 2006; Donaldson et al. 2016). Further experiments with an analysis of the microbiome or more fine-grained analyses of the colonic tissue could provide interesting insights.

Overall, the postulated worsening of the disease course in GR^{dim} mice due to impeded GR dimerization and reduced GC responsiveness, as already demonstrated by Koenen and colleagues in a model of rheumatoid arthritis, could not be demonstrated (Koenen et al. 2018). However, the data at hand need to be complemented by further experiments.

5. Summary

For many decades, GCs such as dexamethasone have been used in the treatment of inflammatory diseases. However, the exact role of the GR in the pathophysiology of inflammatory processes and, above all, in the corresponding therapeutic regimens is still largely unknown. This work has shown that GCs play a central role in both inflammatory and consecutive neoplastic processes of UC and CA-CRC in mice.

In $GR^{villinCreERT2}$ mice it could be demonstrated that switching off GC expression in colonic IECs leads to an exacerbated disease course of DSS-induced colitis and subsequent tumorigenesis of CA-CRC. These findings concerning the relevance of a functioning GR and its anti-inflammatory effects are consistent with those of other inflammatory entities as demonstrated by Koenen and colleagues in a murine model of rheumatoid arthritis (Koenen et al. 2018). A significant effect of the absent GR on the development of CA-CRC after UC could also be shown, although it was not possible to distinguish whether GC have a direct effect on neoplastic events or whether they are indirectly responsible for the stronger neoplastic growth via the preceding increased inflammation during colitis. Nevertheless, it must be emphasized that the findings related to colitis, as well as those related to CA-CRC, can initially only be referred to the mouse model and cannot be readily applied to humans.

In GR^{dim} mice, however, no clear effect could be observed so far that could be linked to the structural change of the modified GR. It was assumed that GR^{dim} mice were to provoke a more severe disease by the increased pro-inflammatory effect of the modified GC, but this assumption could not be proven in the experiments conducted so far. Nevertheless, cytokine concentrations, like those of IL-6, showed increased inflammation in GR^{dim} mice, suggesting higher inflammatory activity. Future protocols with prolonged DSS application may prove this conjecture.

This work has helped to show that a functional GR in IECs can be confirmed as an essential clinical target of inflammatory processes. It is hoped that further analysis of its function and downstream signaling cascades will reveal more possible intervention sites that may help to target UC and other inflammatory processes more specifically and with fewer side effects in the future.

6. References

Abreu MT (2010): Toll-like receptor signalling in the intestinal epithelium: How bacterial recognition shapes intestinal function. Nat Rev Immunol 10, 131–143

Adcock IM, Mumby S (2017): Glucocorticoids. Handb Exp Pharmacol 237, 171–196

Ahluwalia B, Magnusson MK, Öhman L (2017): Mucosal immune system of the gastrointestinal tract: maintaining balance between the good and the bad. Scand J Gastroenterol 52, 1185–1193

Ahmed A, Schmidt C, Brunner T, Brunner T (2019): Extra-Adrenal Glucocorticoid Synthesis in the Intestinal Mucosa : Between Immune Homeostasis and Immune Escape. Front Immunol. 10, 1438.

Artis D (2008): Epithelial-cell recognition of commensal bacteria and maintenance of immune homeostasis in the gut. Nat Rev Immunol 8, 411–420

Berg JM, Tymoczko JL, Lubert S (Eds.): Stryer Biochemie. 7th edition; Springer-Verlag Berlin, Heidelberg 2013

Berg S, Kutra D, Kroeger T, Straehle CN, Kausler BX, Haubold C, Schiegg M, Ales J, Beier T, Rudy M, et al. (2019): ilastik: interactive machine learning for (bio)image analysis. Nat Methods 16, 1226–1232

Bevins CL, Salzman NH (2011): Paneth cells, antimicrobial peptides and maintenance of intestinal homeostasis. Nat Rev Microbiol 9, 356–368

Böcker GW, Kreipe H, Moch H (Eds.): Pathologie. 5th edition; Urban and Fischer, Berlin 2012

Bonda U, Jaeschke A, Lighterness A, Baldwin J, Werner C, De-Juan-Pardo EM, Bray LJ (2020): 3D Quantification of Vascular-Like Structures in z Stack Confocal Images. STAR Protoc 1, 100180

Brenner H, Kloor M, Pox CP (2014): Colorectal cancer. Lancet 383, 1490–1502

Brierley JD, Gospodarowicz MK, Wittekind C: TNM Classification of Malignant Tumours. 8th edition; John Wiley & Sons 2016

Buettner M, Bode U (2012): Lymph node dissection--understanding the immunological function of lymph nodes. Clin Exp Immunol 169, 205–212

Bürtin F, Mullins CS, Linnebacher M (2020): Mouse models of colorectal cancer: Past, present and future perspectives. World J Gastroenterol 26, 1394–1426

Busillo JM, Cidlowski JA (2013): The five Rs of glucocorticoid action during inflammation: ready, reinforce, repress, resolve, and restore. Trends Endocrinol Metab 24, 109–119

Cain DW, Cidlowski JA (2017): Immune regulation by glucocorticoids. Nat Rev Immunol 17, 233–247

Cario E, Podolsky DK (2000): Differential Alteration in Intestinal Epithelial Cell Expression of Toll-Like Receptor 3 (TLR3) and TLR4 in Inflammatory Bowel Disease. Infect Immun 68, 7010–7017

Chrousos GP (1995): The Hypothalamic–Pituitary–Adrenal Axis and Immune-Mediated Inflammation. N Engl J Med 332, 1351–1363

Cole TJ, Blendy JA, Monaghan AP, Krieglstein K, Schmid W, Aguzzi A, Fantuzzi G, Hummler E, Unsicker K, Schütz G (1995): Targeted disruption of the glucocorticoid receptor gene blocks adrenergic chromaffin cell development and severely retards lung maturation. Genes Dev 9, 1608–1621

Crielaard BJ, Lammers T, Morgan ME, Chaabane L, Carboni S, Greco B, Zaratin P, Kraneveld AD, Storm G (2011): Macrophages and liposomes in inflammatory disease: Friends or foes? Int J Pharm 416, 499–506

Cruz-Topete D, Cidlowski JA (2015): One Hormone, Two Actions: Anti- and Pro-Inflammatory Effects of Glucocorticoids. Neuroimmunomodulation 22, 20–32

Danese S, Fiocchi C (2011): Ulcerative Colitis. N Engl J Med 365, 1713–1725

Danese S, Sans M, Fiocchi C (2004): Inflammatory bowel disease: The role of environmental factors. Autoimmun Rev 3, 394–400

Dieleman LA, Ridwan BU, Tennyson GS, Bucy RP (1994): Dextran sulfate sodium-induced colitis occurs in severe combined immunodeficient mice. Gastroenterology 107, 1643–52

Dignass AU, Bokemeyer B, Adamek H, Mross M, Vinter-Jensen L, Börner N, Silvennoinen

J, Tan G, Pool MO, Stijnen T, et al. (2009): Mesalamine Once Daily Is More Effective Than Twice Daily in Patients With Quiescent Ulcerative Colitis. Clin Gastroenterol Hepatol 7, 762–769

Donaldson GP, Lee SM, Mazmanian SK (2016): Gut biogeography of the bacterial microbiota. Nat Rev Microbiol 14, 20–32

Donnelly RP, Young HA, Rosenberg AS (2009): An overview of cytokines and cytokine antagonists as therapeutic agents. Ann N Y Acad Sci 1182, 1–13

el Marjou F, Janssen K-P, Chang BH-J, Li M, Hindie V, Chan L, Louvard D, Chambon P, Metzger D, Robine S (2004): Tissue-specific and inducible Cre-mediated recombination in the gut epithelium. Genesis 39, 186–193

Enders G: Darme mit Charme. Ullstein Buchverlage GmbH, Berlin 2014

Etzerodt A, Moestrup SK (2013): CD163 and inflammation: biological, diagnostic, and therapeutic aspects. Antioxid Redox Signal 18, 2352–2363

Ford MJ, Camilleri M, Wiste JA, Hanson RB (1995): Differences in colonic tone and phasic response to a meal in the transverse and sigmoid human colon. Gut 37, 264–269

Fumery M, Singh S, Dulai PS, Gower-Rousseau C, Peyrin-Biroulet L, Sandborn WJ (2018): Natural History of Adult Ulcerative Colitis in Population-based Cohorts: A Systematic Review. Clin Gastroenterol Hepatol Off Clin Pract J Am Gastroenterol Assoc 16, 343-356.e3

Garrett WS (2019): The gut microbiota and colon cancer. Science 364, 1133–1135

German S3-Guideline Colorectal Cancer German Guideline Program in Oncology (German Cancer Society, German Cancer Aid, AWMF): S3-Guideline Colorectal Cancer, long version 2.1, 2019, AWMF registration number: 021-007OL. 2019

German S3-Guideline Ulcerative Colitis (2020): Updated S3-Guideline Ulcerative Colitis German Society for Digestive and Metabolic Diseases (DGVS). Z Gastroenterol 57, 162–241

Gill SR, Pop M, DeBoy RT, Eckburg PB, Turnbaugh PJ, Samuel BS, Gordon JI, Relman DA, Fraser-Liggett CM, Nelson KE (2006): Metagenomic Analysis of the Human Distal Gut Microbiome. Science (80-) 312, 1355 LP – 1359

Girardi M, Oppenheim DE, Steele CR, Lewis JM, Glusac E, Filler R, Hobby P, Sutton B, Tigelaar RE, Hayday AC (2001): Regulation of cutaneous malignancy by gammadelta T cells. Science 294, 605–609

Goldstein N, Dulai M (2006): Contemporary morphologic definition of backwash ileitis in ulcerative colitis and features that distinguish it from Crohn disease. Am J Clin Pathol 126, 365–376

Grandt D, Lappe V, Schubert I: Arzneimittelreport 2018. volume 10; 2018

Hamers AAJ, Van Dam L, Duarte JMT, Vos M, Marinković G, Van Tiel CM, Meijer SL, Van Stalborch AM, Huveneers S, Te Velde AA, et al. (2015): Deficiency of nuclear receptor Nur77 aggravates mouse experimental colitis by increased NFκB activity in macrophages. PLoS One 10, 1–22

Hanly WC, Artwohl JE, Bennett BT (1995): Review of Polyclonal Antibody Production Procedures in Mammals and Poultry. ILAR J 37, 93–118

Hehlgans T, Pfeffer K (2005): The intriguing biology of the tumour necrosis factor/tumour necrosis factor receptor superfamily: players, rules and the games. Immunology 115, 1–20

Helander HF, Fändriks L (2014): Surface area of the digestive tract - revisited. Scand J Gastroenterol 49, 681–689

Heller F, Florian P, Bojarski C, Richter J, Christ M, Hillenbrand B, Mankertz J, Gitter AH, Bürgel N, Fromm M, et al. (2005): Interleukin-13 is the key effector Th2 cytokine in ulcerative colitis that affects epithelial tight junctions, apoptosis, and cell restitution. Gastroenterology 129, 550–564

Hermoso MA, Matsuguchi T, Smoak K, Cidlowski JA (2004): Glucocorticoids and Tumor Necrosis Factor Alpha Cooperatively Regulate Toll-Like Receptor 2 Gene Expression. Mol Cell Biol 24, 4743–4756

Hudcovic T, Stepankova R, Cebra J, Tlaskalova-Hogenova H (2001): The Role of Microflora in the Development of Intestinal Inflammation : Acute and Chronic Colitis Induced by Dextran Sulfate in Germ-Free and Conventionally Reared Immunocompetent and Immunodeficient Mice. Folia Microbiol 46, 565–572

Hunter MM, Wang A, Parhar KS, Johnston MJG, Van Rooijen N, Beck PL, McKay DM

(2010): In Vitro-Derived Alternatively Activated Macrophages Reduce Colonic Inflammation in Mice. Gastroenterology 138, 1395–1405

Jass JR (2007): Classification of colorectal cancer based on correlation of clinical, morphological and molecular features. Histopathology 50, 113–130

Kagnoff MF (2014): The intestinal epithelium is an integral component of a communications network. J Clin Invest 124, 2841–2843

Kaiserling E, Kröber S, Geleff S (2003): Lymphatic vessels in the colonic mucosa in ulcerative colitis. Lymphology 36, 52–61

Kaistha A, Levine J (2014): Inflammatory Bowel Disease: The Classic Gastrointestinal Autoimmune Disease. Curr Probl Pediatr Adolesc Health Care 44, 328–334

Kerr TA, Ciorba MA, Matsumoto H, Davis VRT, Luo J, Kennedy S, Xie Y, Shaker A, Dieckgraefe BK, Davidson NO (2012): Dextran Sodium Sulfate Inhibition of Real-Time Polymerase Chain Reaction Amplification: A Poly-A Purification Solution. Inflamm Bowel Dis 18, 344–348

Kiesslich R, Fritsch J, Holtmann M, Koehler HH, Stolte M, Kanzler S, Nafe B, Jung M, Galle PR, Neurath MF (2003): Methylene blue-aided chromoendoscopy for the detection of intraepithelial neoplasia and colon cancer in ulcerative colitis. Gastroenterology 124, 880–888

Kitajima S, Morimoto M (2001): Dextran Sodium Sulfate-Induced Colitis in Germ-Free IQI / Jic Mice. Exp Anim 50, 387–395

Kitajima S, Takuma S, Morimoto M (1998): Tissue Distribution of Dextran Sulfate Sodium (DSS) in the Acute Phase of Murine DSS-Induced Colitis. 1–4

Kitajima S, Takuma S, Morimoto M (2000): Histological Analysis of Murine Colitis Induced by Dextran Sulfate Sodium of Different Molecular Weights. Exp Anim 49, 9–15

Klaßen C: Airway Epithelial Cells as Targets of Glucocorticoid Theraoy in Inflammatory Lung Disease. Med. Diss., Göttingen 2016

Klaßen C, Karabinskaya A, Dejager L, Vettorazzi S, Van Moorleghem J, Lühder F, Meijsing SH, Tuckermann JP, Bohnenberger H, Libert C, Reichardt HM (2017): Airway Epithelial Cells Are Crucial Targets of Glucocorticoids in a Mouse Model of Allergic

Asthma. J Immunol 199, 48–61

Koenen M, Culemann S, Vettorazzi S, Caratti G, Frappart L, Baum W, Krönke G, Baschant U, Tuckermann JP (2018): Glucocorticoid receptor in stromal cells is essential for glucocorticoid-mediated suppression of inflammation in arthritis. Ann Rheum Dis 77, 1610–1618

Kojouharoff G, Hans W, Obermeier F, Männel DN, Andus T, Schölmerich J, Gross V, Falk W (1997): Neutralization of tumour necrosis factor (TNF) but not of IL-1 reduces inflammation in chronic dextran sulphate sodium-induced colitis in mice. Clin Exp Immunol 107, 353–358

Kumar V, Abbas A, Fausto N (Ed.): Pathologic Basis of Disease. 8th edition; Saunders & Elsevier, Chicago 2016

Laroui H, Ingersoll SA, Liu HC, Baker MT, Ayyadurai S, Charania MA, Laroui F, Yan Y, Sitaraman S V, Merlin D (2012): Dextran sodium sulfate (DSS) induces colitis in mice by forming nano-lipocomplexes with medium-chain-length fatty acids in the colon. PLoS One 7, e32084

Laroux FS, Grisham MB (2001): Immunological Basis of Inflammatory Bowel Disease: Role of the Microcirculation. Microcirculation 8, 283–301

Lawrence T (2009): The Nuclear Factor NF- B Pathway in Inflammation. Cold Spring Harb Perspect Biol 1, a001651–a001651

Leslie A, Carey FA, Pratt NR, Steele RJC (2002): The colorectal adenoma-carcinoma sequence. Br J Surg 89, 845–860

Li D, Dong H, Kohan AB (2019): The Isolation, Culture, and Propagation of Murine Intestinal Enteroids for the Study of Dietary Lipid Metabolism. Methods Mol Biol 1576, 195–204

Li H, Kaiser TK, Borschiwer M, Bohnenberger H, Reichardt SD, Lühder F, Walter L, Dressel R, Meijsing SH, Reichardt HM (2019): Glucocorticoid resistance of allogeneic T cells alters the gene expression profile in the inflamed small intestine of mice suffering from acute graft-versus-host disease. J Steroid Biochem Mol Biol 195, 105485

Lin J-F, Chen J-M, Zuo J-H, Yu A, Xiao Z-J, Deng F-H, Nie B, Jiang B (2014): Meta-

analysis: fecal calprotectin for assessment of inflammatory bowel disease activity. Inflamm Bowel Dis 20, 1407–1415

Loftus E V. (2004): Clinical epidemiology of inflammatory bowel disease: Incidence, prevalence, and environmental influences. Gastroenterology 126, 1504–1517

Longo D (Ed.): Harrison' s Principles of Internal Medicine. volume II; 18th edition; McGraw-Hill Companies, Inc., New York 2012

Louw A (2019): GR Dimerization and the Impact of GR Dimerization on GR Protein Stability and Half-Life. Front Immunol 10, 1693

Magaki S, Hojat SA, Wei B, So A, Yong WH (2019): An Introduction to the Performance of Immunohistochemistry. Methods Mol Biol 1897, 289–298

Mähler M, Bristol IJ, Leiter EH, Workman AE, Birkenmeier EH, Elson CO, Sundberg JP, Bristol IJ, Leiter EH, Workman AE, et al. (1998): Differential susceptibility of inbred mouse strains to dextran sulfate sodium-induced colitis. Am J Physiol 274, 544–551

Mason KL, Huffnagle GB, Noverr MC, Kao JY (2008): Overview of gut immunology. Adv Exp Med Biol 635, 1–14

Meers GK, Bohnenberger H, Reichardt HM, Lühder F, Reichardt SD (2018): Impaired resolution of dss-induced colitis in mice lacking the glucocorticoid receptor in myeloid cells. PLoS One 13, 1–15

Melgar S, Karlsson A, Michaelsson E (2005): Acute colitis induced by dextran sulfate sodium progresses to chronicity in C57BL/6 but not in BALB/c mice: correlation between symptoms and inflammation. AJP Gastrointest Liver Physiol 288, G1328–G1338

Michael Ross WP (Ed): Histology - A Text and Atlas. 7th edition; Wolters Kluwer Health 2016, 156 - 159

Mills CD (2012): M1 and M2 Macrophages: Oracles of Health and Disease. Crit Rev Immunol 32, 463–488

Mosser DM, Edwards JP (2008): Exploring the full spectrum of macrophage activation. Nat Rev Immunol 8, 958–969

Muanprasat C, Chatsudthipong V (2013): Cholera: pathophysiology and emerging

therapeutic targets. Future Med Chem 5, 781–798

Murphy K, Weaver C: Janeway Immunologie. Springer Berlin Heidelberg, Berlin, Heidelberg 2018, 378 - 398

Mutalib M, Borrelli O, Blackstock S, Kiparissi F, Elawad M, Shah N, Lindley K (2014): The use of sirolimus (rapamycin) in the management of refractory inflammatory bowel disease in children. J Crohns Colitis 8, 1730–1734

Newberry RD, Lorenz RG (2005): Organizing a mucosal defense. Immunol Rev 206, 6–21

Nielsen HG, Øktedalen O, Opstad P-K, Lyberg T (2016): Plasma Cytokine Profiles in Long-Term Strenuous Exercise. J Sport Med Hindawi Publ Corp 2016, 7186137

Oakley RH, Cidlowski JA (2013): The biology of the glucocorticoid receptor: new signaling mechanisms in health and disease. J Allergy Clin Immunol 132, 1033–1044

Okayasu I, Hatakeyama S, Yamada M, Ohkusa T, Inagaki Y, Nakaya R (1990): A novel method in the induction of reliable experimental acute and chronic ulcerative colitis in mice. Gastroenterology 98, 694–702

Page AR, Hansen AE, Good RA (1963): Occurrence of leukemia and lymphoma in patients with agammaglobulinemia. Blood 21, 197–206

Pastorelli L, De Salvo C, Mercado JR, Vecchi M, Pizarro TT (2013): Central Role of the Gut Epithelial Barrier in the Pathogenesis of Chronic Intestinal Inflammation: Lessons Learned from Animal Models and Human Genetics. Front Immunol 4, 1–22

Perše M, Cerar A (2012): Dextran Sodium Sulphate Colitis Mouse Model: Traps and Tricks. J Biomed Biotechnol 2012, 1–13

Phillips SF, Giller J (1973): The contribution of the colon to electrolyte and water conservation in man. J Lab Clin Med 81, 733–746

Pithadia AB, Jain S (2011): Treatment of inflammatory bowel disease (IBD). PharmacolRep 63, 629–642

Pivonello R, Isidori AM, De Martino MC, Newell-Price J, Biller BMK, Colao A (2016): Complications of Cushing's syndrome: state of the art. lancet Diabetes Endocrinol 4, 611–629

Podolsky DK (2002): Inflammatory Bowel Disease. N Engl J Med 347, 417–429

Puthia M, Storm P, Nadeem A, Hsiung S, Svanborg C (2014): Prevention and treatment of colon cancer by peroral administration of HAMLET (human α-lactalbumin made lethal to tumour cells). Gut 63, 131–142

Rahier JF, Ben-Horin S, Chowers Y, Conlon C, De Munter P, D'Haens G, Domènech E, Eliakim R, Eser A, Frater J, et al. (2009): European evidence-based Consensus on the prevention, diagnosis and management of opportunistic infections in inflammatory bowel disease. J Crohn's Colitis 3, 47–91

Ramakrishna BS (2007): The Normal Bacterial Flora of the Human Intestine and Its Regulation. J Clin Gastroenterol 41, S2–S6

Reichardt HM, Kaestner KH, Tuckermann J, Kretz O, Wessely O, Bock R, Gass P, Schmid W, Herrlich P, Angel P, Schütz G (1998): DNA Binding of the Glucocorticoid Receptor Is Not Essential for Survival. Cell 93, 531–541

Reichardt SD, Föller M, Rexhepaj R, Pathare G, Minnich K, Tuckermann JP, Lang F, Reichardt HM (2012): Glucocorticoids Enhance Intestinal Glucose Uptake Via the Dimerized Glucocorticoid Receptor in Enterocytes. 153, 1783–1794

Rex DK (2010): Preventing colorectal cancer and cancer mortality with colonoscopy: What we know and what we dont know. Endoscopy 42, 320–323

RKI Report on Cancer R (2016): Bericht zum Krebsgeschehen in Deutschland 2016. 274

Rutgeerts P, Sandborn WJ, Feagan BG, Reinisch W, Olson A, Johanns J, Travers S, Rachmilewitz D, Hanauer SB, Lichtenstein GR, et al. (2005): Infliximab for induction and maintenance therapy for ulcerative colitis. N Engl J Med 353, 2462–2476

Säemann MD, Böhmig GA, Osterreicher CH, Burtscher H, Parolini O, Diakos C, Stöckl J, Hörl WH, Zlabinger GJ (2000): Anti-inflammatory effects of sodium butyrate on human monocytes: potent inhibition of IL-12 and up-regulation of IL-10 production. FASEB J Off Publ Fed Am Soc Exp Biol 14, 2380–2382

Sandle GI (1998): Salt and water absorption in the human colon: a modern appraisal. Gut 43, 294–299

Sapolsky RM, Romero LM, Munck AU (2000): How Do Glucocorticoids Influence Stress

Responses? Integrating Permissive, Suppressive, Stimulatory, and Preparative Actions. Endocr Rev 21, 55–89

Sartor RB (2008): Microbial Influences in Inflammatory Bowel Diseases. Gastroenterology 134, 577–594

Sender R, Fuchs S, Milo R (2016): Revised Estimates for the Number of Human and Bacteria Cells in the Body. PLoS Biol 14, e1002533

Servier Medical Art by Les Laboratoires Servier, Suresnes (2018): Servier Medical Art

Shankaran V, Ikeda H, Bruce AT, White JM, Swanson PE, Old LJ, Schreiber RD (2001): IFNgamma and lymphocytes prevent primary tumour development and shape tumour immunogenicity. Nature 410, 1107–1111

Shao L, Kamalu O, Mayer L (2005): Non-classical MHC class I molecules on intestinal epithelial cells: mediators of mucosal crosstalk. Immunol Rev 206, 160–176

Snider AJ, Bialkowska AB, Ghaleb AM, Yang VW, Obeid LM, Hannun YA (2016): Murine Model for Colitis-Associated Cancer of the Colon. Methods Mol Biol 1438, 245–254

So AY-L, Chaivorapol C, Bolton EC, Li H, Yamamoto KR (2007): Determinants of cell- and gene-specific transcriptional regulation by the glucocorticoid receptor. PLoS Genet 3, e94

Stange EF, Travis SPL, Vermeire S, Reinisch W, Geboes K, Barakauskiene A, Feakins R, Fléjou JF, Herfarth H, Hommes DW, et al. (2008): European evidence-based Consensus on the diagnosis and management of ulcerative colitis: Definitions and diagnosis. J Crohn's Colitis 2, 1–23

Stremmel W, Staffer S, Jochen M, Gan-schreier H, Wannhoff A, Stuhrmann N (2017): Genetic Mouse Models with Intestinal-Specific Tight Junction Deletion Resemble an Ulcerative Colitis Phenotype. 1247–1257

Surjit M, Ganti KP, Mukherji A, Ye T, Hua G, Metzger D, Li M, Chambon P (2011): Widespread negative response elements mediate direct repression by agonist-liganded glucocorticoid receptor. Cell 145, 224–241

Suzuki R, Kohno H, Sugie S, Tanaka T (2005): Dose-dependent promoting effect of dextran sodium sulfate on mouse colon carcinogenesis initiated with azoxymethane. 492, 14670

Tanaka T (2009): Colorectal carcinogenesis: Review of human and experimental animal studies. J Carcinog 8, 5

Tanaka T, Kohno H, Suzuki R, Yamada Y, Sugie S, Mori H (2003): A novel inflammation-related mouse colon carcinogenesis model induced by azoxymethane and dextran sodium sulfate. Cancer Sci 94, 965–973

Tomita M, Tsumoto K (2011): Hybridoma technologies for antibody production. Immunotherapy 3, 371–380

Tronche F, Kellendonk C, Kretz O, Gass P, Anlag K, Orban PC, Bock R, Klein R, Schütz G (1999): Disruption of the glucocorticoid receptor gene in the nervous system results in reduced anxiety. Nat Genet 23, 99–103

Turnbaugh PJ, Ley RE, Hamady M, Fraser-Liggett CM, Knight R, Gordon JI (2007): The Human Microbiome Project. Nature 449, 804–810

Uhlenhaut NH, Barish GD, Yu RT, Downes M, Karunasiri M, Liddle C, Schwalie P, Hübner N, Evans RM (2013): Insights into negative regulation by the glucocorticoid receptor from genome-wide profiling of inflammatory cistromes. Mol Cell 49, 158–171

Vagnerová K, Kverka M, Klusoňová P, Ergang P, Mikšík I, Tlaskalová-Hogenová H, Pácha J (2006): Intestinal inflammation modulates expression of 11β-hydroxysteriod dehydrogenase in murine gut. J Endocrinol 191, 497–503

van Dalen FJ, van Stevendaal MHME, Fennemann FL, Verdoes M, Ilina O (2018): Molecular Repolarisation of Tumour-Associated Macrophages. Molecules 24

Van Hauwermeiren F, Vandenbroucke RE, Grine L, Lodens S, Van Wonterghem E, De Rycke R, De Geest N, Hassan B, Libert C (2015): TNFR1-induced lethal inflammation is mediated by goblet and Paneth cell dysfunction. Mucosal Immunol 8, 828–840

Van Staa TP, Leufkens HGM, Abenhaim L, Begaud B, Zhang B, Cooper C (2000): Use of oral corticosteroids in the United Kingdom. QJM - Mon J Assoc Physicians 93, 105–111

Vandevyver S, Dejager L, Tuckermann J, Libert C (2013): New insights into the anti-inflammatory mechanisms of glucocorticoids: an emerging role for glucocorticoid-receptor-mediated transactivation. Endocrinology 154, 993–1007

Vinay DS, Ryan EP, Pawelec G, Talib WH, Stagg J, Elkord E, Lichtor T, Decker WK, Whelan RL, Kumara HMCS, et al. (2015): Immune evasion in cancer: Mechanistic basis and therapeutic strategies. Semin Cancer Biol 35 Suppl, S185–S198

Zhang Z, Dong L, Jia A, Chen X, Yang Q, Wang Yufei, Wang Yuexin, Liu R, Cao Y, He Y, et al. (2020): Glucocorticoids Promote the Onset of Acute Experimental Colitis and Cancer by Upregulating mTOR Signaling in Intestinal Epithelial Cells. Cancers (Basel) 12